RUHR-UNIVERSITÄT BOCHUM

RUB

Efficiency of Electrocatalytic Gas Evolution on Transition Metal-Oxides - from Spatial Distribution of Morphological Pattern Towards Understanding of Electrocatalysis as Resonance Phenomenon

DISSERTATION

Submitted for the Degree of Doctor of Natural Sciences (Dr. rer. nat.)

by

Aleksandar R. Zeradjanin

(from Belgrade, Serbia)

Department of Analytical Chemistry – Elektroanalytik & Sensorik

Faculty of Chemistry, Ruhr University Bochum, Germany

July, 2012

RUHR-UNIVERSITÄT BOCHUM

RUB

Efficiency of Electrocatalytic Gas Evolution on Transition Metal-Oxides - from Spatial Distribution of Morphological Pattern Towards Understanding of Electrocatalysis as Resonance Phenomenon

DISSERTATION

zur Erlangung des Grades eines Doktors der Naturwissenschaften

vorgelegt von

Aleksandar R. Zeradjanin

(aus Belgrad, Serbien)

Analytische Chemie – Elektroanalytik & Sensorik

Fakultät für Chemie, Ruhr Universität Bochum, Deutschland

Juli, 2012

DEDICATION

This thesis I dedicate to my family: my father Radisav, my mother Milena and my brother Igor to whom I am grateful for all the love, faith and patient sacrifice. Even in this world some things are sacred and immortal…

Ову дисертацију посвећујем мојој породици: оцу Радисаву, мајци Милени, и брату Игору, којима сам неизмерно захвалан за сву љубав, поверење и стрпљиво пожртвовање. Чак и у овом свету неке ствари су свете и бесмртне...

“By the rivers of Babylon there we sat down and there we wept when we remembered Zion

Psalms 137:1

“And you, my son Solomon, know the God of your father, and serve him with single mind and willing heart; for the Lord searches every mind, and understands every plan and thought. If you seek him, he will be found by you… be strong, and act.” *1. Chronicles 28:9*

David said further to his son Solomon: “Be strong and of good courage, and act. Do not be afraid or dismayed; for the Lord God, my God, is with you.” *1. Chronicles 28:20*

When David’s time to die drew near, he charged his son Solomon, saying: ”I am about to go the way of all the earth. Be strong, be courageous, and keep the charge of the Lord your God, walking in his ways and keeping his statutes, his commandments, his ordinances, and his testimonies, as it is written in the Law of Moses, so that you may prosper in all that you do and wherever you turn.” *1. Kings 2:1*

“For now we see in a mirror, dimly, but then we will see face to face. Now I know only in part; then I will know fully, even as I have been fully known” *1. Corinthians 13:12*

Research for this doctoral study was carried out from April of 2009 till April of 2012 in the working group of Prof. Wolfgang Schuhmann, in the Department of Analytical Chemistry at the Faculty of Chemistry, Ruhr University Bochum, Germany.

Date of submission:

Date of examination:

Chair of examination commission:

Referee: Prof. Dr. Wolfgang Schuhmann

Co-referee: Prof. Dr. Martin Muhler

ACKNOWLEDGEMENTS

Knowledge accumulated in this doctoral thesis is a result of many years of effort initiated long before my arrival to Germany. Being witness of times where many great people from my country are erased from history, I must mention at least some of the names who are much more than just my personal inspiration: Nikola Tesla, Ruđer Bošković, Pavle Savić, …. they are true giants of the human family. With their brilliance and generosity they contributed to civilization in a best sense, despite their name was stolen and their work shamefully attributed to others. Their impact was so profound that it can be understood as providential.

My beginnings in electrochemistry are rooted at Belgrade University, at the Department of Physical Chemistry and Electrochemistry. I was lucky enough to be part of a department that exists more than 70 years, which propelled many excellent electrochemists to the scientific community. One of the most inspiring figures was certainly Aleksandar Despić, president of the Serbian Academy of Science and an outstanding scholar. John Bockris, one of the two or three most important electrochemists of the Western world [1] stated: „...I had an unusually clear view of electrochemistry in the Eastern countries between about 1956 and Gorbachov... Despić stood out among these people in breadth of comprehension and ability to take up virtually any theme. Indeed, in my opinion he stands historically second only to A.N. Frumkin“ [2]...who was considered to be *primus inter pares* [3]. In years when I was growing up where everything was distorted and approaching to complete nihilism, the possibility to identify with somebody who is a world class was of major importance.

With nice memories I recall most of my professors from Belgrade, they gave me some encouraging remarks. Especially important for me was Prof. Branimir Grgur who introduced me into electrochemistry and helped me to make some important decisions for my future. *Hvala Bane!*

Special gratitude I own to Prof. Wolfgang Schuhmann from several important reasons. I started to search for position abroad on 6th of October 2008. I sent an email to Wolfgang on 14th of October and I received invitation letter from him already on 18th of October. Knowing experience of others, everything happened amazingly fast. My first thought about Wolfgang was: „This is a pragmatic 'maniac'...very good... this is exactly what I need“. In those days I was not aware that Wolfgang is one of the eminent world figures in analytical electrochemistry. Arrival in Bochum was on 9th of January 2009 and PhD project started at 21st of April 2009. From the beginning, I had an impression that Wolfgang trusts my abilities. As the project was ongoing he delivered me more and more independence until I practically took over full responsibility for the project. This was very important in building of self-confidence. Due to Wolfgang and the financial support that he provided I had opportunity to make my PhD research according to my own vision, to present my work at some prestige conferences and to meet some of the best electrochemists in the world...I learned a lot and I visited some beautiful places. Although scientific (and nonscientific) discussions between Wolfgang and me could burst into flame, with time I learned to respect more an more his experience. Whenever I consider his point of view I could be sure that there will be some integrity there. Many good things came to me through Wolfgang Schuhmann... *Thanks Man!*

Thanks to Prof. Martin Muhler for his kind acceptance to be in the examination commission. This was a particular honor for me, knowing that Prof. Muhler is an eminent scientist in the field of catalysis.

Gratitude goes to BMBF (German Federal Ministry of Education and Research) for financial support. The work was financially supported by the BMBF in the framework of the project: „Innovative Technologien für Ressourceneffizienz rohstoffintensiver Produktionsprozesse: Effizienzsteigerung bei der Chlor-Herstellung“ (FZ 033R018E)“.

Certainly, I own gratitude to many people who helped me in realizing this thesis in direct or indirect way:

Many thanks to Bettina Stetzka and her enormous patience, without her it would be impossible to realize any administrative task, all necessary burocratic procedures etc.

Thanks to Prof. Michael Bron for the help during my first days in Germany. Before official start of my PhD, during my first three months in Bochum, we worked together on oxygen reduction reaction. Michael believed that I have a potential do achieve something serious in that field...time will tell.

Thanks to Dr. Leonard Stoica for his kind scientific help during my first days. He always had time for me, despite I interrupted him too often.

Thanks to Dr. Thomas Erichsen for help with computer network, without him work in the lab would not be as easy as it was.

Thanks to PD Dr. Sabine Seisel for administrative support in the BMBF project.

Thanks to Dr. Fabio La Mantia and Dr. Aliaksandr Bandarenka, junior group leaders at the Center for Electrochemical Sciences for scientific discussions and for lifting up the level of electrochemistry in the group.

Thanks to colleagues from industry (AG Bayer Materials Science): Dr. Jürgen Kintrup, Andreas Bulan and Bruno Sawaryn for the friendly atmosphere. With their help I learned about real problems in industrial electrochemistry.

Thanks to other collaborators: Prof. Strasser's group (Nadine Menzel...TU Berlin); Prof. Hempelman's group (Chen, Trieu, Natter, Schley....UdS Saarbrücken); Prof. Schmuki's group (Robert Hahn...FAU Erlangen); Prof. Rosiwal's group (Hanadi Ghanem...FAU Erlangen); NanoX (Elin Hamaberg...), Prof. Schlögl's group (Dr. Detre Teschner...Fritz Haber Inst. Berlin); Prof. Kulesza's group (Anna Dobrzeniecka...University of Warsaw)...

Special thanks to the group of people who contributed to this dissertation with experimental measurements and data: Dr. Rolf Neuser, Matthias Born, Dr. Dominik Schäfer, Stefan Klink, Sandra Schmidt for SEM/EDX mapping; Dr. Edgar Ventosa and Artjom Maljusch for AFM

measurements; Dr. Stefanie Schwamborn for Raman spectroscopy measurements; Dr. Thomas Reinecke for supplying XRD data.

An important contribution was improving of English language for the papers, reports and this thesis where thanks goes to Justus Masa and Dr. John Henry.

Finally and with great respect, I would like to thank to some important scientists from the field of electrocatalysis and catalysis who encouraged me for the future: Dr. Nenad Markovic, (Argonne National Laboratory, US), Prof. Dr. Peter Strasser (TU Berlin), Dr. Karl Mayrhofer (Max Planck Inst., Düsseldorf); Dr. Detre Teschner (Fritz Haber Inst. Berlin); Prof. Dr. Jose Zagal (University of Santiago de Chile)…

…and thanks to all members of ELAN staff and ELAN guests who contributed to the nice working atmosphere: Nicolas, Dmitrii, Thara, Xingxing, Magda, Christian, Michaela, Lutz, Andrea, Stefanie G, Kiril, Julia, Yvonne, Mauro, Kasia,… Prof. Salim Abdali, Prof. Miklos Gratzl, Prof. Bhavik Patel, Prof. Sergey Schleev, Dr. Juan Jose Carlos Santana, … and all the others…Thanks!

TABLE OF CONTENTS

1. INTRODUCTION – Chemical industry and sustainable development

One of the imperatives of technological development is a sustainable use of resources extracted from the natural environment. One critical aspect, on a global scale, is the generally accepted view for a necessity of constant industrial growth. Irreversible changes generated to the natural environment are evidently beyond measures of control. The main question now is how to provide a sustainable development that will overcome already present elements of ecological disaster [4]. A typical scheme, which illustrates the concept of sustainable development, is given in Figure 1.1.

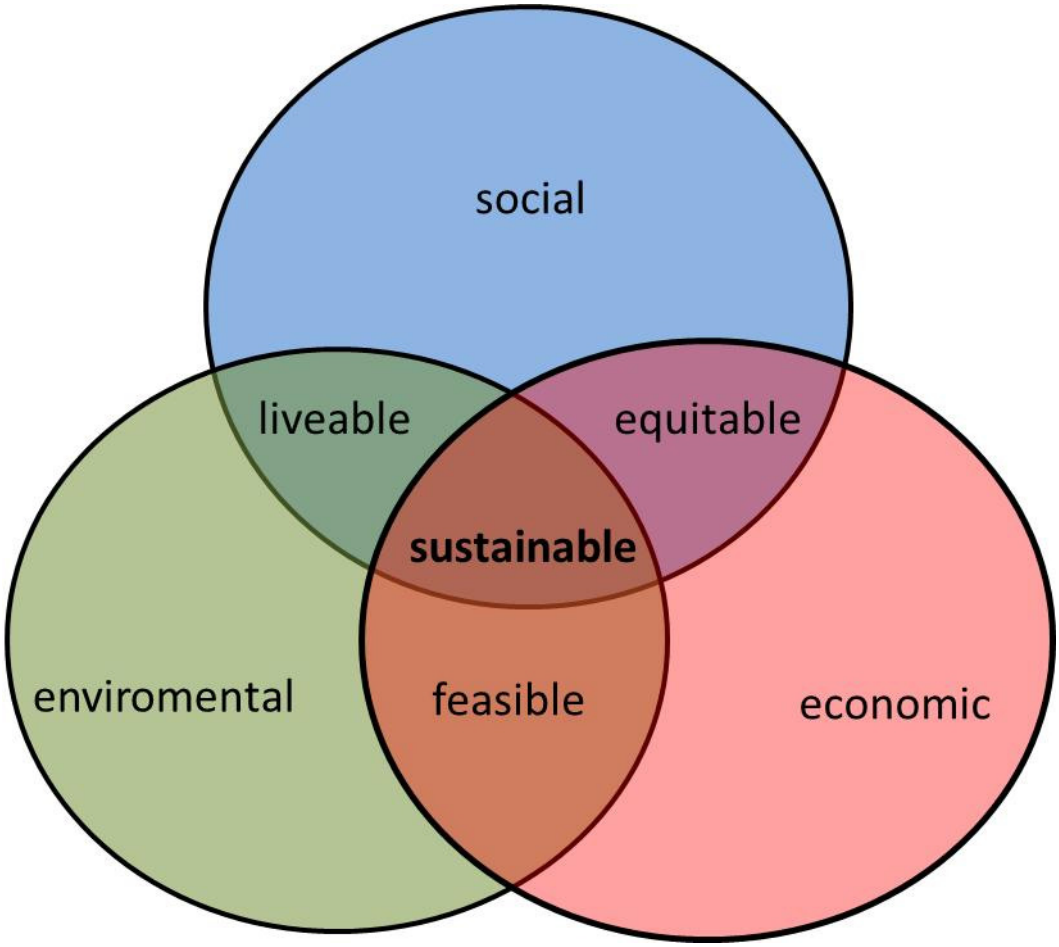

Figure 1.1. Graphical illustration of a concept of sustainable development (based on [5])

A certainly important part of the solution of this *conundrum* are new technological solutions that will either revolutionarily change the industrialized world or at least reduce energy and materials consumption in existing technologies. Reality suggests that new “clean” technologies like solar cells, photo-electrochemical cells, fuel cells… are still far away to become conventional technologies [6], while energy intensive technologies with detrimental effects on the environment are in constant growth [7]. However, even in conventional technologies we face a serious lack of understanding concerning how to improve the overall efficiency of industrial processes [8]. From this perspective, it looks more rational to deal with challenges connected with technologies that are more conventional. Progress in the field of conventional technologies will certainly be a good indicator that accumulated technical and fundamental scientific knowledge is ready to be transferred into the area of “clean” technologies.

In this particular case, the intention is to improve the efficiency of chlorine production, an integral part of chlor-alkali industry. According to official data [7], chlorine as a product is interconnected with more than 50 % of the worldwide turnover in chemical industry. Some of the most important applications of chlorine are: a) the production of a large number of organic chloroderivatives used in processing or producing paper, textiles, paints, dyes, medicines, antiseptics, petrochemicals, pesticides, plastics, foodstuffs, solvents, and other consumer products. b) the use as a disinfectant and bactericide in water treatment and purification. c) the application as oxidizing agent. d) the use as a substituent agent in a number of organic reactions, and e) in making chlorinated lime (bleaching powder) for bleaching fabrics and other substances. Other applications are in food processing; shrink proofing wool; and removal of tin and zinc from iron. Chlorine is used as tracer for studying corrosion of steel by salt water; to determine chloro-substitution mechanisms in organics; and to measure the geological age of meteorites [9].

The overall consumption of electrical energy in chlor-alkali industry is enormously high. Reduction in energy consumption is of high importance not just from from the point of savings in raw materials but also as part of environmental policy. Most of the electrical energy in the world is still produced using fossil fuels and nuclear power plants. By reduction in the consumption of electrical energy less nuclear waste would have to be disposed and the emission of CO_2 could substantially drop. Moreover, increasing the emission of Cl_2 and its derivatives into the atmosphere is one of the main sources of ozone depletion. [10].

However, the chlorine evolution reaction (CER) is considered to be a very good model system for studying of gas evolving reactions. Increasing interest in the oxygen evolution reaction (OER) and the hydrogen evolution reaction (HER), particularly in the field of water electrolysis and photoelectrolysis stimulates efforts in direction of a better general understanding of gas-evolving electrocatalytic reactions. The complexity of these reactions is due to coupling of electrochemistry (electrocatalysis in particular) with surface physics at the electrode/electrolyte interface. In this way, strategies for efficiency improvement require an in depth understanding of the physico-chemical phenomena occurring at the electrode/electrolyte interface.

2. AIM AND SIGNIFICANCE OF THE STUDY – Efficiency of chlorine production

Approaching from a more general overview towards a more precise definition of the goal of the study, one can say that a possible efficiency improvement of the electrolytic Cl_2 production will have multilateral significance.

The continuous expansion of the demand for Cl_2 supply reaches about 65 Mton in 2010 worldwide [11]. In the energy-intensive chlor-alkali process, the most efficient membrane process consumes around 2500 kWh per ton Cl_2, accounting for 50% of the manufacturing

costs [11]. The total European chlorine production was *ca.* 9 Mton where Germany was the main producer with a quota of 43.5% [7].

In Figure 2.1. the growth of chlor-alkali industry in the world through the last four decades is displayed. The turnover increased by more than 350 %.

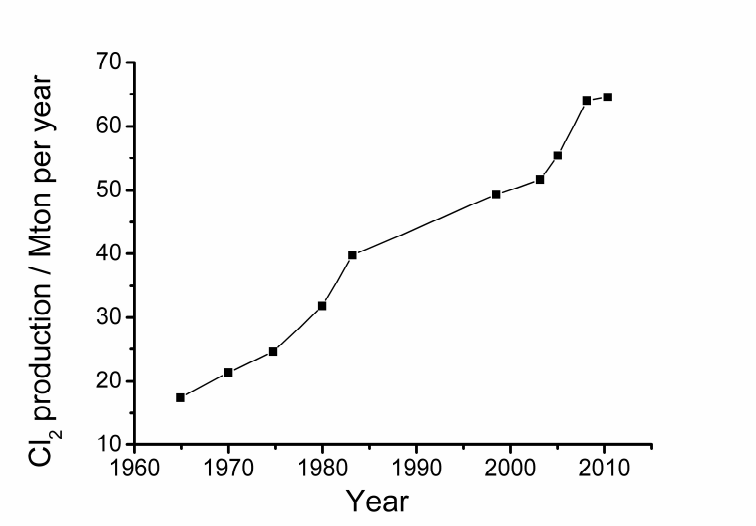

Figure 2.1. Growth of chlorine production during the last 4 decades (data adopted from [12])

From a practical point of view, 1) a reduction in consumption of electrical energy in an electrochemical reactor will decrease overall costs and reduce the pollution of the environment by several means (smaller loss of raw materials from the natural environment, reduced emission of CO_2, drop in the amount of disposed nuclear waste); 2) reduction in the consumption of noble metals, usually used as catalysts (for CER most commonly ruthenium (Ru) is used), or the complete replacement of noble metals, will decrease the overall costs and make industrial production less vulnerable to changes in the price of noble metals. The sensitivity of the market of noble metals is illustrated in Figure 2.2. using Ru as example. From a more fundamental point of view, despite some very impressive chapters considering electrocatalysis and electrochemistry in general are written using CER as model system [13], still a serious lack of general understanding of electrocatalytic reactions is obvious [14]. Moreover, from today's perspective it becomes evident that gas evolving/consuming reactions

will have a dominant place in applied electrochemistry. Hence, an universal point of view on the electrocatalysis with gas reactants/products is more than desirable. Furthermore, despite CER is a two-electron transfer reaction while OER is four electron transfer reaction, experimental activity trends for this two reactions are almost identical on several transition metal-oxides [13]. This is an encouraging perspective which suggests a possible transfer of knowledge from the field of CER to problems of OER.

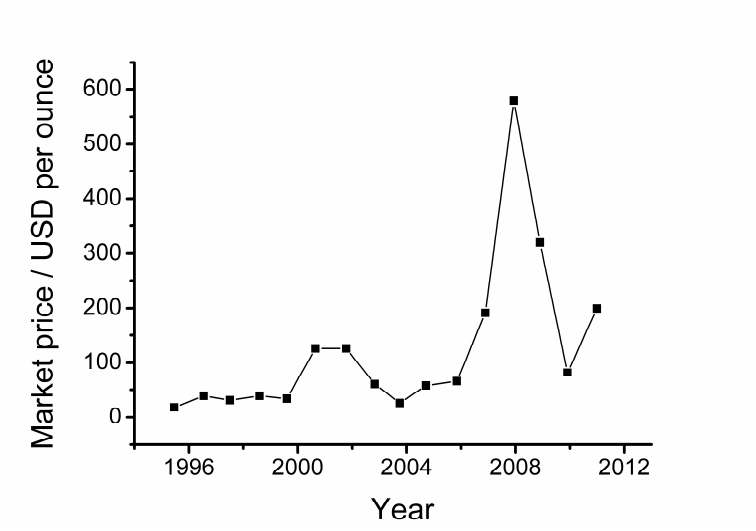

Figure 2.2. Fluctuations of the price of Ru during the last two decades (data adopted from [12])

Based on these considerations, the focus in this study is on expanding of the in-depth knowledge about gas-evolving electrocatalytic reactions, thus shining light on the general understanding of surface science and at the same time being applicable for real industrial problems. In this sense, particular accent is on the development of analytical approaches and techniques that should be part of methodology used in investigation of electrode/electrolyte interface.

3. STATE OF THE ART AND PROBLEM IDENTIFICATION

A central part in the production line in chlor-alkali industry is the electrochemical reactor. A scheme of one electrochemical reactor is given in Figure 3.1.. It is essentially a chemical

reactor in which the anodic oxidation reaction and the cathodic reduction reaction are spatially separated. Electrochemical reactions proceed at the electrode/electrolyte interface, which essentially represents a boundary between an electronic conductor and an ionic conductor. The interface between electrode and electrolyte is called electrochemical double layer and represents the region where electric energy is transformed into chemical energy (or *vice versa*). This is an essential line of differentiation between all other fields of chemistry and electrochemistry. While in chemical reactors energy stored in chemical bonds is transformed into heat, in electrochemical reactors heat production is a consequence of irreversibility, while chemical energy is mainly converted into electricity (*and vice versa*). Worth to mention is that the conversion of electrical to chemical energy is a driven (non-spontaneous) process. A minimal amount of electrical energy which is necessary for electrolysis is defined by the change in Gibbs free energy of the observed reaction. In reality, the amount of electrical energy necessary to drive the process is larger than thermodynamics predicts due to kinetic losses, losses in mass transport, as well as ohmic drops etc. Practically, the goal of all efforts is to reduce the energy consumption in an electrochemical reactor to a value which is as much as possible close to thermodynamical predictions.

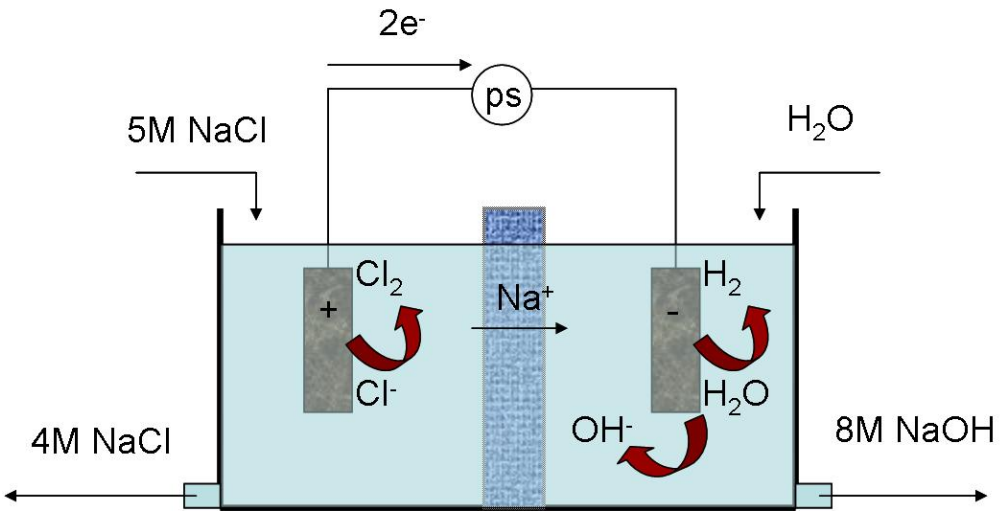

Figure 3.1. Scheme of an electrochemical reactor for NaCl electrolysis. The reactants are NaCl and water and the products are chlorine (at the anode), hydrogen (at the cathode) and sodium hydroxide in the cathode compartment formed in a homogenous chemical reaction

The theoretical part of this thesis will deal in more details with explaining of the exact physical meaning of particular quantities and concepts used in electrochemistry. It is important to remember that the energy efficiency in one electrochemical reactor can be monitored by measuring of the voltage during the electrochemical reaction. All phenomena, which are causing that voltage to be higher than thermodynamical predictions are called sources of overvoltage. In this sense, a first necessary step in the investigation should be to gather information on sources of overvoltage in the electrochemical reactor (or electrolyzer). In Figure 4 an electrochemical reactor for NaCl electrolysis is schematically shown. Despite chlorine can be produced by the Deacon process [12,15-17] based on heterogeneous catalysis and by electrolysis of hydrochloric acid (HCl) [18] the most common way to produce chlorine is NaCl electrolysis. The analysis of available technical data from DeNora [8] illustrates voltage drops in the electrolyzer (Table 3.1.).

Table 3.1. Performance of electrochemical reactors at a current density of 10 kAm^{-2} given for graphite (previously used anode) and DSA (state of the art, so called dimensionally stable anode).

		Graphite	DSA
Anode potential	(V)	1.47	1.37
Cathode potential	(V)	-1.85	-1.85
Anode ohmic drop	(V)	0.15	0.15
Electrolyte ohmic drop	(V)	0.60	0.40
Gas-bubble effect	(V)	0.90	0.13
Current efficiency	(%)	96.00	97.00
Energy consumption	($kWh\ t^{-1}$)	3910	3040

If we analyze carefully the data in Table 3.1., it can be observed that replacing graphite (or carbon based material) with DSA reduced the overvoltage by almost 1V. This was the biggest

known breakthrough in industrial electrochemistry [8,19]. DSA (dimensionally stable anodes) are essentially mixed oxides of transition metals supported by a valve metal. Most commonly, the catalyst layer consists of a mixed oxide (TiO_2+RuO_2) supported with metallic Ti.

Despite the fact that the DSA exhibits obviously superior performance as compared with graphite, it is important to notice that the anode potential (which responds to effect of electrode material on the kinetics of the anode reaction) was reduced by approximately 100 mV i.e. around 10 % of the overall improvement. The new anode design allowed for decrease the distance between anode and membrane what saved additionally 200 mV through the reduction of the overall ohmic drops. However, the largest impact on the overall reduction in overvoltage came from the gas-bubble effect, around 770 mV. Gas-bubble formation in the electrolyte supersaturated with the product is causing that parts of the active surface area is blocked by physical adhesion of the gas phase. Blockage of surface area causes that in a galvanostatic regime the current density is increasing causing an additional overpotential. Finally, the faradaic efficiency is quite high with more than 96 %.

Important to mention is that the analyzed technical data originate from measurements made at a current density of 10 kAm^{-2} with a mercury cathode in a cell, which is today replaced due to ecological and health issues. Nowadays, in membrane technology, the working current density is around 4-5 kAm^{-2}. This suggests that the analysis of the shown technical data has the purpose of an illustration of energy losses, however, it cannot be exact for the presently investigated systems.

The focus of this work was predominantly on weaknesses of the anodic process, what is in agreement with the introductory statement that one of the goals of the work is to transfer knowledge and better understanding of anodic OER. Cathodic reactions, i.e. the hydrogen evolution reaction (HER), although intensively studied [20-32], additionally also requires an efficiency improvement. However, anodic reactions are occupying more attention, simply due to the fact that these reactions proceed at oxidized, reconstructed surfaces, which differs

substantially from the open circuit conditions both in the case of CER and OER. An additional obstacle, considering anodic reactions at oxidized surfaces, is how to justify the application of classical diagnostic criteria of electrode kinetics for their analysis. Focusing on problems of anodic reactions certainly does not diminishes the importance of further analysis of HER, especially in alkaline media [32],. Definitively, some conclusions from the investigation of CER can be applied to HER, also a gas-evolving reaction. In HER like in CER two electrons are exchanged, which suggests that both reactions proceed with the participance of one intermediate [33]. From this point of view choosing CER is seen as an excellent model system for studying of electrocatalytic gas-evolving reactions.

From a formal point of view, an improvement in efficiency of anodic processes at a DSA can be achieved by reducing:

1) the activation overpotential – the impact of the nature of the electrode material on the rate of the electrode reaction (rate of charge transfer, an essential aspect of electrode reactions)
2) ohmic drop in the electrolyte – distance between membrane and anode
3) ohmic drop in the anode – conductivity of semiconductive transition metal-oxides
4) gas-bubble effect coupled with diffusional overpotential – impact of hydrophilicity, surface morphology…

After a detailed literature study (about 400 publications are dealing with DSA for Cl_2 evolution) the following can be concluded:

1) Improvement of intrinsic catalytic properties of the state of the art electrode material remains only as theoretical possibility. a) The activity trend for a significant number of transition-metal oxides is almost identical for OER and CER. b) The kinetics of CER is superior as compared with CER, while OER is thermodynamically more favorable. c) According to the “volcano”-curve (predictive model in electrocatalysis based on the

expression of maximal kinetics as function of an optimal catalytic descriptor) for OER, RuO_2 is the material of choice being at the top of the “volcano”-curve [13].

2) Reducing the distance between anode and membrane is possible if the detachment radius of the gas-bubbles becomes smaller.
3) The ohmic drop in the anode is hard to reduce. Changing of bulk conductivity of the coating is very delicate and not just only because of stability issues. In this particular case, the ohmic drop is already identical to the ohmic drop in previously used graphite electrodes considering that the coating consists of RuO_2 (with almost metallic conductivity) and TiO_2 (semiconductor with large band gap). Due to the tendency to further reduce the loading of RuO_2 as more conductive component, a better conductivity of the anode is hard to achieve.
4) If the chemical composition of the coating is kept unchanged, then hydrophilicity which is considered to be a parameter which can influence gas-bubble detachment remains the same. However, the surface morphology can be changed despite the chemical composition of the coating remains, if adequate synthetic procedures can be applied. Finally, surface morphology can influence mass-transport and reduce diffusion overpotential.

In summary, an in-depth understanding of the properties of a DSA becomes only possible by combining knowledge beyond electrochemistry including aspects from surface physics and chemical engineering. Obviously, a major factor is seen in reducing the size of gas-bubbles which can additionally influence the ohmic drop in the electrolyte by decreasing the distance between the anode and the membrane.

4. THEORETICAL PART

4.1. Energy efficiency in electrochemistry

Energy consumption in an electrochemical reactor is determined by several factors:

1) the thermodynamics of electrode reactions
2) the kinetics of electrode reactions
3) ohmic drops
4) the spatial distribution of overpotentials and the current density

4.1.1. Thermodynamics of electrode reactions

The main relation of electrochemical thermodynamics defines the driving force for an electrode reaction as given in Equation 1:

$$\Delta G_r = -nF(E^o_{rev,c} - E^o_{rev,a}) = -nF\Delta E^o \qquad \textit{Equation 1}$$

where, n is the number of exchanged electrons, F the Faraday's constant (96500 C/mol), $E°_{rev,c}$ and $E°_{rev,a}$ are reversible electrode potentials of the cathodic and anodic reactions, respectively, $\Delta E°$ is the difference in electrode potentials between cathode and anode at standard conditions, and ΔG_r is the Gibbs free energy of the reaction.

The electrode potential conceptually responds to the chemical potential of a half cell in which the electric potential difference at the electrode/electrolyte interface is established. The electrode potential can be understood as an additional degree of freedom in the description of electrochemical systems as compared with chemical systems.

For the equilibrium state, the electrode potential is defined by Nernst's equation. For the electrode Reaction 1:

$aA + ne \rightleftharpoons bB$ *Reaction 1*

the reversible electrode potential is given by Equation 2 :

$$E_{rev}(A|B) = E^{\circ}_{rev}(A|B) - \frac{RT}{nF} \ln \frac{a_i^{\,b}(\mathrm{B})}{a_i^{\,a}(\mathrm{A})} \qquad \textit{Equation 2}$$

where, R is the universal gas constant, T the absolute temperature, A is the reactant, B is the product, a is the stoichiometric coefficient for the reactant, b is the stoichiometric coefficient for the product, a_i are chemical activities. Since thermodynamic considerations are defined for equilibrium conditions a correlation between driving force and equilibrium constant (K) for the electrode Reaction 1 can be established, formally by combining the main relation of electrochemical thermodynamics (Equation 1) and the Nernst equation:

$$\ln K = -\frac{\Delta G_r}{RT} \qquad \textit{Equation 3}$$

The Gibbs free energy of any electrode reaction shows a characteristic temperature dependence (Equation 4):

$$\left(\frac{\partial \Delta_{\mathrm{r}} G}{\partial T}\right)_{\mathrm{p}} = -\Delta_{\mathrm{r}} S \qquad \textit{Equation 4}$$

essentially representing the entropy of the given reaction. The entropy of the electrode reaction can be understood as a temperature coefficient of the electrode potential, suggesting a quite simple procedure for the estimation of the entropy of a reaction in electrochemistry.

The overall change in energy during the chemical reaction or the enthalpy of the reaction is expressed with Equation 5:

$\Delta_r H = \Delta_r G + T\Delta_r S$ *Equation 5*

and represents the sum of the change in Gibbs free energy and the reversible exchanged heat during the reaction.

Based on Equation (1) and Equation (4) one can write (Equation 6):

$$\Delta_r H = -nF\Delta E + nFT\left(\frac{\partial \Delta E}{\partial T}\right)_p$$ *Equation 6*

Finally, the energy efficiency of the electrode reaction is given as ratio of Gibbs free energy of the reaction and enthalpy of the reaction (Equation 7):

$$\varepsilon = \frac{\Delta_r G}{\Delta_r H} = -\frac{nF\Delta E}{\Delta_r H}$$ *Equation 7*

Surprisingly, the energy efficiency of an electrochemical reaction can be more than 100 % [34]. This is certainly not any kind of *perpetuum mobile,* but just a consequence of the existence of reactions with positive temperature coefficient (or negative change in entropy). Despite being rare, such reactions exists such as e.g. the electrochemical oxidation of carbon to carbon-monoxide [34]. Practically, the fundamental limitations of the Carnot cycle do not impose on electrode reactions.

In case of CER

$2Cl^- \rightleftharpoons Cl_2 + 2e^-$ $E°= 1.36$ V/NHE ($t = 25$ °C, $p = 1$ bar, $a(Cl^-) = 1$) Reaction 2

the temperature coefficient of the reaction is estimated to be dE°/dT = -1.248 mV/K using a normal hydrogen electrode (NHE) as reference electrode.

The eversible potential of CER is obtained from the corresponding Nernst equation (Equation 8):

$$E_{rev}(Cl^-/Cl_2) = E^{\circ}_{rev}(Cl^-/Cl_2) + \frac{RT}{nF} ln \frac{f(Cl_2)}{\gamma^2 c^2(Cl^-)}$$ Equation 8

where f(Cl_2) is the fugacity of the chlorine gas (analogue to the activity of solvated species), estimated to be about 1.2 under real industrial conditions; γ is the activity coefficient of the chloride ion which is in 5 M NaCl is 0.803 (at 100°C) or 0.873 (at 25°C).

From Equation 8 and considering the industrial working temperature of around 90°C the reversible potential is approximately 1.24 V /NHE. At a working temperature of around 25°C it is around 1.32 V/NHE.

The correction for the temperature coefficient of the standard electrode potential is made according to Equation 9:

$$E(T) = E°(T°) + \frac{dE}{dT}(T - T°)$$ Equation 9

where T° is the standard temperature.

Following Equations (6), (7) and (9) the theoretical energy efficiency as expressed in Reaction (2) should be around 73 %.

4.1.2. Kinetics of electrode reactions

Opposite to other types of chemical reactions, the rate of an electrochemical reaction can be measured directly due to its proportionality to the current density (Equation 10):

$$v = \frac{j}{nF} \qquad \textit{Equation 10}$$

where *j* is a current density defined by Equation 11:

$$j = I/A \qquad \textit{Equation 11}$$

where *I* the current intensity and *A* the real surface area of the electrode.

The main model of electrode kinetics is known as Butler-Volmer equation (Equation 12):

$$j = j_0 \left\{ \frac{c_s(\mathrm{R})}{c(\mathrm{R})} \exp\left[\frac{(1-\beta) nF \eta_a}{vRT} \right] - \frac{c_s(\mathrm{O})}{c(\mathrm{O})} \exp\left[-\frac{\beta nF \eta_k}{vRT} \right] \right\} \qquad \textit{Equation 12}$$

where j_0 is the exchange current density or rate of reaction in equilibrium, c_s(R) is the surface concentration of the reduced species, c(R) is the concentration of the reduced species in bulk, ß is the symmetry factor of the activation barrier (usually assumed to be around 0.5), v is the stoichiometric number giving the number of repetitions of the rate determining step before the whole reaction proceeds ones, and η is the overpotential of the reaction which essentially represents the difference in the electrode potential. The overpotential is characteristical for some finite kinetics and the reversible electrode potential as given with Equation 13:

$$\eta = E - E_{rev} \qquad \textit{Equation 13}$$

While the electrode potential is considered as an additional degree of freedom that describes the state of electrochemical system at the same time the control of the electrode potential is the most common approach in controlling of the rate of the electrode reaction.

Dependent on different parameters, including concentration gradients in the proximity of the electrode surface or the reversibility of the reaction or the magnitude of the overpotential (known also as polarization), the Butler-Volmer equation can be shown in various forms.

Of particular significance is the so-called Tafel's approximation which is valid for irreversible reactions at overpotentials larger than 100 mV, where it is assumed that the concentration of chemical species at the electrode surface is equal to the concentration in bulk. In the case of an anodic reaction like CER the Tafel's approximation leads to Equation 14:

$$\eta = -\frac{2,3RT}{\alpha_a F}\log j_0 + \frac{2,3RT}{\alpha_a F}\log j_a \qquad \textit{Equation 14}$$

in which α_a is the so-called transfer coefficient defined for an anode reaction as shown in Equation 15:

$$\alpha_a = \frac{(1-\beta)n}{\nu} \qquad \textit{Equation 15}$$

The transfer coefficient can be interpreted as the portion of the overpotential that is really used for changing the activation energy of the observed anodic reaction.

Worth to mention is that the transfer coefficient together with partial orders of the reaction and the stoichiometric number represents typical diagnostic criteria for mechanistic studies of electrode reactions [35].

Equation (14) can be transformed into a more simplified form (Equation 16):

$\eta = a + b \log j_a$ *Equation 16*

where the coefficient *b* is known as Tafel's slope, which has a particular importance in electrode kinetics as parameter for kinetic studies of electrode reactions. In the case of CER it is usually expected that the Tafel's slope is around 40 mV/dec. With Equation 16 a semilogarithmic interdependence between the rate of the electrode reaction (current density) and the driving force (overpotential) can be established.

The overpotential caused by the electrode reaction itself without interference from mass transport limitations is usually called activation overpotential. However, mass transport limitations are present during the electrode reactions. In Equation 12, the significance of the mass transport is implicitly noted. More generally, mass transport limitations represent an additional resistance in a system that should be overcome to sustain a desired rate of the reaction. The presence of a diffusion overpotential leads to the observation that the exponential dependence of the current density from the electrode potential starts to deviate towards linear dependence.

Equation 17 demostrates how the overall current density is dependent from both, the intrinsic kinetic properties and the (usually diffusional) mass transport:

$$\frac{1}{j} = \frac{1}{j_k} + \frac{1}{j_d}$$ *Equation 17*

where j is the measured current, j_k is the kinetic current, and j_d is the diffusional current.

Using 1st Fick's law the diffusional currentcan be expressed as (Equation 18):

$$j = \frac{nFD(c - c_s)}{\delta}$$ *Equation 18*

where D is the diffusion coefficient and δ is the magnitude of the diffusion layer. When the concentration of the reactant at the electrode surface becomes equal zero, Equation 17 is reduced to the diffusional term which is then called diffusion limited current density. The diffusion limited current density has importance in electrochemistry as the maximal current density that can be reached in the system. Besides diffusion, the mass transport in electrochemical cell can be influenced by natural convection (density gradient), forced convection (pressure gradients) or migration (electric field gradients). Generally it is difficult to gain a precise quantitative interpretation of the influence of the mass transport on the overall kinetics due to complicated mathematical models. One of the few well-defined models of mass transport is obtained using a rotating disk electrode (RDE) [36]. The diffusion limited current density at a RDE is given by the Levich equation, in case of linear diffusion (Equation 19):

$$j_d = 0.62nFD^{2/3}\nu^{-1/6}c\omega^{1/2} = Bc\omega^{1/2}$$ *Equation 19*

where v is the kinematic viscosity, ω is the rotation rate, B is the Levich slope. In addition, the diffusion limited current is also well-defined in case of microelectrodes due to the hemispherical diffusion [36] (Equation 20):

$$I = 4nFcDr$$ *Equation 20*

where r is the radius of the microelectrode.

The overpotential caused by diffusional limitations is given as (Equation 21):

$$\eta_{\mathrm{d}} = \frac{RT}{nF} \ln \frac{c_s}{c} = \frac{RT}{nF} \ln\left(1 - \frac{j}{j_{\mathrm{d}}}\right)$$ *Equation 21*

The overpotential at a certain current density is the additional energy that will be consumed during the electrode reaction and it will contribute to the overall potential at the electrode (or voltage in the reactor).

4.1.3. Ohmic drops

Ohmic drops in the electrochemical cell, although not directly part of investigations in electrochemistry, have mayor importance on the overall energy consumption in an electrochemical reactor. Besides ohmic drops in cables, contacts, electrodes itself, etc. of particular importance for CER are ohmic drops in the electrolyte that contains gas-fraction. The ohmic resistance is given by Equation 22 which shows that besides the nature of the resistor the geometry of the electrochemical cell is very important.

$$R = \frac{U}{I} = \rho \frac{l}{S}$$ *Equation 22*

The gas fraction in the electrolyte can decrease the cross section of the ionic conductor (S) but even more importantly the resistivity of the electrolyte (ρ) will be increased [37] as given by Equation 23:

$$\rho = \rho_o (1 - \varepsilon_g)^{-3/2}$$ *Equation 23*

Ohmic drops are in addition to the thermodynamics and kinetics of the reaction the third most important contribution to the overall energy consumption. Consequently, the overall anode

potential will be (Equation 24):

$E_a = E_{a,rev} + \sum\eta + \sum RI$ *Equation 24*

The energy consumed at the anode is given as a function of the electrode potential multiplied by the current intensity in a given period of time (Equation 25):

$W_{an} = E_a I t$ *Equation 25*

This holds analogously for the entire electrochemical reactor, where instead of the anode potential the voltage in the reactor is considered.

From this perspective, it is convenient to express the energy efficiency as the ratio between the reversible potential (or voltage) and the potential (or voltage) at working conditions (Equation 26):

$$\varepsilon = \frac{E_{a,rev}}{E_a}$$ *Equation 26*

Thus, all efforts considering the conversion of electrical energy into chemical energy (and *vice versa*) is to conduct the process as close as possible to equilibrium conditions or as close as possible to the reversible potential.

Besides the reversible potential, which is defined by the thermodynamics of the reaction and represents a reference point for the energy consumption, an important quantity in the analysis of the electrode reactions is open the circuit potential which represents a “close-to-equilibrium” state influenced by the surface properties of the electrode material.

4.1.4. Spatial distribution of overpotential and current density

While electrochemical thermodynamics is the basis for the estimation of the driving force and the energetics of the electrochemical reaction, electrode kinetics predicts how fast the reaction may occur. Predictions of the reaction mechanism based on analysis of the reaction at the molecular scale are defined as microkinetics. Microkinetics combined with the spatial distribution of the (over)potential and current density influenced by transport phenomena, cell design and electrode design leads to a macrokinetic description of an electrochemical reactor [38].

Spatial distribution of the (over)potential and current density can be rigorously mathematically treated in electrochemical engineering, which would be, however, beyond the scope of this thesis. Here, some basic aspects of the distribution of the (over)potential and current density, predominantly at a qualitative level, will be discussed.

Three types of distribution of the (over)potential and current density are usually defined in the literature, classified according to the types of the resistances which are predominant during the reaction:

1) primary - the influence of the ohmic resistance

2) secondary - the influence of the activation overpotential

3) ternary - the influence of the diffusion overpotential

The thernary is the most uniform one, while the primary is the most non-uniform one. A detailed explanation can be found in [35,39]. In general terms, it is desirable to have as much as possible uniformly distributed current density in the electrochemical cell.

The current density distribution can be expressed using a group of dimensionless so-called Wagner numbers (Equation 27):

$$W_a = \frac{d\eta}{dj}\frac{\kappa}{l}$$ *Equation 27*

where $d\eta/dj$ is the polarization resistance, κ is the conductivity of the electrolyte and l is the characteristic length.

A more uniform current density distribution (i.e. a larger Wagner number) will be defined by a 1) smaller characteristic length (depending on the geometry of the cell), a 2) larger conductivity of the electrolyte, and a 3) larger polarization resistance.

A larger polarization resistance can be understood as a tendency opposite to the kinetic requirement to have an as small as possible Tafel's slope. This indicates the reality of macrokinetics where the optimal performance of the electrochemical reactor differs from conclusions of microkinetics.

One aspect that was previously not in the literature is the spatial distribution of the current density as a function of the spatial distribution of the activity or the spatial distribution of active sites on the electrode surface. In this case, it is also intuitively assumed that a more uniform distribution of active sites will promote an increased overall performance [11,40]. However, until now no experimental methodology was proposed to estimate the spatial distribution of catalytic activity.

4.2. Chemistry of Cl_2 evolution reaction

Chlorine is produced during the electrode process via the anodic oxidation of Cl^- given by Reaction 2. The produced molecular chlorine is according to Henry's law dissolved following the equilibrium given by Reaction 3. The amount of dissolved chlorine responds to the partial pressure of chlorine gas above the electrolyte. Dissolved chlorine is further disproportionated according to Reaction 4.

$2Cl^- \rightleftharpoons Cl_2 + 2e^-$		*Reaction 2*
$Cl_{2(g)} \rightleftharpoons Cl_{2(aq)}$	$K_1 = 0.062$	*Reaction 3*
$Cl_{2(aq)} + H_2O \rightleftharpoons H^+_{(aq)} + Cl^-_{(aq)} + HOCl_{(aq)}$	$K_2 = 4.2 \cdot 10^{-4}$	*Reaction 4*

One critical aspect during the anodic Cl_2 evolution is the control of the pH value (see Reaction 4). The optimal pH value should be between 1 and 3 in order to avoid side reactions of a product given by Reactions 5 and 6 which are domination at basic conditions as well as the destruction of the membrane in extreme acidic environment.

$Cl_2 + 2\ NaOH \longrightarrow NaClO + NaCl + H_2O$ *Reaction 5*

$3\ NaClO \longrightarrow NaClO_3 + 2NaCl$ *Reaction 6*

An additional importance of the control of the pH value is reflected by the intensity of oxygen evolution as a side reaction. Oxygen evolution is generally thermodynamically favored as compared with Cl_2 evolution. The reversible potential of oxygen evolution is 1.23 V/NHE and declines 60 mV for each pH unit. Thus, the higher the pH value the more oxygen evolution will be thermodynamically significant.

Three reaction paths [41] have been proposed:

1) The Volmer-Heyrovsky (or Volmer-Tafel) reaction path starts with electrochemical discharging of Cl^- ions under formation of adsorbed species on the surface and continues with electrochemical recombination (or recombination). This reaction path, although accepted by many authors, may not respond to reality because of the significant impact of the pH value on the kinetics (in aqueous solution), that cannot be explained by the shown reactions (Reaction 7 to 9).

$Cl^- \rightleftharpoons Cl_{ads} + e^-$ *Reaction 7*

$Cl_{ads} + Cl^- \longrightarrow Cl_2 + e^-$ *Reaction 8*

$Cl_{ads} + Cl_{ad} \longrightarrow Cl_2$ *Reaction 9*

2) A reaction path that starts with Volmer's elementary step, but then continues with a reaction between the adsorbed chlorine species (Cl_{ad}) and water yielding hypochloric acid that subsequently disproportionates. This reaction path includes the existence of an adsorbed species on the surface but additionally includes the influence of water and can be considered more realistic than the Volmer-Heyrovsky pathway (Reaction 7, 10-11).

$Cl^- \rightleftharpoons Cl_{ads} + e^-$ *Reaction 7*

$Cl_{ads} + H_2O \longrightarrow HClO + H^+ + e^-$ *Reaction 10*

$HClO + H^+ + Cl^- \rightleftharpoons Cl_2 + H_2O$ *Reaction 11*

3) A third reaction path starts with the anodic discharge of water, continues with reaction between Cl^- ions and the formed OH_{ad} species producing hypochloric acid. This reaction also includes an adsorbed species and the influence of the pH value (Reaction 12 - 14).

$H_2O \rightleftharpoons OH_{ad} + H^+ + e^-$ *Reaction 12*

$Cl^- + OH_{ad} \longrightarrow HClO + e^-$ *Reaction 13*

$HClO + H^+ + Cl^- \rightleftharpoons Cl_2 + H_2O$ *Reaction 14*

The existence of an adsorbed species was confirmed by the pseudocapacitance measurements [42], a transient electrochemical method which can provide information on the surface coverage of an adsorbed species. However, pseudocapacitance measurements do not give any information on the nature of the adsorbed species at the surface. Here, two types of adsorbed species, namely Cl_{ad} and OH_{ad} are expected, however, in aqueous solution OH_{ad} and Cl_{ad} cannot be distinguished by pseudocapacitance measurements. Thus, *in situ* spectroscopic techniques have to be employed.

There is a theoretical possibility that Cl_{ad} is a blocking species for CER suggesting reaction path 3 to be more likely in aqueous solutions. This would be a classical example how the solvent can influence kinetics by enabling lower activation energies. Practically, the solvent itself is transformed into an adsorbed species that reacts with a Cl^- ion which can keep partially its solvation sphere. In case of reaction path 2, Cl_{ad} is free of a solvation sphere and it is necessary to remove the solvent from the sites where Cl^- will be adsorbed, what requires additional energy.

While it was previously reported that the Tafel's slope is changing from 40 to 120 mV [43] when approaching very high current densities, it should be possible with a good catalyst to sustain the slope of 40 mV even at very high current densities. Assuming that the rate determining steps (rds) are Reaction 10 and Reaction 13, for pathways (2) and (3), respectively, the effect of pH value on the equilibrium of step (12) could help to distinguish which of these two pathways is more likely. Step (12) is not the rds, but in extremely acidic environment this step can become irreversible and cause the increase of the Tafel slope to 120 mV. This is considered as a sign that reaction (12) was in equilibrium before changing the pH value. In opposite, pathway 2 should be less susceptible to pH changes despite water participates in the reaction.

The most important gas evolving/consuming reactions are inner sphere reactions, in which electron transfer is coupled with adsorption/desorption of intermediates. Resolving of the reaction path certainly can help to learn how to achieve a more efficient adsorption/desorption of intermediates from the electrode surface.

4.3. Transition metal-oxides as gas-evolving electrodes

Electrode reactions like CER, which proceeds in highly corroding environment (pH = 2-3, t = 90°C, the presence of chloride ions, oxygen evolution as a side reaction…) require electrocatalytically active stable materials which can last at minimum for three years. For an

anodic reaction like CER it hence is necessary to utilize oxides as electrode materials. Importantly, some transition metal-oxides like RuO_2 or IrO_2 exhibit almost metallic conductivity [44].

4.3.1. Characteristics of the support material

Pourbaix diagrams [45] are illustrating the corrosion stability at a given pH value and at a given applied potential for the chosen metal. Hence, they are good starting points for choosing of support materials. Despite Pourbaix diagrams are based on pure thermodynamic considerations they are sufficiently reliable in predicting corrosion stability. Support materials for dimensionally stable anodes (DSA) are ususally “valve” metals, most often Ti.

Ti as d^2 metal is covered even in air with a thin oxide film layer which passivates and protect from further corrosion. Ti posseses excellent mechanical stability and high electronic conductivity. Before the deposition of an oxide based catalytic layer it is necessary to remove the passivating layer which would induce a significant ohmic drop. Ti is usually used in a form of a mesh or in form of a chip for model DSA samples. Pretreatment of the Ti-support before coating with the catalyst layer is allowing for modifying structural properties of the catalyst coating.

4.3.2. TiO_2 as a matrix for the catalytically active component

Despite titanium dioxide exists in polymorphal structures (anatase, brookite, rutile) the rutile form is of particular importance in electrocatalysis of CER. Rutile has a tetragonal unit cell, with unit cell parameters of a = 4.584 Å and c = 2.953 Å [46]. The titanium cations are coordinated with 6 oxygen atoms forming an octahedron. The crystal structure of rutile TiO_2 is shown in Figure 4.3.1.. Rutile TiO_2 is a semiconductor with a bandgap of 3 eV. However, it posseses mechanical and chemical stability and hence it can be used as matrix for

catalytically active components such as RuO_2. The catalytically active component has to be in direct contact with the metallic substrate.

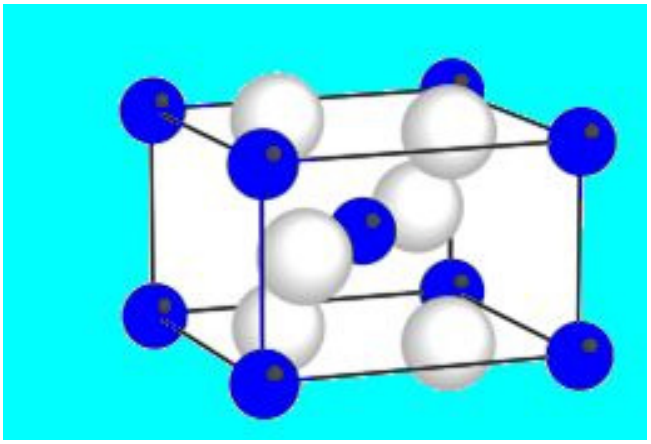

Figure 4.3.1. Scheme of the crystal structure of TiO_2 rutile form; Ti – blue, O -white

4.3.3. RuO_2 as electrocatalyst for CER

RuO_2 also has a rutile type crystal structure similar to TiO_2 with slightly different crystal lattice parameters; a = 4.492 Å and c = 3.100 Å [47]. Strong catalytic activity for some oxidation reactions, including CER, is attributed to the acid-base properties of RuO_2. The hydrated form of RuO_2 can reversibly exchange protons with the aqueous solutions [48]. The reaction is usually written as faradaic process, although the current response in the corresponding cyclic voltammogram resembles a capacitive current (Reaction 15):

$$RuO_x(OH)_y + zH^+ + e^- \rightleftharpoons RuO_{x-z}(OH)_{y+z} \qquad \textit{Reaction 15}$$

Probably the best way to address this phenomenon is a pseudocapacitive behavior, due to the fact that the redox transition is causing changes of the double layer capacitance. Upon deprotonation Cl^- ions start to populate more and more the outer Helmholtz plane of the

double layer. Due to this pseudocapacitive behavior, RuO_2 is known to be an exceptional capacitor [49].

In the past, several catalytic descriptors were employed to explain the quality of electrocatalysts for CER, including [42]:

1) the dissociation energy of the M-Cl bond

2) the d-band vacancy

3) the level of oxidation of the surface during the CER.

Trasatti found an interesting correlation between the potentials for CER and OER at the same current density [13] to qualify oxide-based electrocatalysts. The slope was almost equal one, suggesting that any good electrocatalyst for CER is at the same time a good electrocatalyst for OER and *vice versa*. Trasatti constructed so called “volcano”-curve for OER where RuO_2 was close to the top. As catalytic descriptor the enthalpy for transition of the oxide with the lower oxidation state towards the oxide with the higher oxidation state of the cation was used. This is, essentially a bulk property which optimal value correlated with the maximum of the “volcano” curve. This was not the first time that a bulk property had a good predictable power for intrinsic surface catalytic properties [25], despite some authors [31] still give (maybe unjustified) significance to the surface properties. Considering bulk or surface properties the redox transition from lower towards higher oxidation state of the cation seems to be of mayor importance both for CER and OER. However, an exact interpretation of this phenomenon does not exist. Particularly, it is still not clear how to correlate the obviously necessary redox transition with structural properties of the oxide layer.

4.3.4. Mixed oxides of TiO_2 and RuO_2

Due to the fact that TiO_2 and RuO_2 have similar crystal lattice dimensions mixed oxide films can be easily prepared. Commercial catalyst coatings usually consist of not more than 30

mass. % of RuO_2, while TiO_2 contributes with at least 70 mass. % to the coating. A morphological picture of a typical DSA coating is shown in Figure 4.3.2..

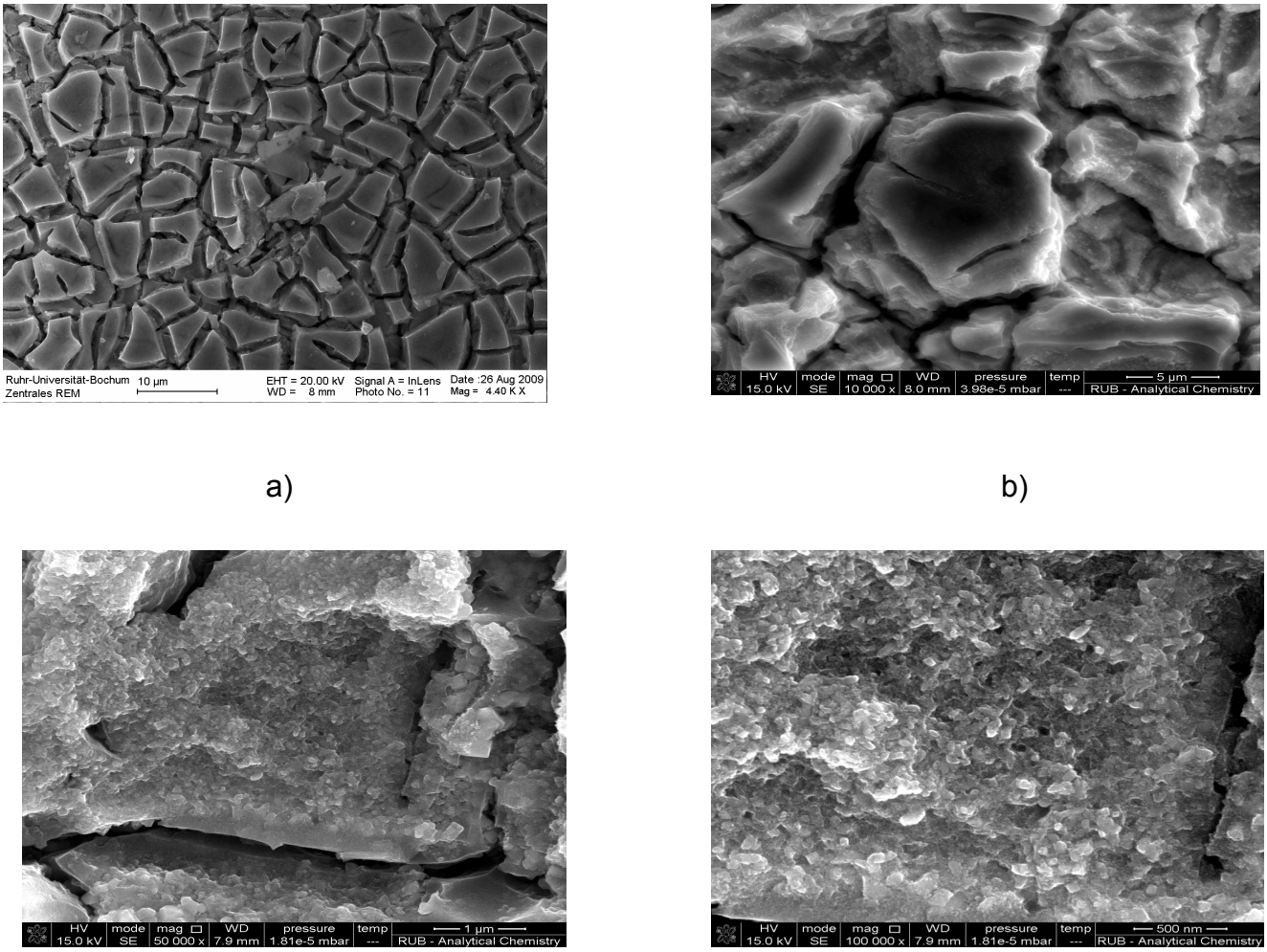

Figure 4.3.2. Morphological images of a standard DSA coating.The “mud-crack” microstructure (a,b) contains nanopores and nanoclusters (c,d)

More than 40 % of RuO_2 cause serious changes in the selectivity promoting intensively OER [43,48]. Despite RuO_2 is known as an excellent catalyst for OER the observed phenomenon of changing selectivity as function of the RuO_2 loading, still cannot be explained. On the other hand, the mass percentage of RuO_2 should not be below 20 % due to the then observed exponential decrease in electronic conductivity of the coating [50]. Percolation [51] is

unavoidable and the RuO_2 clusters must not loose ohmic contact with the Ti support. Even more important, an increase in the Tafel's slope above the expected value of 40 mV/dec is characteristic for coatings with less than 20 % of RuO_2 [50,52,53]. The phase diagram of the binary system TiO_2-RuO_2 [51] reveals that the mixed oxide of TiO_2 and RuO_2 is essentially a solid solution of RuO_2 in TiO_2, where besides the rutile structure the anatase structure is partially present if the calcination temperature was below 900°C. For the preparation of DSA the calcination temperature is usually less than 600°C in order to avoid the growth of TiO_2 at the Ti support which can induce a serious ohmic drop in the anode itself. An additional reason for using temperatures of less than 600 °C is that active surface area, usually expressed as the voltammetric surface charge is reaching a maximum at around 450°C [54].

Practically, the usually obtained coating is a compromise between on one side the highest possible presence of the stable and highly active rutile structure and on the other side the presence of a large number of active sites., An additional limitation for obtaining as much as possible of the rutile crystal is the ohmic drop induced at the support/coating interface by growth of TiO_2.

Most of the oxides used for CER or OER have rutile structure. Some spinels, like Co_3O_4, showed respectable activity however, spinels cannot be used as catalysts for CER due to their instability in acidic environment [55].

From XRD data it is, for example, evident that RuO_2 and Co_3O_4 have significantly different unit cells [47,56] or in other words significantly different crystal lattice parameters. This finding suggest that the lattice constant cannot be the only parameter determining the catalytic performance.

4.3.5. Interface between transition-metal oxides and electrolyte

When an oxide electrode is immersed into the electrolyte, a potential difference is established between the oxide surface and the bulk of the electrolyte due to the difference in chemical

potentials of electrons in the oxide and in the electrolyte species (Cl^- ions and water molecules). The potential of zero charge [57], (E_{pzc}), refers to the potential at which no net charge is located at the electrode surface which at the same time represents the point of the maximal entropy in the double layer.

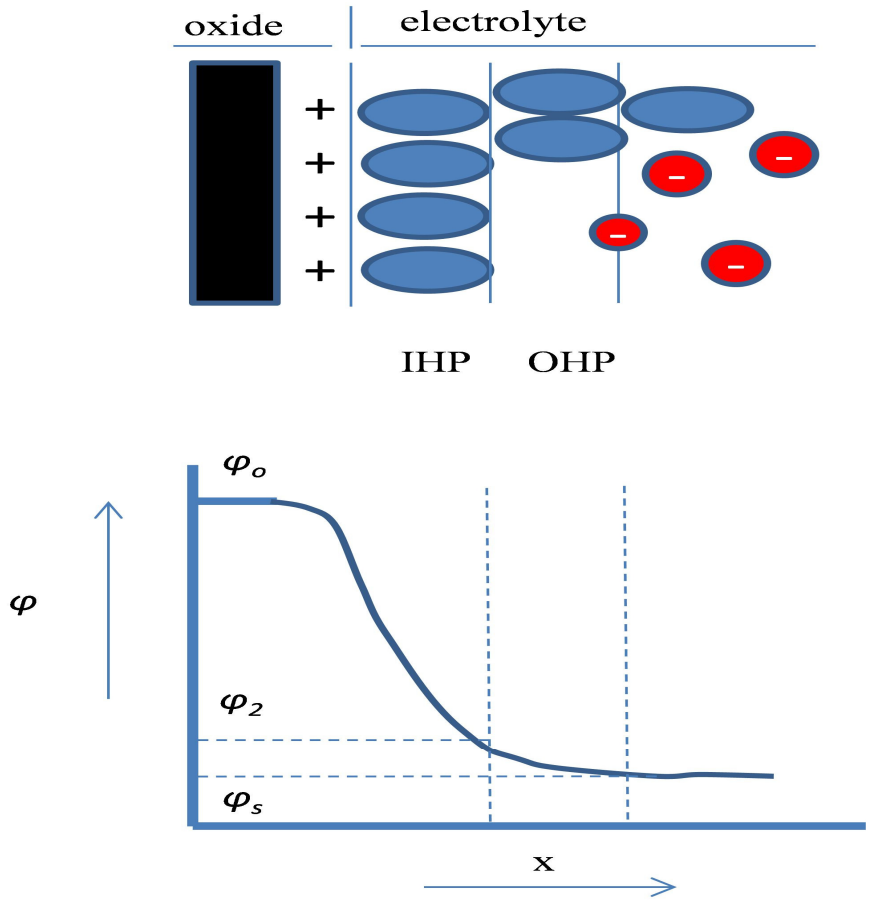

Figure 4.3.3. Scheme of the double layer between oxide electrode and electrolyte in the equilibrium state together with the scheme of potential drop at the interface where φ_o is the potential at the electrode surface , φ_2 is the potential in the inner Helmholtz plane, φ_s *is the* potential at the outer Helmholtz plane. Blue spheres represent solvent molecules oriented with the oxygen atoms towards the electrode surface, while Cl^- ions are marked with red.

At relevant pH values (pH 1-3), the open circuit potential (OCP) is always more positive than E_{pzc}, suggesting that solvent molecules are oriented with the oxygen towards the positively charged surface. Additionally, the positively charged electrode surface increases the

probability that Cl^- ions are adsorbed at the oxide surface. In Figure 7, the double layer between the oxide and water that contains Cl^- ions is schematically depicted. It is intentionally shown that in the inner Helmholtz plane only oriented solvent molecules are located while Cl^- ions are situated in the outer Helmholtz plane. It can be assumed that an additional arrangement of the outer Helmholtz plane or even a penetration of Cl^- ions towards the water dipoles inside the double layer occurs due to the imposed overpotential. Na^+-ions are deliberately not shown in the illustration in Figure 4.3.3. because they do not contribute to the established potential difference. According to a general assumption cations have a stable solvation sphere which can be removed only by polarization at the cathode.Magnitude of the d-band vacancy will determine how intensive the attraction between the water molecules or chloride ions and the electrode surface will be, what will essentially influence the OCP which will probably influence the value of the exchange current density during gas evolution.

4.3.6. Electrocatalysis of CER on rutiles and spinels

Theoretical analysis by Rossmeisl et al. [58] predicts that active centers for CER and OER are coordinately unsaturated sites (CUS). The analysis is based on Pourbaix diagrams of RuO_2 (110) facets in which it can be traced which adsorbed species will dominate at the electrode surface in dependence from the pH value as a function of the electrode potential. It is a reasonable assumption that active centers on the transition metal oxides are favouring both, Cl^- ions oxidation and water discharge. The impact of O_2 evolution during Cl_2 evolution will be determined by the pH value, the electrode potential, the concentration of Cl^- ions and the temperature (Cl_2 evolution exhibits a more negative temperature coefficient of the electrode potential than O_2 evolution [59]). In Figure 4.3.4. the overpotentials of Cl_2 and O_2 evolution for variety of transition metals oxides are shown. As supposed, the trend in activity for both reactions is the same, only the overpotentials are different showing that OER has generally a lower rate.

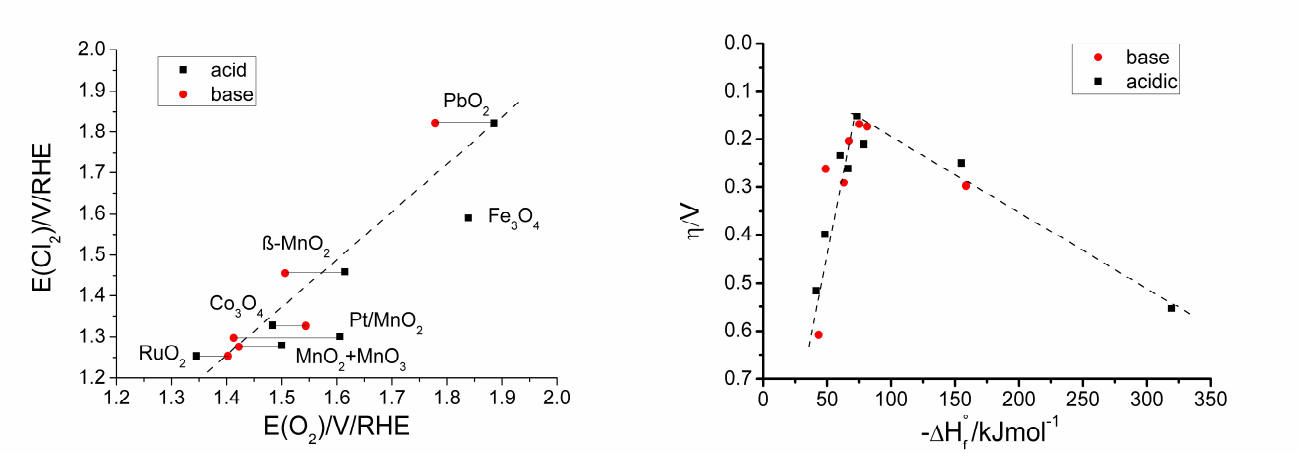

a) b)

Figure 4.3.4. a) Comparison of catalytical activity for CER and OER at a variety of transition metal oxides at the same current density. b) Volcano plot for OER using the enthalpy of the transition from the lower toward the higher oxidation state of the oxide as catalytic descriptor (Figures reploted according to [13])

One important consequence of the Marcus theory [60,61] which is describing outer sphere reactions is that the simultaneous transfer of two electrons requires an activation energy which is four times larger than that of a single electron transfer [33]. Thus, the lower rate of OER as compared with CER can be understood as a consequemce of the higher activation energy in a case of $4e^-$ transfer process (OER) as compared with a $2e^-$ transfer process (CER).

Furthermore, most reaction pathways assumed for OER consider that recombination steps are unavoidable (see Reaction 12 for example):

$H_2O = OH_{ad} + H^+ + e^-$	*(2 times)*	*Reaction 12*
$OH_{ad} = O_{ad} + H^+ + e^-$	*(2 times)*	*Reaction 16*
$O_{ad} + O_{ad} = O_2$		*Reaction 17*

Hence, a sufficiently large spatial separation between active sites can seriously inhibit the rate of OER, while CER remains with the same intrinsic rate because molecules such as Cl_2 can

be produced at one single active site according to the Erenburg pathway [41].

In case of RuO_2 in acidic electrolyte the potential for OER is around 100 mV higher than for CER (Figure 8a). Considering the volcano curve for OER given in Figure 8b it is clear that RuO_2 is at the top with the lowest overpotential of around 150 mV for this reaction. Based on an identical trend in the activity for the different transition metal oxides for OER and CER, the expected volcano curve for CER should be similar, however, with the top of the volcano curve lifted by about 100 mV. A rough estimation is that there are around 50 mV difference between a "state of the art" DSA and the theoretical value from thermodynamics which practically represents the "space" for improvement. The data in Figure 8. are given for a current density of 10 kAm^{-2}. Hence, at 5 kAm^{-2} the overpotential will be between 35 and 40 mV. that the related Tafel slope is around 40 mV opening the perspective to increase the catalytic activity by one order of magnitude.

As previously stated, the number of active sites is counted indirectly using the acid-base properties of RuO_2 [48,62,63] (and some other transition metal-oxides) according to Reactions 15 and 18:

$$RuO_x(OH)_y + zH^+ + e^- \rightleftharpoons RuO_{x-z}(OH)_{y+z} \qquad \textit{Reaction 15}$$

$$RuO_x(OH)_y + zOH^- \rightleftharpoons RuO_{x+z}(OH)_{y-z} + H^+ + e^- \qquad \textit{Reaction 18}$$

which indicate redox transitions from the lower towards the higher oxidation state [64] and *vice versa*. The charge consumed for this reaction during potential cycling in a potential range which corresponds to the thermodynamic stability of the solvent, used for the estimation of the active surface area, is called voltammetric surface charge (q*). There is a correlation between the BET surface and q* [48,62] despite findings obtained with radiotracers that protons can penetrate into the bulk of RuO_2 [65] causing a solid state transition. Also the partial order of

the reaction with respect to q* is equal one [66], what additionally suggesst that q* is proportional to the number of active sites.

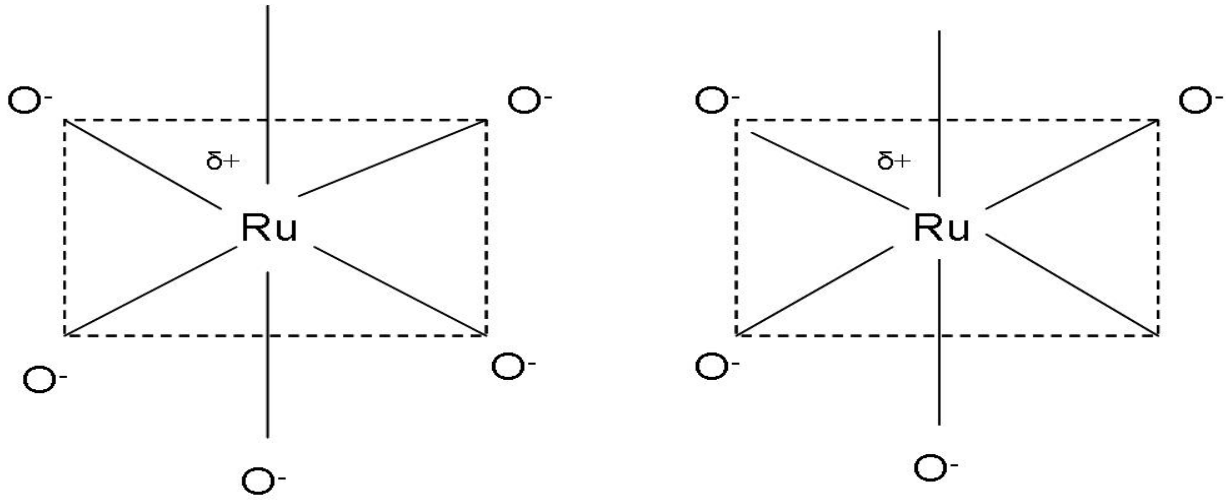

Figure 4.3.5. Schematic interpretation of two different nonstoichiometric rutile structures of RuO_2

Non-stoichiometric oxides which are formed at lower calcination temperatures show a higher activity as compared with stoichiometric oxides which are formed at higher temperatures due to the increase in activation energy of the reaction with the calcination temperature [54]. The structural properties as shown in Figure 4.3.5. suggest that the stoichiometric RuO_2 can exchange more protons with the solution indicated by a higher q* and a higher active surface area. However, this does not seem to be true. Possibly, only unsaturated sites can be (de)protonated and hence contribute to the reaction itself. Increasing the calcination temperature is increasing E_{pzc} [53] due to a particle size effect [67] leading to an concomitant increasing of Tafel's slope [53,54]. Obviously, non-stoichiometric hydrated oxides exhibit better properties concerning the charge transfer resistance and higher surface area, while the stoichiometric oxide exhibits a higher crystalinity and hence probably better adsorption properties manifested by the higher exchange current density. This is based on the assumption that the transfer coefficient and the exchange current density should be inversely proportional despite the opposite was reported before [55]. In case of inner sphere reactions

catalysts with very high current densities, reach full coverage very leading to an increase in the Tafel's slope. A fraction of the activation energy in that case is consumed by adsorption of intermediates, which becomes more difficult due to lateral interactions between adsorbed species. The assumed relation between the transfer coefficient and the exchange current density resembles a relation that exists between the pre-exponential factor and the activation energy in the Arrhenius equation which was previously discussed in the analysis of the oxygen reduction reaction (ORR) [68,69].

In previous works the nature of the relation between the number of active sites and the turnover frequency was discussed [50,66]. The availability of active sites for the reaction can be strongly influenced by the morphology and at the atomic level by the specific structure of crystal lattice, which is important also for gas-bubble detachment. Hence, conclusions of electrocatalysis will overlap with conclusions of surface physics.

Basic kinetic considerations in case of inner sphere reactions are based on the application of an adsorption isotherm for defining of a rate law. The Langmuir isotherm is usually applied in case of low coverage (close to zero) or high coverage (close to unity) with the main assumption that lateral interactions between adsorbed species can be neglected [35]. In case of middle coverage Frumkin's isotherm is usually employed that includes interaction parameters [35]. A specially important form of Frumkin's isotherm is Temkin's isotherm for which a linear dependence between electrode potential and coverage exists in a range of $0.2<\theta<0.8$ [35]. As previously stated, the coverage depends strongly on the exchange current density. A high exchange current density causes full coverage for low overpotentials increasing the Tafel's slope. The highest exchange current densities and lowest Tafel's slopes (30 mV/dec) which are following the Volmer-Tafel's pathway are characteristic for catalysts containing a transition metal cation with filled t_{2g} orbitals or half filled t_{2g} orbitals and partially filled e_g orbitals such as Ti/PtO_2, Pt/MnO_2, $LaNiO_3$, $La_{0.6}Sr_{0.4}CoO_3$ while less active and more stable catalysts (RuO_2 or IrO_2) have partially filled t_{2g} orbitals and empty e_g orbitals

and follow the Volmer-Heyrovsky reaction path with a Tafel's slope of around 40 mV/dec [70]. The former catalysts keep the value of the Tafel' slope even at high current densities. Obviously, the number of electrons in the e_g orbitals defines the overall activity, while at the same time it is assumed that activation energy is a linear function of the energy difference between the conduction band of the solid and the energy level of the adsorbed intermediates like Cl_{ad} [71]. Recently it was claimed for perovskites in the case of OER [72,73] that the occupancy of the e_g orbitals has a dominant role in activity. This new findings should be analyzed in a light of well known experimental results from Bockris showing that the activity of perovskites is correlated with number of d-electrons [55] and in light of theoretical predictions based on DFT [74] with the difference in the free binding energy between O_{ad} and OH_{ad} used as catalytic descriptor.

On technically relevant electrodes the Volmer-Heyrovsky reaction path was usually considered due to the typical Tafel slope of around 40 mV/dec. While many authors still accept this pathway [33,75-77] we will show that this pathway does not fulfills the experimental diagnostic criteria. Reaction 7 shows the Volmer's step in which an adsorbed species is formed during the electron transfer reaction defined by the rate constant k_1.

$$Cl^- \xrightarrow{k1} Cl_{ad} + e^- \qquad \textit{Reaction 7}$$

If this step is rate determining than the rate law is given by Equation 28:

$$j_1 = n F k_1 c(Cl^-)(1-\theta)\exp(\beta FE/RT) \qquad \textit{Equation 28}$$

suggesting a coverage of close to zero. The theoretical slope of the Tafel plot describing this case is 118 mV/dec. The rate law can be transformed according to Equation 29:

$j_1 = nFk_1c(Cl^-)exp\ (ßFE/RT)$ $\theta \rightarrow 0$ $b = 120\ mV/dec$ *Equation 29*

If the Volmer's step has a considerably higher rate than the Heyrovsky's step, the Volmer's step can be considered to be in equilibrium. In this case, the rate of forward and backward reactions is the same as given by Equation 30:

$k_1c(Cl^-)(1-\theta)exp\ (ßFE/RT) = k_{-1}\theta exp(-(1-ß)EF/RT)$ *Equation 30*

in which the equilibrium constant is defined as in Equation 31:

$K_1 = k_1/k^{-1}$ *Equation 31*

According to Languimir the surface coverage can be expressed as shown in Equation 32:

$$\frac{\theta}{1-\theta} = Kc(Cl^-)\exp(\frac{FE}{RT})$$ *Equation 32*

The disappearance of the symmetry factor is not only a consequence of the mathematical transformation, but has a physical meaning. The symmetry factor is a pure kinetic parameter and cannot exist in equilibrium [78].

Reaction 8 shows the Heyrovsky step in which the formation of the Cl_2 molecule is coupled with the transfer of a second electron, which is defined by the rate constant k_2.

$$Cl^- + Cl_{ad} \xrightarrow{k2} Cl_2 + e^-$$ *Reaction 8*

This step can be understood as an electrochemical desorption which rate is defined by Equation 33:

$j_2 = Fk_2c(Cl^-)\theta exp(ßFE/RT)$ *Equation 33*

If the coverage is low which is the case at low current densities Equation 34 can be derived from Equations 32 and 33.

$j_2 = nFk_2K_1c^2(Cl^-)\ exp((ß+1)FE/RT)$ $\theta<<1$ *Equation 34*

The theoretical Tafel slope would be 40 mV/dec. However, if the coverage reaches unity, than the current density is given by Equation 35 with a theoretical Tafel slope of 118 mV/dec.

$j_2 = Fk_2c(Cl^-)exp(ßFE/RT)$ *Equation 35*

Analyzing the experimentally derived diagnostic criteria for CER [66,79] one can conclude that the Volmer-Heyrovsky pathway cannot be correct because the partial order of reaction with respect to $[Cl^-]$ is one and the Tafel's slope is 40 mV/dec. In case of the Volmer-Heyrovsky pathway and assuming that the transfer of the second electron is the *rds*, the Tafel's slope is 40 mV/dec for low coverage but the partial order of the reaction with respect to $[Cl^-]$ has to be 2. The partial order of the reaction with respect to $[Cl^-]$ is one at full coverage, however, in this case the Tafel's slope has to be 120 mV/dec. Even if we disregard any impact of the pH value on the kinetics of CER (partial order in respect to $[H^+]$ is -1) the experimental diagnostic criteria suggest that another reaction pathway is necessary for the description of CER.

A Tafel slope of 120 mV/dec will appear if discharging of the Cl^- ion is the rds which is typical for a regime at high current densities or if the electrochemical (or chemical) recombination is rate determining at high coverage. The coverage can be derived from pseudocapacitance

measurements [80] providing a basis for concluding at the *rds*. Moreover, if the rate constant stays constant after a change of the Tafel's slope, one can conclude that the Heyrovsky step is controlling the rate of reaction while only the coverage is changing. The previously mentioned catalysts with partially filled e_g orbitals show Tafel's slope changes from 30 to 120 mV/dec at current densities which are lower than those typically used under industrial conditions probably due to the fact that full coverage was reached rather than a sluggish electroadsorption. This class of catalysts requires two active sites for recombination, while catalysts with empty e_g orbitals and a Tafel's slope of 40 mV/dec requires only one active site for recombination. The remaining question is why the reaction proceeds through electrochemical recombination (directly influenced by the electrode potential) on a catalysts with empty e_g orbitals and through chemical recombination (with indirect influence of electrode potential) in case of catalysts with half-filled e_g orbitals .

Discussing the Tafel's slope as an intensive catalytic property necessarily leads to observations from fundamental investigations at single crystals. Essentially, today's fundamental understanding of electrocatalysis is based on the analysis of characteristic crystal facets, which usually appear also in a polycristaline material. The assumption is that through analysis of the properties of single crystals one is able to easily distinguish electronic from geometric effects in electrocatalysis, and at the same time "deconstruct" the behavior of a polycrystalline material as a function of the behavior of the related single crystals. This approach has serious weaknesses e.g. when comparing the behavior of polycrystalline RuO_2 to single crystals of RuO_2. In fact all relevant single crystal facets of RuO_2 exhibit Tafel'slope for OER in acidic media of minimum 60 mV/dec, while for polycrystalline RuO_2 a slope of less than 40 mV/dec is obtained [81]. Obviously, polycrystalline materials have properties that cannot be derived form the properties of the individual properties of the crystallites and the exposed facets. This property is considered to be a synergy effect and points out that the

Tafel's slope is a result of a certain crystal structure, what opens a variety of possibilities in searching for a new catalysts.

The crystal lattice of the oxide (or metal) should have properties to ensure that the necessary recombination in case of CER or OER (or dissociative adsorption in a case of ORR) does not require a too high activation energy. However, it is difficult to comprehend why parameters of the crystal lattice should be important in case of a catalysts at which electrochemical recombination is catalyzed which proceeds at a single active site.

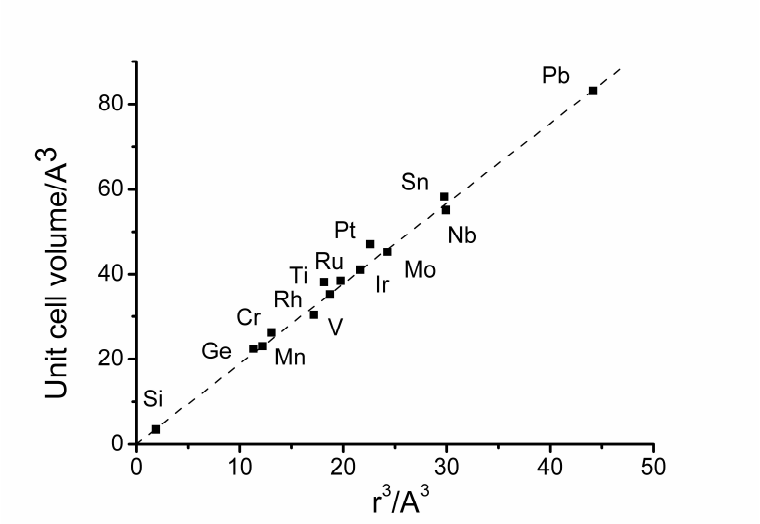

Figure 4.3.6. Unit cell volume as a function of effective ionic volume for several metal oxides with rutile structure. (reploted using data from [82])

TiO_2 and RuO_2 have very similar parameters of the crystal lattice [82] while the intrinsic activity for CER or OER is very low for TiO_2 and at the same time RuO_2 is the best known catalyst for both reactions (Figure 4.3.6.). This is a strong indication that in case of rutiles and for reactions which follow a reaction path based on electrochemical recombination the crystal structure cannot be taken as a criteria for the catalytic activity. Thus, changing of parameters of the crystal lattice [40,83,84] for modifying the selectivity of catalysts is considered to be fundamentally problematic approach. Particularly, it is hard to explain why for example Co_3O_4 has a slightly lower (but comparable) activity than RuO_2 even when the crystal lattice parameters are substantially different [47,56]. This strongly suggests that other properties of

the catalysts are governing the electrocatalytic reactions.

4.4. Weaknesses of conventional electrochemical characterization

The conventional approach for the electrochemical characterization of gas evolving electrodes is based on a sequence of experimental steps [85]:

1) recording the galvanostatic polarization curve from equilibrium conditions towards the technically relevant current density (around 5 kAm^{-2}) with controled hydrodynamics of the system (usually RDE)

2) estimation of the ohmic resistance using impedance spectroscopy or current interruption technique

3) extraction of kinetic parameters (Tafel's slope and exchange current density) from the polarization curve corrected for ohmic drops

Recording of the polarization curve with imposed convective flow of the electrolyte should eliminate concentration gradients near the electrode surface. At a sufficiently high rotation rate of the RDE kinetic control of the reaction can be sustained while the diffusional overpotentials are minimized. However, the mathematical model of RDE experiments is only valid for flat electrodes [35], a fact which is often disregarded without any explanation. Instead of the expected laminar flow, turbulences at the surface are unavoidable [86]. In literature the weaknesses of RDE and rotating ring disc electrode (RRDE) experiments are demonstrated by comparing the number of electrons exchanged during oxygen reduction reaction (ORR) estimated in parallel by RRDE and scanning electrochemical microscopy (SECM) [86]. Errors in kinetic analysis induced by the roughness of the electrode in the RDE or RRDE setup can be severe.

Furthermore, the ohmic drop correction should be conducted incrementally, for each single applied overpotential. This is necessary because the ohmic resistance depends on the gas fraction in the electrolyte which is a function of the overpotential. This is technically very

problematic for current interruption technique. Using electrochemical impedance spectroscopy (EIS), it is possible to monitor ohmic resistance as a function of overpotential, however, the scatter in the data may be significant.

Most problematic is the fact that the correction for the ohmic drop, that can be several hundreds of mV, should reveal an improvement in the performance of the anode reaction that is on a scale of several tens of milivolts. For example, the reversible potential for CER is 1.12 V vs. Ag/AgCl, while the measured potential during the reaction including ohmic drop is about 2 V vs. Ag/AgCl. After ohmic drop correction, the potential is 1.2 V vs. Ag/AgCl suggesting an overpotential of about 80 mV. In order to really observe an improvement of the catalyst on a scale of several tens of milivolts, one has to subtract an ohmic drop of around 800 mV. Thus, an error in estimation of the ohmic resistance of only a few percents would yield a significant error in the estimation of the anode potential and hence give a misleading picture about a possible improvement of the catalyst performance. The accuracy of the measurements could be improved if the ohmic resistance was reduced by positioning of a reference electrode close to the electrode surface using e.g. a Luggin capillary [35]. However, taking into considerations that gas bubbles may block the reference electrode and hence may cause a significant interference with the faradaic current signal, the reference electrode has to be positioned far away from the sample, thus being protected from the intensive gas evolution that unavoidably induces a significant ohmic drop.

Consequently, the extraction of the Tafel's slope for the region of technically relevant current densities (1-13 kA m^{-2} [87]) is not reliable if the ohmic drop correction is not reproducible. Additionally, exchange current densities are a function of time due to the variation of the gas fraction at the electrode surface but also due to the oxidation and reconstruction of the surface during the CER or OER.

Taking all this into account, a conceptually different approach to the characterization of the gas-evolving reactions (GER) is proposed in this thesis.

4.5. Conceptual framework and research approach

The conceptual framework in this work is focusing on three main points:

a) the introduction of new analytical approaches that will provide better insight into the performance of GER

b) providing a better fundamental understanding of electrocatalysis and

c) improving the efficiency of CER and OER.

The proposed approach is based on the application of:

1) stationary electrochemical techniques (potentiometry, amperometry…) for establishing trends in overall activity and energy consumption.

2) transient electrochemical techniques (CV, chronopotentiometry, chronoamperometry, EIS…) for estimation of the electrochemically active surface area, the double layer capacitance , adsorption phenomena etc.

3) *ex situ* UHV microscopic and spectroscopic techniques (SEM, EDX…) for morphology studies and studies of surface composition

4) *in situ* microscopic and spectroscopic techniques (AFM, SECM, Raman…) for topography studies, conductivity studies, local activity studies, insight into the nature of electrocatalytic activity

5. EXPERIMENTAL SECTION

Experimental techniques are:

1) electrochemical techniques (CV, amperometry…)

2) *ex situ* UHV microscopic and spectroscopic techniques (SEM, EDX…)

3) *in situ* microscopic and spectroscopic techniques (AFM, cAFM, Raman spectroscopy…)

5.1. Description of the setup for electrochemical measurements

Two configurations of electrochemical cells were used. A three-electrode system for standard electrochemical measurements and a four-electrode system for local electrochemical measurements. In some cases the four electrode setup was adjusted for standard electrochemical measurements as three electrode setup, while in some cases, for example in case of RDE measurements, it was necessary to use an electrochemical cell with a completely different design. While the setup for RDE measurements used for classical kinetic analysis is described in literature [35,36] we focused on establishing relations between local and global properties of a catalyst layer. Therefore, scanning electrochemical microscopy (SECM) was used for studying electrode kinetics. An example of a SECM setup is shown in Figure 5.1.

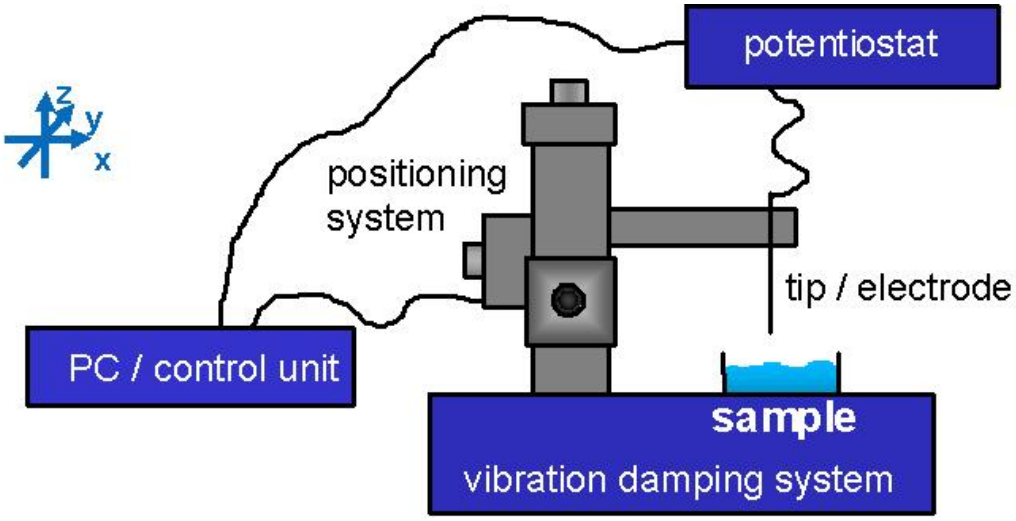

Figure 5.1.. Scheme of a SECM measuring setup (thanks to Sensolytics)

Integral parts of the setup are the electrochemical cell, a potentiostat, the positioning system, a vibration damping system and the PC control unit. The electrochemical cell consisted of four electrodes, namely two working electrodes (sample and a microelectrode tip), a reference electrode and a counter electrode. In dependence from the experiment, different electrolytes were used usually at a temperature of 25°C.

5.1.1. Chemicals

As a redox mediator 5 mM ferrocenemethanol (97 % $C_{11}H_{12}FeO$, Aldrich, Steinheim, Germany) in 0.1 M KCl (95 %, Riedel de Häen, Seelze, Germany) was used. To a 5 M NaCl (99.5 %, J.T. Baker, Deventer, Netherlands) solution HCl (37-38%, J.T. Baker, Deventer, Netherlands) was added until a pH value of 2 was reached. As a chloride-free reference electrolyte a solution of 5 M $NaNO_3$ was used which was prepared from anhydrous $NaNO_3$ (98-100 %, J.T. Baker, Deventer, Netherlands) and addition of HNO_3 (65% J.T. Baker, Deventer, The Netherlands) until a pH value of 2 was reached. All solutions were prepared with deionized water (SG Ultra Clear UV, Barsbüttel, Germany).

5.1.2. Electrodes

The investigated samples were DSA (RuO_2+TiO_2)/Ti disks with a diameter of d = 1.5 cm provided by Bayer MaterialScience AG, Leverkusen, Germany. The diameter 'd_s' of the sample, which was exposed to the electrolyte during analysis, was 0.5 cm. SECM tips were homemade Pt disk microelectrodes with a diameter of 25 µm. Cyclic voltammetry was carried out to verify the diameter of the microelectrode using the value of the diffusion limited current in a redox mediator containing electrolyte which is proportional to the radius of the microelectrode. The reference electrodes were homemade Ag/AgCl/3M KCl electrodes (0.207 V/NHE). All potentials are referred to this reference potential. The counter electrode was a Pt mesh. Before each measurement the microelectrodes were polished with 0.3 µm alumina

paste, sonicated and rinsed with acetone and water. All Pt wires, Pt mesh and Ag wires were provided by Goodfellow (Bad Nauheim, Germany).

5.1.3. Instrumentation

The electrodes were controlled potentiostatically by a bipotentiostat/galvanostat (Jaissle PG 100, Waiblingen, Germany). The position of the tip in the x,y,z directions was controlled by a stepper motor integrated into a SECM (Sensolytics, Bochum, Germany) with HighRes and shearforce options. Increments in x- and y- directions were 10 µm at a speed of 25 μms^{-1}. Ohmic drops were determined using electrochemical impedance spectroscopy at a frequency of 100 kHz using a Gamry Reference 600 potentiostat/galvanostat with an in-built impedance analyzer. Data processing was carried out using OriginPro8G (OriginLab, Northampton MA, USA) and Mira (G. Wittstock, Oldenburg) software.

5.2. Electrochemical characterization

5.2.1. Cyclic voltammetry

Cyclic voltammetry (CV) [36] was used fortesting of the diameter of the fabricated microelectrodes. According to Equation 20 there is a proportionality between the geometry of a microelectrode and the magnitude of current. Using a redox mediators like ferocene-methanol, CV is conducted between potentials of -0.200 and 600 mV /(Ag/AgCl/3M KCl). The steady state current is a function of the diameter of the microelectrode. CV was also applied for the determination of the potentials of Cl_2 evolution/reduction at the working electrodes. The potentials of Cl_2 evolution/reduction at a Pt microelectrode and Cl_2 reduction at the DSA were determined by analyzing the peak currents, while potentials for CER were chosen in a wide range. CV was used for the estimation of the voltammetric surface charge as an analogue of the electrochemically active surface area. The potential was cycled from -0.150 to +0.500 mV/(Ag/AgCl/3M KCl) at a scan rate of 20 mV/s in an acidified solution of NaCl. Moreover, the

level of oxidation of the surface during the CER was determined by means of CV at concentrations of 1, 2, 3 and 4 M NaCl adjusted to a pH value of 2 using HCl and controlling the ionic strength using $NaNO_3$ and the pretreatment of the DSA samples was performed by potential cycling [88] until the voltammograms showed became reproducible.

5.2.2. Chronoamperometry and chronopotentiometry

Besides CV, chronoamperometry [36] was used in this study.The feedback mode of SECM [89] was used for recording tip approach curves for pre-positioning of the SECM tip at a defined distance 'h' of 20 µm from the sample surface. Chronoamperometry at constant potentials was applied to study Cl_2 production and Cl_2 detection. The activities of the samples were determined from the amperometric responses during potentiostatic polarization of the samples at 1400 mV/(Ag/AgCl/3M KCl) while for Cl_2 detection at the SECM tip potential pulses to 950 mV were applied for 0.1 s and the current at the tip was monitored at a frequency of 100 Hz.

Potentiometry [36] was used for a comparative analysis representative for industrial conditions. The experiments were performed using a 3.5 M NaCl electrolyte solution at a pH of 3 using galvanostatic polarization of 5 kAm^{-2} at 55°C.

5.2.3. Linear sweep voltammetry and RDE measurements

Linear sweep voltammetry (LSV) [36] using a RDE setup [36] was employed for standard stationary kinetic analysis. The potential was swept with sweep rate of 5mV/s from OCP to a potential value leading to a current density of approximately 5 kAm^{-2}. Alternatively, the current density was swept from the equilibrium state towards 5 kAm^{-2}. Ohmic drop correction was performed incrementally in order to improve the validity of the obtained kinetic data [85]. Tafel's slopes were estimated for several coatings of interest. Diffusional limitations are minimized using rotation.

5.2.4. Electrochemical impedance spectroscopy

Electrochemical impedance spectroscopy [36] was utilized to estimate predominantly the ohmic resistance in the electrochemical cell at a frequency of 100 kHz which is a prerequisite for the ohmic drop correction of polarization curves recorded with LSV aiming on a for more reliable estimation of the corresponding Tafel' slope. The capacitance of the double layer together with the charge transfer resistance was analysed as a function of applied current density at a frequency of 5 kHz. The sinusoidal perturbation was 10 mV_{pp}. Measurements were performed using a potentiostat/galvanostat with an in-built impedance analyzer.

5.2.5. Local electrochemical measurements

For spatially resolved local electrochemical measurements scanning electrochemical microscopy (SECM) was employed. A modified Sensolytics (Bochum, Germany) SECM set-up was used. The local activity of the prepared electrodes for CER was visualized by performing SECM using a sample generation-tip collection mode [89] and a redox competition mode [90]. Samples with a working area of 15 mm in diameter were used for the measurement. The geometric area of the sample was defined with an O-ring to a diameter of 5 mm. The SECM tip current can be correlated with the catalytic activity of the sample underneath the tip. The tip (Pt microelectrode, 25 µm) was scanned usually over an area of 300 × 300 μm^2 in constant-height mode (tip-to-sample distance of about 20 µm). The sample was polarized at a potential of 1.4 V vs. Ag/AgCl (3M KCl) for the production of Cl_2 by oxidation of Cl^-. The Pt-tip was polarized at a potential of 0.95 V vs. Ag/AgCl/3M KCl to detect the produced Cl_2 or at a potential of 1.4 V vs. Ag/AgCl (3 M KCl) to sense the depletion in the concentration of Cl^- ions. Increments in the x- and y- directions were 10 µm at a speed of 10 µm/s for a scanned area of 300x300 μm^2. For a survey scan over an area of 1000x1000 μm^2, the increments in the x- and y-directions were both 25 µm at a speed of 25 µm/s. The redox competition (RC) mode was additionally used to investigate local equilibriums at chosen

catalyst spots. The sample was polarized at potentials in intervals from 1.3 to 2.0 V vs. Ag/AgCl, while the tip potential was 1.4 vs. Ag/AgCl. The electrolyte was 5M NaCl (pH 2). SECM measurements were carried out at room temperature.

For a more precise visualization of the local catalytic activity in the light of morphological features, imaging of the local catalyst activity was done at a tip-to-sample distance of approximately 1 µm with a Pt disk microelectrode (1 µm diameter). The scanned area of the catalyst was 25 x 25 μm^2. Increments in the x- and y-directions were 0.5 µm.

For local electrochemical measurements by means of SECM the experimental protocol implies electrode testing using CV as denoted in Figure 5.2.1a and the approach to the sample surface as shown in Figure 5.2.1b.

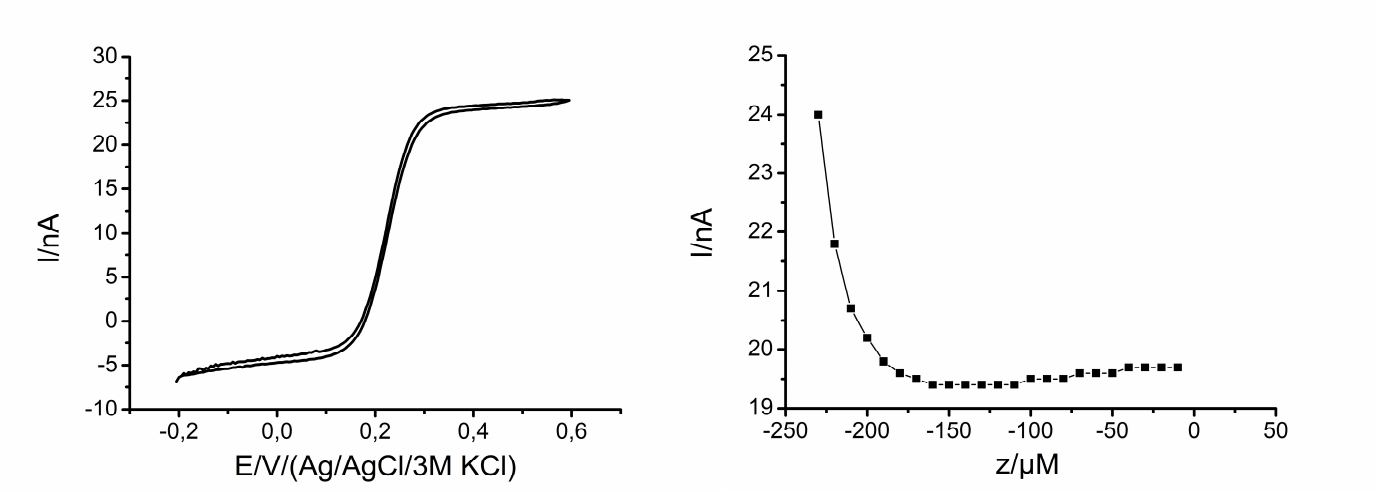

a) b)

Figure 5.2.1.. a) microelectrode testing in a redox mediator by means of CV, b) approach curve to the sample surface

A sigmoidal shape of the CV in an electrolyte containing a redox mediator (feroccene-methanol) with well defined plateau that originates from the diffusional limited current is an indicator of correlation between geometry (diameter) of the microelectrode and the current signal. In Figure 5.2.1a a microelectrode tip with 25 µm shows a current of approximately 25 nA. Approaching to an electrochemically active surface leads to an increase in the current

signal at the tip, while in the case of an approach towards an electrochemically inactive surface the measured tip-current is decreasing. The principle of the feedback mode of SECM used for the approach to a surface is illustrated in Figure 5.2.2.

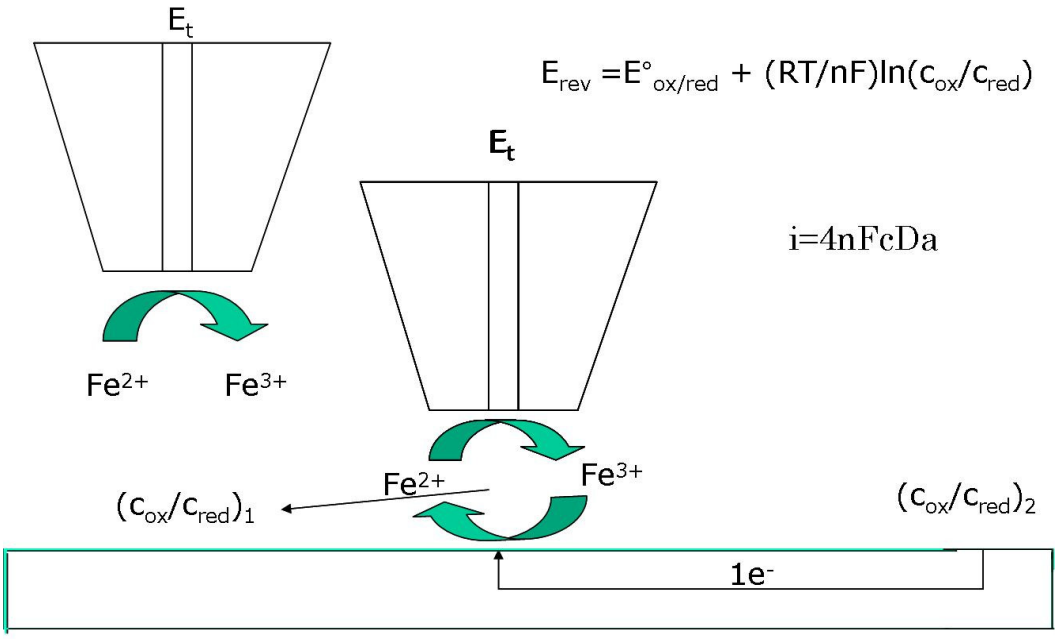

Figure 5.2.2. The feedback mode of SECM. A locally generated equilibrium constant induces a local electrode potential and allows electron flow between the area beneath the tip and area close to the tip.

During the approach of the SECM tip to the surface in feedback mode the sample is not polarized. After approach to the surface the electrolyte containing the redox mediator is replaced with the working electrolyte.

5.3. *Ex situ* UHV microscopic and spectroscopic characterization

5.3.1. Scanning electron microscopy (SEM)

Scanning electron microscopy (SEM) micrographs together with energy dispersive X-ray spectroscopy (EDX) for elemental analysis were recorded using a LEO Gemini 1530 instrument (Zeiss, Weimar, Germany). Insight into morphology at micro- and nano-scale was obtained together with an estimation of the surface composition.

5.3.2. Energy dispersive X ray spectroscopy (EDX) mapping

Spatially resolved EDX mapping was performed using FEI ESEM Dual Beam Quanta 3D FEG electron microscope equipped with an EDX-system (EDAX Genesis XM2i). The spatially resolved surface composition was obtained as a function of morphological features. The analysis was conducted before and after intensively producing Cl_2 with the intention to localizing regions that are subject to corrosion.

5.4. *In situ* microscopic and spectroscopic techniques

5.4.1. Atomic force microscopy (AFM)

AFM images were recorded in air using Si tips (µ-Masch, Estonia) with an ExplorerTM AFM (Topometrix) and TMX 2000 controller (Topometrix) and with a NanoWizard III (JPK, Berlin, Germany) in intermittent contact mode using a silicon cantilever type Acta (N-type, ~340 kHz, ~40 N/m) from AppNano (Santa Clara, CA, USA). Conductive AFM was performed using the JPK cAFM module and cAFM cantilevers provided by JPK (Pt coated, ~40 N/m) in intermittent mode. AFM micropgraphs provide an insight into the spatial distribution of electronic conductivity as a function of morphological features.

5.4.2. Raman spectroscopy

Raman spectroscopy measurements were performed using a Jobin-Yvon iHR550 spectrometer (Horiba, Germany) equipped with a TE cooled charge device. The excitation was achieved with a laser MPC 6000, Model Ventus LP (Laser Quantum Ltd. UK) using a wavelength of 532 mm. The typical laser power was around 10 mW. Experiments were conducted in air and in electrolyte where the potential at the working electrode was controlled by µAutolabIII/Fra2 potentiostat/galvanostat (Metrohm, Herisau, Switzerland). Measurements were performed at 25°C.

5.4.3. Differential electrochemical mass spectroscopy (DEMS)

DEMS measurements were performed at TU Berlin. A mass spectrometer with an integrated gas analytic system OmniStar GSD 301 C (Pfeiffer Vacuum, Asslar Germany), mass range 1-300 amu, was used. A quartz capillary with an inner/outer diameter of 150/220 µm was connected to the gas outlet of the electrochemical cell. A two compartment cell was used with a separate counter electrode (Pt mesh) chamber with pH control and a working electrode chamber (rotating disk electrode, diameter of 15 mm, RuO_2 based DSA).

Measurements were conducted at 25°C with a flow of 100 ml/min N_2 through the working electrode chamber, at pH 3 and electrolyte concentrations of 1, 2, 3 and 4 mol/dm^{-3} NaCl. The reference electrode was a reversible hydrogen electrode (RHE) which was separated from the working electrode chamber via a Haber-Lugin capillary. Calibration of the mass spectrometer with N_2 (100 ml/min), O_2 (50 ml/min) and Cl_2 (50 ml/min) was done using mass flow controllers.

5.4.4. Video imaging of chlorine gas-bubble evolution

Observation of evolving gas-bubbles was carried out at room temperature by using a glass beaker as reaction vessel containing 100 mL 3.5 M NaCl (pH 3) as electrolyte. The working electrode plate with an exposed surface area of 1.76 cm^2 was vertically aligned, immersed in the stagnant electrolyte and polarized galvanostatically at 20 mA cm^{-2}. A CCD camera opposite to the electrode surface was used to image electrolytically generated Cl_2 bubbles. A cold light source was used to illuminate the electrode surface.

6. RESULTS AND DISCUSSION

6.1. Morphology-activity relations

6.1.1. Interplay of morphology and active surface area

It is usually assumed that a catalyst layer with a dense packing of active sites and fast electrode kinetics should guarantee high overall performance, very often overlooking the importance of the accessibility of the active sites. It is, however, perceived that the morphology of a catalyst layer should influence the availability of its active sites during gas evolution. In fact, little attention has been devoted to understanding morphological properties of DSA and their impact on activity.

The intriguing behavior of DSA observed at very high current densities, around 40 kAm^{-2}, suggest possible means for their improvement. Particularly interesting is the phenomenon of "self-acceleration" observed during the chlorine evolution reaction (CER) at DSA. It was proposed that in a regime of very high current densities, the inner parts of the coating start to participate in the reaction due to increased convective flow of the electrolyte in the pores. The arising question is whether it is possible to activate the inner parts of the catalyst coating at a relatively lower constant current density by manipulating certain morphological features.

The activities of four different samples of dimensionally stable anodes (DSA) for the Cl_2 evolution reaction (CER) were analyzed and compared in respect to their geometric properties. The samples were made from the same catalyst material, following a preparation method in which variations in morphological features of the prepared oxide electrodes (mixed oxides of TiO_2 and RuO_2 supported on Ti) were due to changes in the amount of tensile stress delivered to each sample [91]. Samples differ from each other due to the different conditions of breaking of the catalyst layer. Breakage of the catalyst layer or "crack" formation is caused by the thermally induced tensile stress. The volume change of the formed oxide layer during the thermal processing is influenced by the underlying substrate. Once the developed stresses exceed the tensile strength of the formed oxide, cracks develop to relieve the stress.

A different amount of tensile stresses was delivered to each of the coatings by changing the thickness of the deposited catalyst layer [91], but also by pretreatment of the Ti support in direction of changing of coefficient of thermal expansion. The minimum thickness of the coating for observation of this kind of effect was reported to be 0.2 μm [92,93].

Considering the fact that the coatings were prepared from the same material and by the similar preparation procedure, classical diagnostic criteria of electrode kinetics, such as Tafel's slope and exchange current density, were not sufficient for a comparative study. For example, the Tafel's slope for all samples was confirmed in separate experiments to be close to 40 mV/dec, which is the expected value for the standard DSA coatings. Obviously, for the same catalyst loading with almost identical chemical composition differences in activity cannot be exclusively attributed to classical electrocatalytic factors. Geometric effects such as morphology and active surface area are therefore most probably responsible for the eventual discrepancy in the activity of the samples. The influence of geometric factors on the overall activity is usually manifested through more or less effective mass transport, whose investigation can be achieved by analyzing the amperometric response of the samples. Comparative analysis of overall activities was conducted using potentiostatic polarization at low overpotentials. There are three main reasons for using this kind of approach: 1) on the basis of a fundamental kinetic analysis the relative activity is often expressed as current density measured at a fixed electrode potential; 2) intensive gas evolution at high current densities can have an effect on the reference electrode and thus lead to false information about the performance of the coating; 3) the approach used for determining the turnover frequency can only be applied by using potentiostatic measurements.

Comparison of potentiostatic polarization curves of the DSA samples at a fixed potential was the initial step in probing the efficiency of electrolytic Cl_2 evolution. Evidently, the samples manifested different activities as shown in Figure 6.1.a.

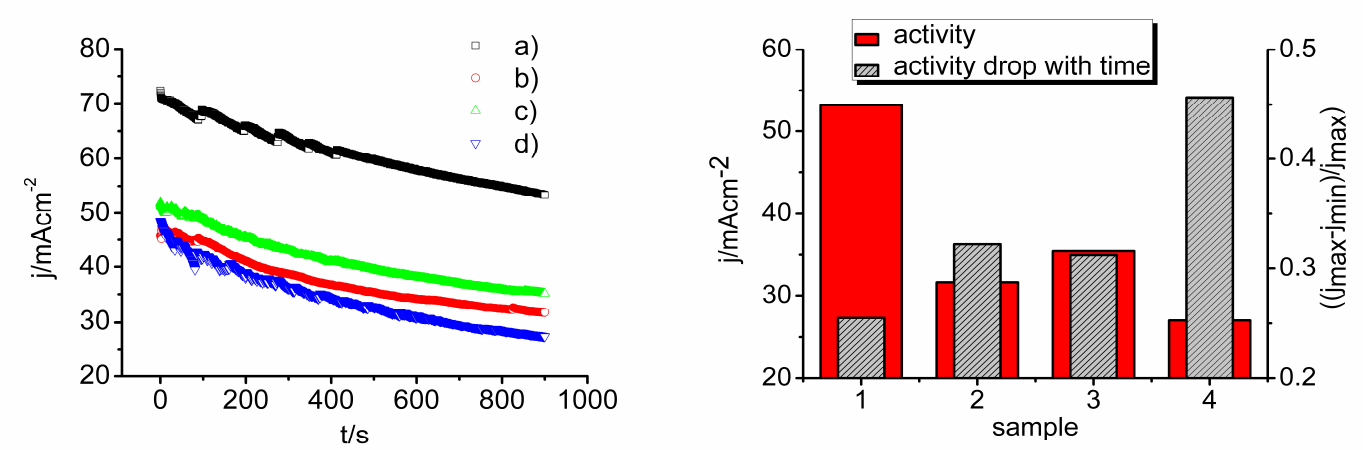

a) b)

Figure 6.1. a) Chronoamperometric measurements of DSA samples (A = 0.196 cm^{-2}; E = 1400 mV; 3.5 M NaCl; pH = 3). Sample 1-black cubes, Sample 2-red circles, Sample 3-green triangles, Sample 4-blue inversed triangles. b) Bar graphs of pseudo-stationary current density (red bars) and loss of activity with time (grey bars).

The first inference arising from this observation is that the state of the surface is not reproducible with regard to either its active surface area, and/or its chemical composition. EDX analysis confirmed almost identical chemical composition:.the mass percentage of Ru is 23.6% (sample 1), 26.7 % (sample 2), 27.4 % (sample 3) and 23.4 % (sample 4). This was reasonable to expect due to the fact that the same nominal loading of ruthenium was used for preparation of all the 4 catalyst coatings. However, during the synthesis it is almost impossible to completely faultlessly reproduce the state of the surface. From this point of view, it was necessary to find a rational approach to normalize activity measurements for the influence of active surface area.

Further, the nonstationary behavior of the recorded current over time is noticeable. The measured ohmic resistances and capacitances of the samples were about 15 Ω and 150 μF, respectively. This implies that discharging of the double layer should happen within approximately 10 ms. Since Cl_2 is generated from a highly concentrated electrolyte, a diffusional limitation of the product is expected as a consequence of its accumulation in the

proximity of the electrode surface. The diffusional overpotential coupled with the “gas-bubble effect” is causing the loss of active surface area due to the produced Cl_2 gas which is masking active spots and thus introduces a decline in activity that can be more than 40 % with respect to the initial value of the current density. It was observed that the current density (calculated with respect to geometric surface area) measured after 900 s in the pseudostationary regime of the potentiostatic measurements, was a suitable representative indicator for the overall activity of each sample. Additionally, the drop in current density between the initial and final times of the measurement was recorded and expressed as a relative change. The general understanding of electrode reactions suggests that geometric regions of an electrode with a higher product turnover should suffer more from transport limitations. Surprisingly, the opposite was observed in this study. The bar graphs of current density and drop in current density with time shown in Figure 6.1b revealed that the activity of the samples is inversely proportional to the loss of activity with time. This may be interpreted as a consequence of significant density gradients caused by gas accumulation near the electrode surface. Supersaturation of the electrolyte near the electrode surface with the produced Cl_2 and gas formation is realistic even at relatively low current densities [94]. The sample with the highest active surface area (the highest density of active spots for the investigated geometric region) should produce more gas per unit of geometric surface area which results in higher density gradients, increased natural convection of the electrolyte and improved penetration of the electrolyte towards the active spots.

Evidently, in order to clarify possible reasons for the distinct behaviour of the DSA samples it was necessary to estimate the electrochemically active surface area. The concept of voltammetric surface charge (q*) was applied, which is based on the acidic-basic properties of RuO_2 manifested through its capability to reversibly exchange protons with the electrolyte as shown above (Reaction 15).

The potential was cycled between -0.15 and 0.5 V, a potential range in which (de)protonation should be the only prevalent process. The influence of Cl^- ions in this region can be excluded as confirmed by cyclic voltammetry (Figure 6.2a). Although it was previously reported that Cl^- ions can be specifically adsorbed on RuO_2 and influence its surface chemistry by changing the potential of zero charge [95], it is shown in Figure 6.2a that the concentration of Cl^- ions does not significantly affect the value of the voltammetric surface charge as assumed by Burke et al. [64].

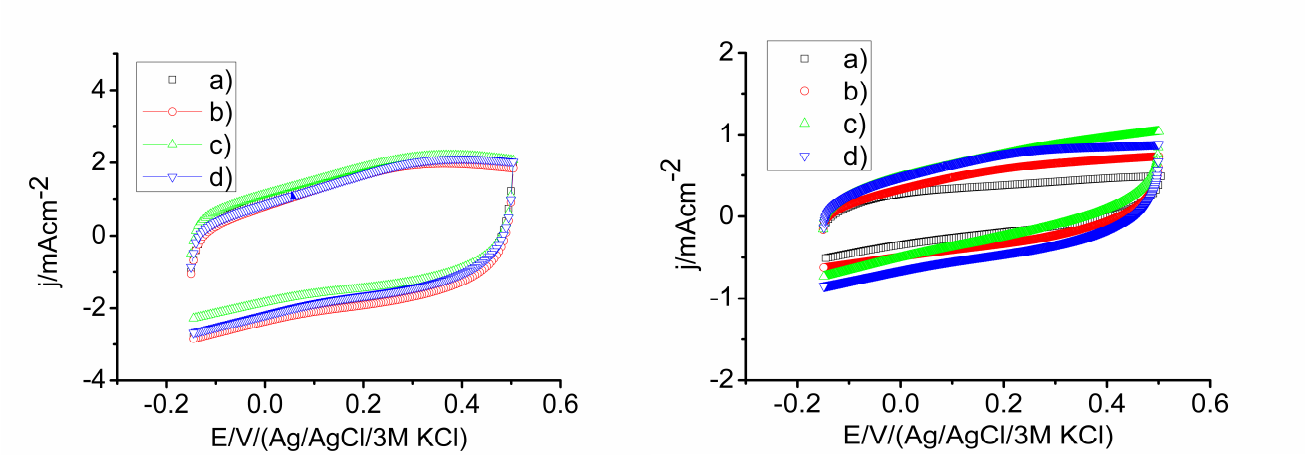

a) b)

Figure 6.2. a) Voltammetric surface charge of a DSA sample for different concentrations of Cl^- ions (a,b,c,d correspond to 1, 2, 3, 4 M NaCl, respectively) at a constant pH value of 2. The ionic strength was adjusted using $NaNO_3$. Scan rate = 100 mVs^{-1}. b) Voltammetric surface charge of the four different DSA samples under identical conditions at a concentration of 3.5 M NaCl, pH 3, scan rate of 20 mVs^{-1}.

For different concentrations of Cl^- ions at a constant pH value, the integrated areas under the cyclic voltammogram were almost identical. This was a clear sign that despite the possibility for specific adsorption of Cl^- ions on RuO_2, protons are essentially the only relevant ions for indirectly determining the number of active sites.

The values of q* should be considered as being mere approximations because the scan rate and the potential range were arbitrarily chosen. The real value of q* should be independent of the scan rate. A method for estimation of the real value q* has been proposed [96,97] but it is

not definitive [98] and requires additional studies. Nevertheless, the approach is justifiable since the sole intention was to observe trends in the properties of the different catalytic layers. Figure 6.2b shows the cyclic voltammograms from which the voltammetric surface charges of the four samples were estimated according to Equation 6.1.1:

$$q^* = INT/(2vA_{geo}) \qquad \textit{Equation 6.1.1.}$$

where, A_{geo} is the geometric surface area of the sample, INT is integrated area of the cyclic voltammogram and v is the scan rate.

It is evident that the samples have different active surface areas and therefore different numbers of active sites although the trend is opposite from what was expected. It seems that the sample with the largest number of active sites exhibits the lowest activity and suffers the highest loss of activity with time. This is a clear indication that additional parameters influence mass transport and finally the overall activity.

Furthermore, the current density was normalized with respect to the voltammetric surface charge. In this way, any differences in activity caused by differences in the magnitude of the active surface area are eliminated. From the ratio of current density and voltammetric surface charge, an estimate of the turnover frequency (TOF) is obtained which is essentially the charge that passes through all the active sites in unit time divided by the charge needed to cover all the active sites with a monolayer of adsorbed species.

Analysis of the gathered data revealed that the trends for the voltammetric surface charge (1<2<3<4) and turnover frequency (1>2>3>4) are inversely proportional. This can be interpreted as a consequence of an inefficient usage of the available surface area. The effectiveness of the active surface area of DSA has been a subject of investigation in only a few studies [99-101]. As the active surface area becomes larger it seems that the accessibility of active sites becomes more difficult. In order to understand the geometrical features

responsible for variations in the accessibility of active sites, the analysis was focused on morphological features of the catalyst layers. The correlation between morphology and resistivity is already known [102], but the relationship between the morphology of DSA and mass transport is still not clearly established.

Scanning electron microscopy (SEM) as shown in Figure 6.3 was employed representing an area of approximately 300x300 μm^2 at a magnification scale of 10000, where typical morphological features can be observed.

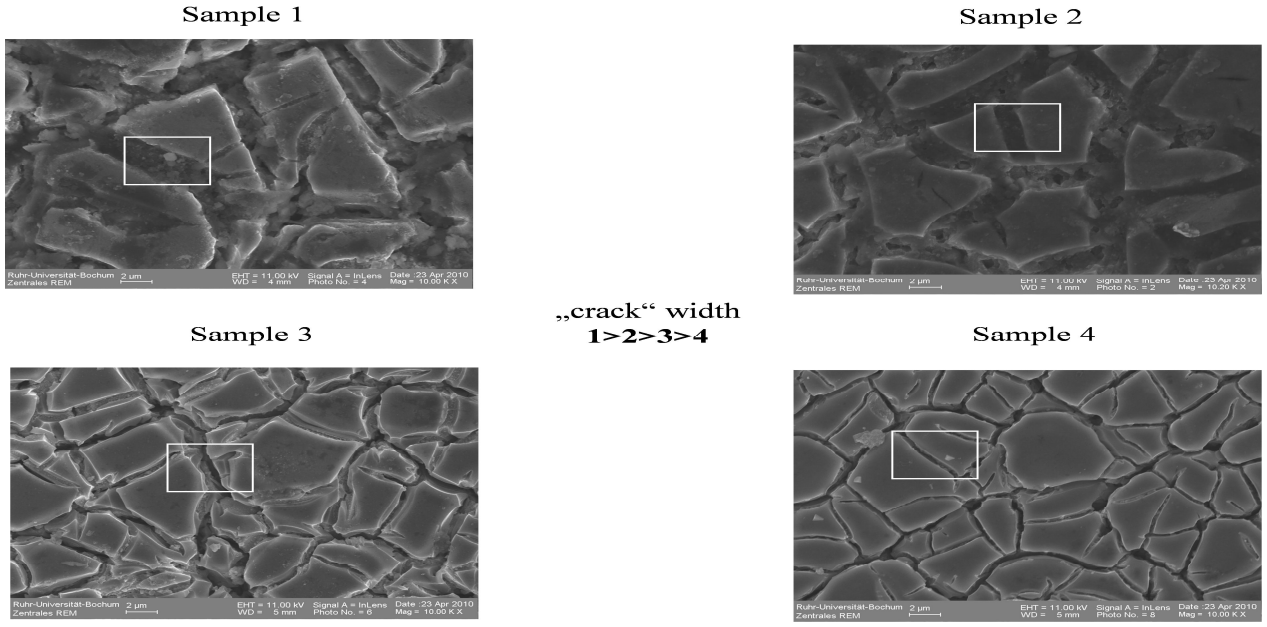

Figure 6.3. SEM micrographs of the DSA samples. The size of the “cracks” was estimated in an area of 300x300 μm^2 (magnification 10000). For the samples 1, 2, 3, 4 the “cracks” have average widths of 2, 1.6, 1, 0.5 µm, respectively.

The so-called “mud-crack” structure reveals that the surface of DSA samples is composed of “islands” and “channels” (or “cracks”). The average size of the “islands” is not easy to estimate, but the size of the “cracks” is characteristically different for each of the samples. In this case, the size of the “cracks” can be regarded as a sort of porosity whose sizes influence mass transfer into the inner parts of the catalyst layer. It was possible to estimate the average widths of the “cracks” for each sample from the micrographs shown in Figure 6.3. For the samples tested in this study, the width decreased in the order 1>2>3>4, which was exactly

similar to the trend observed for the turnover frequency and inversely proportional to the voltammetric surface charge. Inverse proportionality between voltammetric surface charge and turnover frequency was also observed for “crack-free” electrodes (shown in chapter 6.5). The results of the analysis are summarized in Table 6.1.

Table 6.1. Values of voltammetric surface charge, current density, turnover frequency and “crack width” for the DSA samples 1, 2, 3 and 4.

sample	q*/mCcm^{-2}	j/mAcm^{-2}	v/Hz	d/μm
1	9.5	53.6	5.7	2.0
2	13.7	31.6	2.3	1.6
3	16.6	35.7	2.2	1.0
4	18.4	27.6	1.5	0.5

It is rational to construct graphically correlations between activity, active surface area and morphological features. The activity and active surface area which are expressed by means of turnover frequency and voltammetric surface charge, respectively, were obtained from electrochemical measurements and expressed as functions of the widths of the “cracks”. In this way, it was possible to establish clear morphology/activity correlations, which should contribute to a better understanding of the performance of DSA.

Figure 6.4 shows current density, turnover frequency and voltammetric surface charge plotted as function of “crack” widths, which essentially expresses how morphological features influence the overall performance of DSA coatings.

The current density that is an absolute parameter for the overall activity follows a trend which is very similar to that of the turnover frequency. With increasing “crack” widths, the voltammetric surface charge decreases, which generally affects the performance of the DSA negatively. However, the turnover frequency increases with increasing “crack” widths more rapidly than the rate at which the voltammetric surface charge decreases.

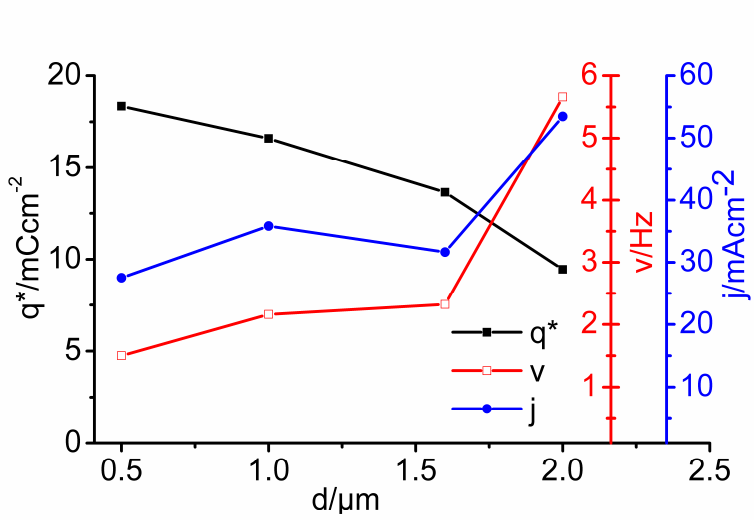

Figure 6.4. Voltammetric surface charge (black cubes), turnover frequency (red empty cubes) and current density (blue circles) as functions of "crack" width.

In summary, the overall activity of DSA is more affected by an increase in the turnover frequency than by a decrease of the active surface area, which suggests that it would be desirable to additionally increase the "crack" widths. Whereas the trend for the variation of the turnover frequency with "crack" width was the same for all samples and inverse to the trend for the voltammetric surface charge, in the trend for the overall activity, samples 2 and 3 exchanged their positions. Considering the fact that the measured ohmic drop of all four samples at a fixed distance of 1 cm between the reference electrode and the working electrode was about 15 Ω, the discrepancies observed above may be attributed to differences in spatial distribution of activity.

According to the general principles of electrode kinetics, a decrease in the number of active sites should lead to a proportionate decrease in current density (calculated with respect to the geometric surface area). However, the opposite was observed in this study. It is hence apparent that the widths of the "cracks" determine the availability of the surface area for the reaction. One of the most important aspects for effective utilization of DSA is the necessity for effective transport of the electrolyte to the active sites. It is reasonable to argue that due to the density gradient caused by the produced Cl_2 gas, the electrolyte is transported into "cracks"

more or less effectively depending on the geometry of the “cracks”. It may thus be concluded that “cracks” with larger widths contribute more efficiently to effective mass transport and thus allow for higher product turnover than those with narrower widths. This experimental result fits into some theoretical expectations made by Evdokimov [92,93], based on role of the surface physics, on the role of capillary forces in particular. However, Evdokimov did not notice the potential relevance of the oscillatory behavior of GER.

6.1.2. Efficiency of the gas-bubble detachment from the viewpoint of surface physics

It is very important to note that the critical radius for gas-bubble nucleation at 25°C and 1 bar is about 1 μm [103], which corresponds to the size of the “cracks” observed on DSA. This fact accounts for the sudden raise in turnover frequency as shown in Figure 6.4. Nucleation of gas-bubbles is a phenomenon where electrocatalysis couples with surface physics. The primary goal in electrocatalysis is often to have a material with a very high exchange current density. Certainly, this is a necessary but not sufficient condition for the overall good performance of a catalyst. For gas evolution reactions, supersaturation of the electrolyte with the dissolved product would cause substantial diffusion overpotentials if gas-bubbles are not formed. Gas-bubbles essentially act as a sink for dissolved molecular Cl_2 that caused supersaturation [104]. The entire gas evolution process can be divided into three crucial steps involving: 1) nucleation, 2) bubble growth, and 3) detachment. If gas-bubble nucleation proceeds inside the cracked regions of the electrode, the growth of gas bubbles would be limited. Because of this, detachment of gas-bubbles from inner regions of the “cracks” should happen with smaller bubble radii and more frequently than for detachment from the outer surfaces of DSA. At the same time, when a gas-bubble is detached from inner regions of a “crack”, the electrolyte will flow into the “crack” thus enabling the pores in the inner parts of the coating to participate in the reaction. This is one of the possible explanations for the experimentally observed correlations. A very interesting and insightful analogy can be drawn

between gas evolution driven by electrode potential and gas evolution during boiling. During boiling, there is clear inverse proportionality between the frequency of gas-bubble detachment and the radius of the gas-bubbles [105]. It is known that the oscillation frequency of smaller bubbles causes more frequent displacement of the surrounding liquid than in the case of larger bubbles. The agitation of a gas bubble due to periodic oscillations of the liquid in its proximity finally causes its detachment. In the case of electrolysis on “cracked” electrodes, due to the limited growth of bubbles inside the “cracks”, the excess energy delivered to the solid/liquid interface due to the applied overpotential is dissipated after the electrochemical reaction and gas-bubble nucleation to the nucleated gas bubbles thereby amplifying their oscillations. The increased oscillation of the gas-bubbles inside the “cracks” leads to their eventual detachment with a considerably higher frequency.

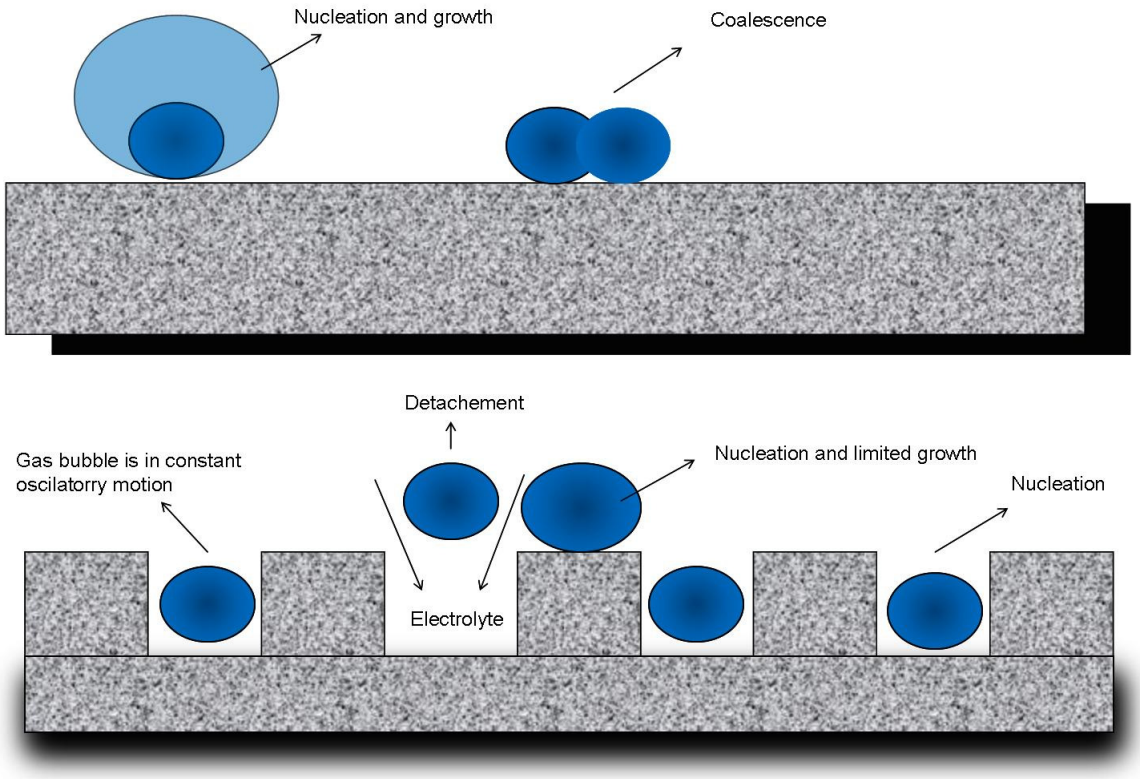

Figure 6.5. Schematic illustration of bubble behavior in case of “crack”-free and “cracked” DSA electrodes

This phenomenon is schematically depicted in Figure 6.5 in which the gas-bubble behaviour on flat “crack”-free and “cracked” DSA is compared. Obviously, in case of a “crack”-free electrode, after nucleation the growth and coalescence can proceed without any interference. In contrary, a “cracked” electrode exibit the possibility to limit the growth of gas bubbles inside the “cracks” and consequently induce higher frequency of detachment. This indirectly influences the growth of gas-bubbles on the outer surface of the “cracked” DSA due to a frequent flow of liquid towards the “cracks”.

6.1.3. Efficiency of gas-bubble detachment from the viewpoint of local chemistry induced by thermal stress

The entire analysis described above is based on geometrical aspects where the morphology of an electrode is considered to be crucial in utilization of existing active sites because of its influence on the nucleation of gas bubbles.

However, it is reasonable to assume that the “cracked” regions can exhibit different local crystallinities induced by the unsystematic rupture of the catalyst layer during synthesis, which can influence the local conductivity. The AFM micrographs shown in Figure 6.6 were used to substantiate this hypothesis. In Figure 6.6a a micrograph in the tapping mode of AFM was used to map the morphology/topography profile of the scanned region. A measurement in the conductive mode of AFM (C-AFM) was executed over the same region and the conductivity pattern can be seen in Figure 6.6b. Finally, Figure 6.6c shows a transparent reconstruction of Figure 6.6b overlaid with Figure 6.6a, displaying the local conductivity as a function of morphology. It is clear from Figure 6.6c that “cracked” regions exhibit locally higher conductivity. Our preliminary conclusion is that the reason for the spatial variation of conductivity is due to different crystallinities or due to non-uniform local enrichment with Ru due to the fact that Ru has a lower affinity for oxygen compared to Ti. This causes Ti to

diffuse more towards the outer surfaces of the catalyst coating to form TiO_2 during thermal synthesis while Ru exhibits a higher concentration in the inner layers of the DSA coating.

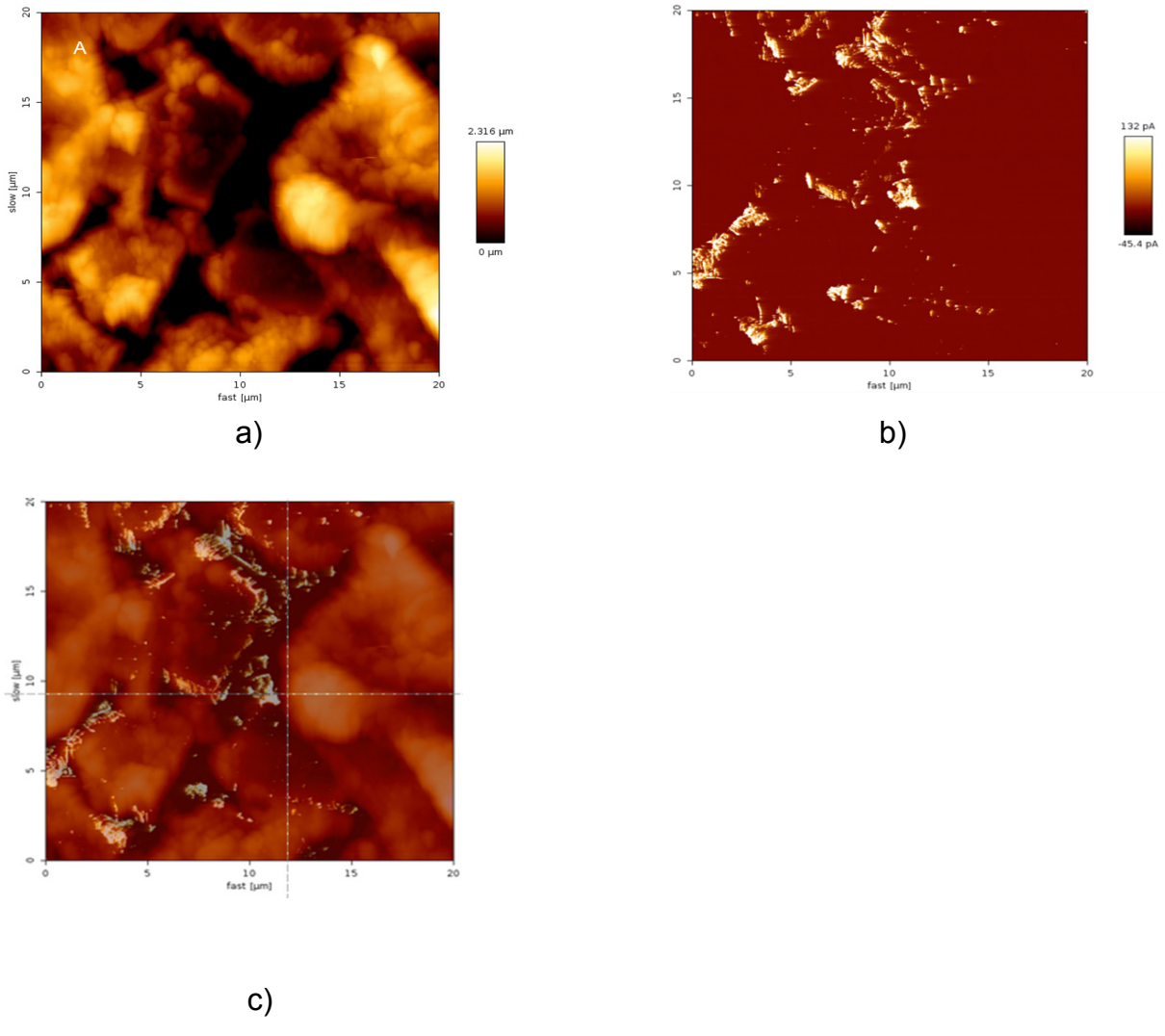

Figure 6.6. a) Topography/morphology micrograph recorded using the tapping mode of AFM, b) conductivity map recorded using the conductive mode of AFM c) transparent image of (b) overlaid with (a) to depict conductivity as a function of morphology. The scanned region was 20 x 20 μm^2

Results from AFM were considered as an initial hint that the “cracks” induced by thermal stress has to be some local chemistry impact behind. For an adequate spatially resolved analysis, it was necessary to establish local morphology/conductivity/composition/activity relations. The main difficulty was how to locally estimate the activity and how to interpret the origin of local activity at a particular region.

6.2. Principles of local activity measurements - detection and visualization of CER at the microscale

Investigation of the local activity appears necessary due to the fact that the activity itself is the consequence of a local equilibrium potential (which is a consequence of the local chemical composition), the local overpotential (which is a consequence of local kinetics) and the local ohmic drop. Hence, local activity measurements are seen as an important part for understanding the complex behaviour of the electrochemical interface. An adequate tool for this purpose is SECM, in which in opposite to all other techniques that deal with morphology, structure, topography, composition…etc. the experimental result is imaging a chemical process.

SECM was previously predominantly used to detect and visualize the electrocatalytic activity of different materials. A number of papers describe the application of SECM for exploring hydrogen oxidation/evolution and oxygen reduction/evolution [86,106-114]. However, chlorine evolution at DSA has not been a subject of detailed investigations by means of SECM. On a fundamental level it is challenging to find more detailed correlations between macrokinetics and local physico-chemical properties. Following this line of thoughts, the spatially resolved visualization of electrocatalytic activity can provide valuable information about the distribution of electrocatalytic activity and the reaction rate at the microscale. SECM is proposed as analytical tool for exploring the electrocatalytic activity of DSA for Cl_2 evolution. A method for the detection and visualization of the electrocatalytic activity for this specific reaction was developed.

6.2.1. SG-TC mode of SECM for the detection and visualization of Cl_2 evolution at DSA

The SECM feedback mode was used to position the tip in close proximity of the sample. Using 5 mM ferrocenemethanol in 0.1 M KCl as a mediator during the approach of the tip to the sample, the tip current increased in the vicinity of the DSA sample indicating that the tip is

approaching an electrochemically active surface. The tip was lowered until the tip current increased by approximately 20 % which corresponds to a tip-to-sample distance of about 20 µm. This distance was used as typical working distance in all further experiments.

In Figure 6.7. the concept of the sample-generation/tip-collection mode for Cl_2 detection is displayed together with an optical image of a DSA sample. The sample with a defined geometry (diameter d_s) was polarized to a potential E_s at which Cl_2 is produced. The tip (diameter d_t) was polarized to a potential E_t at which Cl_2 is reduced.

In this way, the current at the tip is a function of the catalytic activity of the spot on the sample directly underneath the tip. However, the properties of the DSA sample can be only derived in the generation-collection mode at a tip-to-sample distance (h) which is similar to the diameter of the tip. Local properties of the sample can be evaluated through a semiquantitative approach, in which the tip current describes activity fluctuations at the sample. A quantitative analysis requires knowing the collection efficiency of the tip which depends on the geometry of the system including the diameter of the sample, the diameter of the tip, the RG value (ratio between glass shield diameter and microelectrode diameter) and the tip-to-sample distance.

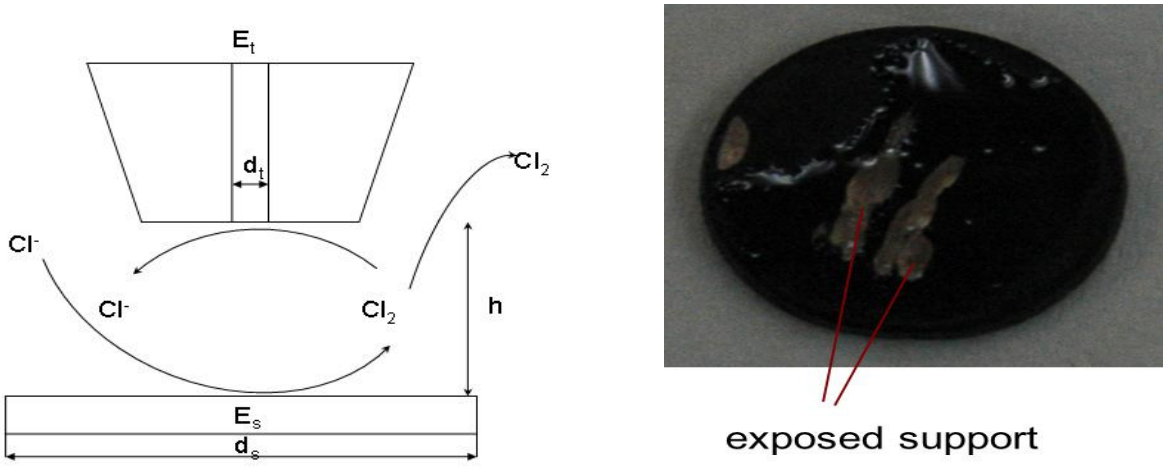

a) b)

Figure 6.7. a) Concept of SG-TC mode for detection of Cl_2 and b) optical image of the used DSA sample showing two scratches with removed catalyst

a)

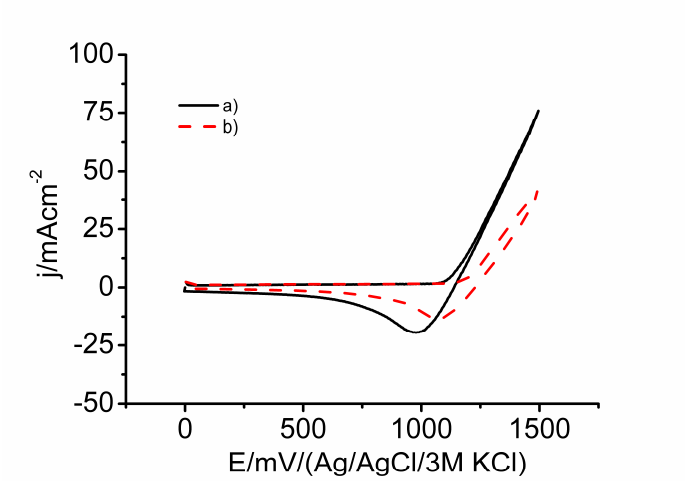

b)

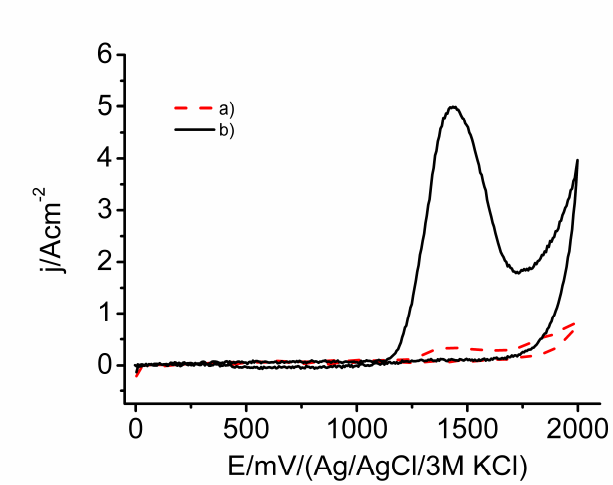

c)

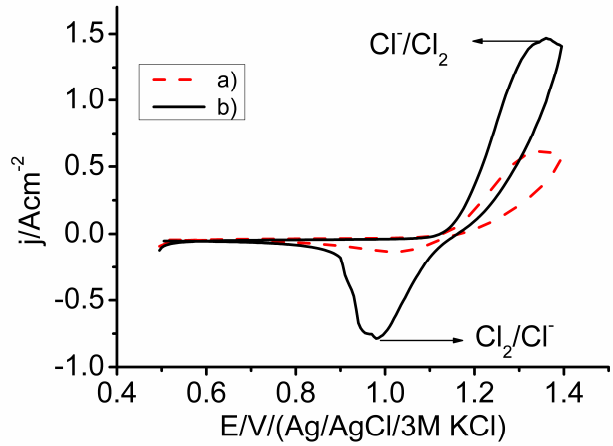

Figure 6.8. a) Cyclic voltammogram of the DSA (v = 100 mVs^{-1}; T = 298 K). Solid line: in 5 M NaCl adjusted to pH 2 by addition of HCl. Dashed line: in 5 M $NaNO_3$ adjusted to pH 2 by addition of HNO_3. b) Cyclic voltammogram of a Pt microelectrode (v = 100 mVs^{-1}; T = 298 K). solid line: in 5 M NaCl, pH 2. dashed line: in 5 M $NaNO_3$, pH 2. c) Cyclic voltammogram of a Pt microelectrode in 5 M NaCl compared with the cyclic voltammogram of the pre-reduced Pt microelectrode in Cl_2-saturated 5 M NaCl solution (v = 100 mVs^{-1}).

To evaluate the electrochemical characteristics of the electrodes and to derive suitable potentials for further SECM studies the DSA as well as a Pt-microelectrode were characterized using cyclic voltammetry. The measurements were carried out at a scan rate of 100 mVs^{-1} in a 5 M NaCl and in 5 M $NaNO_3$ solutions, both at a pH value of 2. The peak potential for Cl_2 evolution at the Pt tip was 1.36 V as shown in Figure 6.8. Cl_2 evolution can hence be easily distinguished from O_2 evolution which occurs at higher potentials. Similar observations were reported elsewhere [115]. This was confirmed by a comparative analysis of the CV recorded in 5 M $NaNO_3$ and 5 M NaCl. Both electrolytes had the same pH value and ionic strength. Thus, the observed differences in the voltammograms have to be attributed exclusively to the presence of Cl^- ions assuming that NO_3^- ions are electrochemically inert at the experimental conditions. Inert behavior of NO_3^- ions was confirmed during estimation of the potential of zero charge on some DSA coatings using as KNO_3 as supporting electrolyte [95,116,117].In contrast, Cl_2 evolution at DSA cannot be doubtlessly identified since no distinctive peak was observed in the related voltammogram (Figure 6.8a). Using the Nernst equation for Cl_2 and O_2 evolution, the respective Nernst potentials at 25 °C at the experimental condition (5 M NaCl; pH = 2) were calculated (Equation 6.21a and 6.21b):

$$E(Cl^-/Cl_2)_{rev} = E°(Cl^-/Cl_2) + (RT/nF)ln(1/c^2_{Cl^-}) \quad = 1.12\ V \quad \text{Equation 6.21a}$$

$$E(H_2O/O_2)_{rev} = E°(H_2O/O_2) - 0.059\ pH \quad = 0.91\ V \quad \text{Equation 6.21b}$$

Obviously, under these conditions O_2 evolution is thermodynamically favored. However, as seen from the voltammograms, Cl_2 evolution is dominating kinetically over O_2 evolution. This assumption is supported by *i)* the shift of the onset potential of the oxidation process by about 100 mV and *ii)* the substantially increased anodic currents in presence of Cl^- ions (Figure 6.8a). The exact ratio of anodically generated O_2 and Cl_2 is unknown. However, it is important

to keep in mind that the simultaneously produced O_2 may influence the cathodic current at the SECM tip which is assumed to be due to Cl_2 reduction.

In a previous kinetic analysis [42] the overpotential for Cl^- oxidation was not more than 400 mV, due to the intensive oxidation of the catalyst on highly anodic potentials. Taking this into account, all further experiments were performed at a maximum sample potential of 1.5 V. Finally, it was necessary to find a suitable potential for Cl_2 reduction at the Pt tip electrode for a successful application of the SG-TC mode of SECM. The CV in Figure 6.8b demonstrates that Cl_2 evolution, O_2 evolution and the formation of Pt oxides (Pt_xO_y) occur at potentials more positive than 1.1 V. Reduction of Cl_2, however, cannot be observed in the cathodic scan of the same CV. Reduction of Cl_2 was previously shown to occur on Pt at potentials between 0.9 and 1.125 V [118]. By changing the anodic vertex potential to 1.4 V a reduction peak for Cl_2 was observed at these potentials (Figure 6.8c). However, this reduction process may also at least in part be due to the reduction of Pt oxides [59].

In order to confirm that Cl_2 is indeed reduced at these potentials, Cl_2 was produced at a DSA in a 4-electrode SECM setup for 40 min to assure Cl_2 saturation of the electrolyte solution. A Pt microelectrode was conditioned at 0.9 V for 5 min and subsequently a CV was performed at the microelectrode to an anodic vertex potential of 1.4 V to limit the formation of O_2 and Cl_2. A significant increase in cathodic peak current can be observed after saturation of the electrolyte with Cl_2, which is clearly attributed to Cl_2 reduction. The increase in anodic peak current is most likely due to the pre-conditioning of the Pt electrode assuming that a reduced Pt surface shows higher activity towards Cl_2 evolution [42].

Based on these evaluations, the parameters for the SG-TC mode of SECM were set to 1.4 V at the DSA for the production of Cl_2 and to 0.95 V for Cl_2 reduction at the Pt microelectrode used as SECM tip. The reduction of O_2 is thermodynamically excluded above potentials of 0.912 V. It is expected that by applying these potentials an at least qualitative description of the local electrocatalytic activity of a DSA can be obtained. In order to evaluate the ability to

visualize local differences in the electrocatalytic evolution of Cl_2, the catalyst layer was partially removed from the DSA (Figure 6.7b) to have a clear contrast between the active areas and the bare Ti support. A SECM image in the SG-TC mode with the above-mentioned parameters is shown in Figure 6.9. together with a corresponding line scan at the y-coordinate of 600 µm. Darker colors in the SECM image in Figure 6.9a denote high currents for Cl_2 reduction at the SECM tip, indicating high local catalytic activity for Cl_2 production at the sample area opposite of the SECM tip. As expected, Cl_2 evolution only takes place over sites with intact catalyst layer whereas the Ti support did not show any significant activity. Thus, by means of a proper adjustment of the applied potentials at both the tip and the sample, the SG-TC mode of SECM can be applied for the local visualization of Cl_2 production at a DSA.

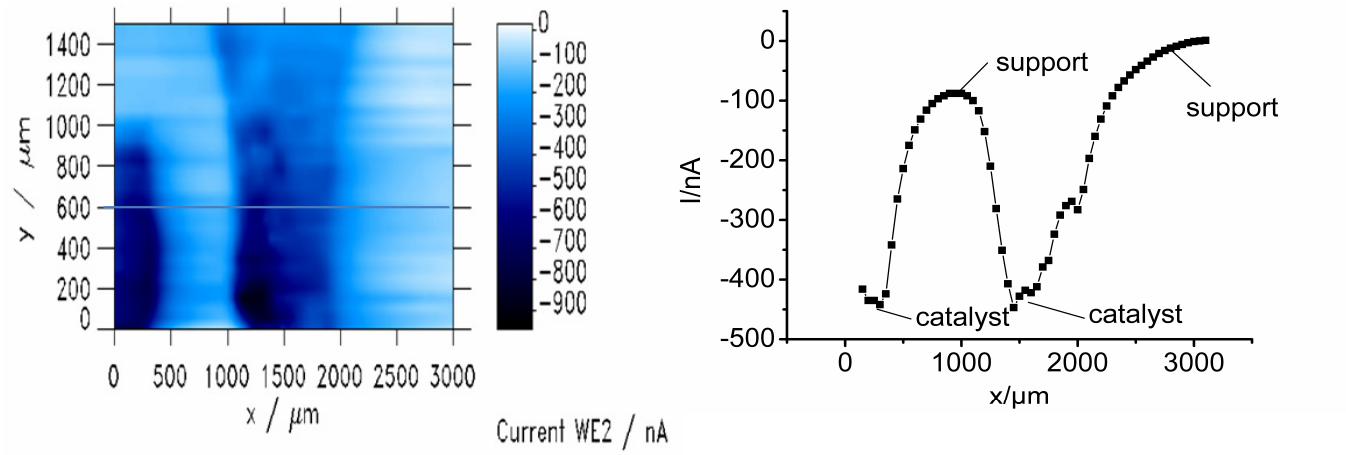

Figure 6.9. Visualization of Cl_2 generated at the DSA (E_s = 1400 mV) and detected at the SECM tip (E_t = 950 mV) in 5 M NaCl solution at pH 2 by means of the SG-TC mode of SECM:
a) 2D image of the electrocatalytic activity for Cl_2 evolution at the DSA
b) line-scan at y = 600 µm

6.2.2. Limitations of the SG/TC mode at high current densities for Cl_2 evolution.

Under industrial conditions, Cl_2 is produced at high current densities leading to a supersaturation of the electrolyte with gaseous Cl_2. Since at the tip only Cl_2, which is

dissolved in the electrolyte, can be detected the tip current in a SG-TC arrangement does not necessarily represent the local catalytic activity of the catalyst-modified sample. By increasing the applied potential at the DSA sample, the current due to Cl_2 evolution is increasing and the reduction current at the tip is following this increased Cl_2 concentration up to a DSA current of about 25 mA corresponding to an applied potential of 1.65 V (Figure 6.10.).

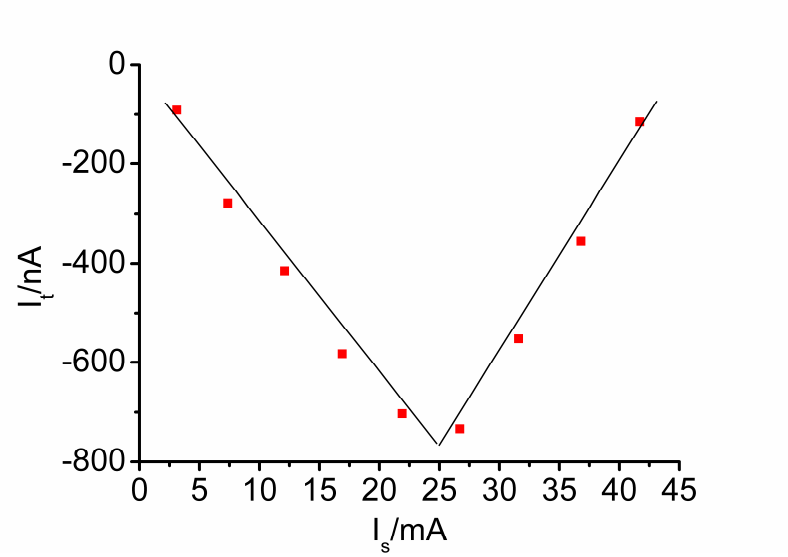

Figure 6.10. Change of cathodic current on a tip (E_t = 950 mV) as a function of the anodic current at the sample. Each data point corresponds to an average current at the sample during the polarization for 60 s. The potential was changed from 1200 mV (first point) to 2000 mV (last point)

By further increasing the sample current the tip current decreases. Although the increased gas fraction in the electrolyte with increasing sample current is leading to an additional ohmic drop in the gap between SECM tip and sample, the decrease in the tip current is connected with the non-sufficient amount of solvent necessary for dissolving the gaseous Cl_2. Thus, the SG-TC mode is only suitable for rather low sample currents but cannot identify the local catalytic activity of the DSA sample at industrial conditions. Consequently, a SECM mode has to be conceived which is not relying on the reduction of Cl_2 at the tip and is hence avoiding the problems occurring at supersaturation with Cl_2 gas. Maximal current density according to Figure 6.10 (respecting surface area of 0.196 cm^{-2}) at which produced Cl_2 could be collected

was around 130 mA cm^{-2}. Practical requirement, which corresponds to the industrial system, should be around 400 mA cm^{-2}.

6.2.3. The redox competition mode of SECM for visualization of Cl_2 evolution at DSA

Evaluation of general aspects of the reaction path of Cl_2 evolution may be helpful to overcome the limitations of the SG-TC mode of SECM. The reaction pathway for CER, predominantly used in literature, is shown with the Reactions 6.22:

$Cl^- = Cl_{ad} + e^-$	*Volmer step*	*Reaction 6.22a*
$Cl^- + Cl_{ad} = Cl_2 + e^-$	*Heyrovsky step*	*Reaction 6.22b*
$Cl_{ad} + Cl_{ad} = Cl_2$	*Tafel step*	*Reaction 6.22c*

Equations are given as stoichiometric one, without indication of (ir)reversibility, what will depend from applied overpotential and used material. Despite it was already illustrated (chapter 4.2.) that this reaction path is not adequate, its even recently still considered [33]. Being fully aware of weaknesses of this pathway, it still can be used to evaluate local equilibria and the interplay between thermodynamics and kinetics that can be used for local detection and visualization of the catalytic activity.

In the case of Cl_2 evolution at Pt electrodes, the Tafel reaction is considered to be the second step. One of the most often used methods for the evaluation of the kinetics of electrode reactions is the method of pseudo-equilibrium [35]. This method is based on the assumption that all steps of the reaction, with exception of the rate-determining step, are in equilibrium. At high current densities, most authors agree that the rate-determining step is the discharge of the Cl^- ion according to the Volmer reaction [119]. Thus, the second step, namely the recombination of the adsorbed Cl atoms is assumed to be in equilibrium. Evidently, this equilibrium is dependent on the concentration of the dissolved Cl_2 in the solution. Considering

that dissolved Cl_2 is in physical equilibrium with the Cl_2 gas, an increase in the partial pressure of Cl_2 gas will cause concomitantly an increase in the concentration of dissolved Cl_2. If the concentration of Cl_2 in the vicinity of the SECM tip is high, it will shift the Tafel reaction to the left and hence inhibit the recombination of the adsorbed chlorine atoms Cl_{ad}. Additionally, this can inhibit the further formation of the adsorbed chlorine atom Cl_{ad} and consequently negatively effect on the primary Volmer reaction. Practically, accumulation of the product can decrease the rates of both the Volmer and the Tafel reaction, which are determining the rate of Cl_2 evolution. However, if the above mentioned lack of solvent (here water) is true then inhibition of the reaction by the produced Cl_2 will be certainly important additionally due to the fact that the lack of solvent will decrease electroadsorption in Volmer's step and consequently the rate of the reaction.

In the following, these considerations about the reaction pathway are combined with the concept of the transient redox competition (RC) mode of SECM [90]. In the RC mode, the microelectrode and the sample are competing for the same redox species in solution. A decrease of the current at the microelectrode occurs when the local concentration of the redox species in proximity of the microelectrode decreases due to an electrochemical conversion of the same redox species at active sites of the sample. Previously [120-123], monitoring the local change in concentration of the redox species in the gap between SECM tip and sample caused by the sample reaction was possible due to the fact that the experiments were conducted in diluted solutions. However, in this specific case the reactant, namely Cl^- ions, is available in very high concentrations, a substantial decrease in its concentration due to the sample reaction is unlikely, and consequently the current at the tip over a Cl_2 producing spot should not be substantially changed. However, as discussed above, the reaction rate at the tip and hence the tip current should be dependent on the increased Cl_2 concentration by its impact on the rate of both the Tafel and the Volmer reaction. The concept

of the RC mode of SECM for highly concentrated solutions is schematically shown in Figure 6.11.

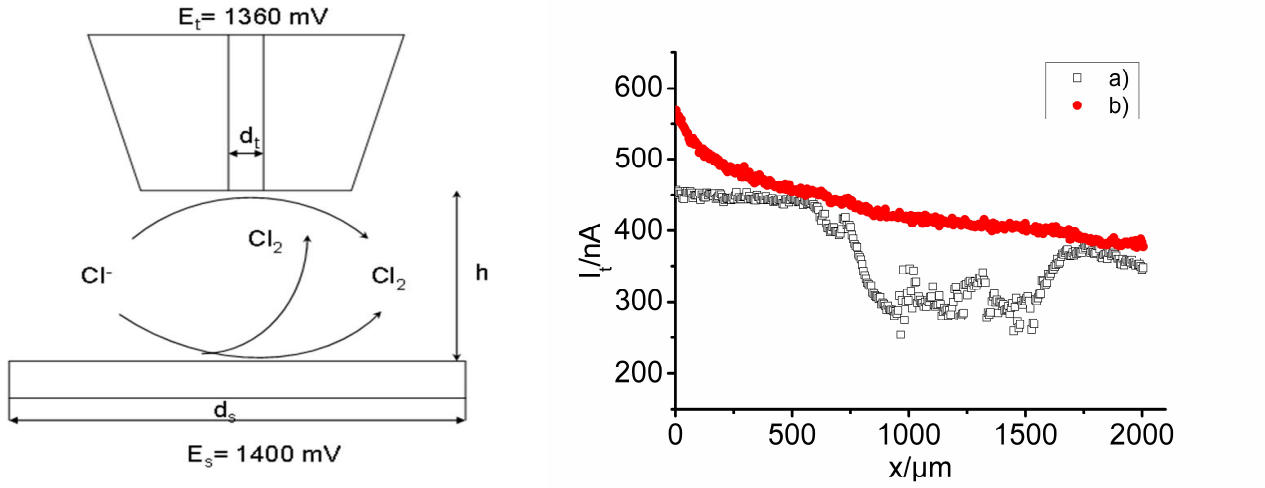

Figure 6.11. a) Schematic representation of the concept of the RC mode of SECM for highly concentrated solutions. b) RC mode line scan over a catalyst-modified area of a DSA (E_t = 1.36 V; E_s = 1.4 V; 5 M NaCl) when sample is polarized (black cubes) and when sample is at OCP (red circles)

The potential value for the tip reaction corresponds to the peak potential for Cl_2 evolution (see Figure 6.8b). A high local catalytic activity of the sample is reflected by an increase in the local Cl_2 partial pressure which will in turn reduce the production of Cl_2 at the SECM tip in proximity of an active sample site leading to a decreased tip current. The experimental proof of this concept is shown in Figure 6.11b. In a first line scan across the sample, which was previously used for the SG-TC experiments, no potential was applied to the DSA sample leading to a rather constant Cl^- oxidation current at the SECM tip overlaid by a slow decrease of the underlying background current with time until steady-state conditions at the sample are reached. After polarizing the sample to a potential of 1.4 V and repeating the line scan a pronounced decrease of the tip current occurs at coordinates above the active catalyst. In order to further evaluate the suggested RC mode for high concentrations and to compare its

sensitivity to the SG-TC mode, the same area of the DSA sample was visualized with the two SECM modes (Figure 6.12).

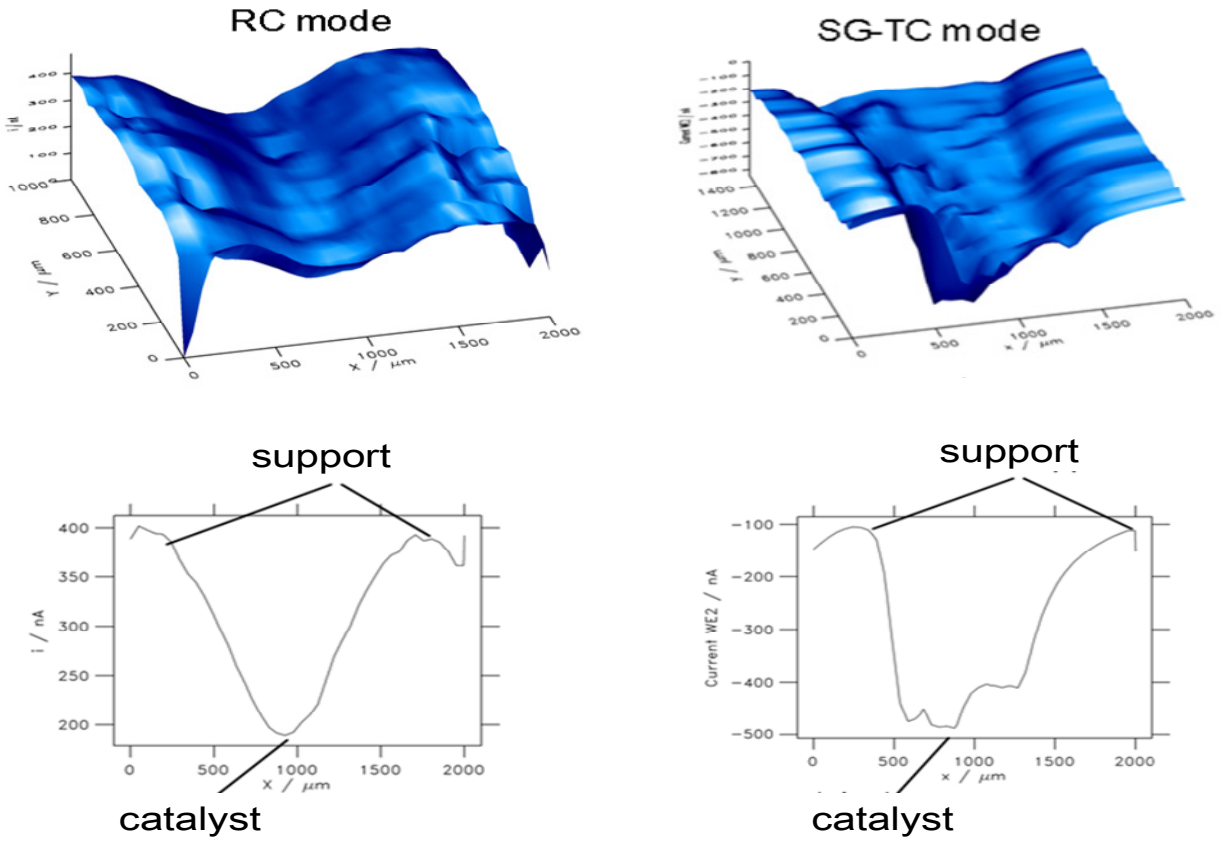

Figure 6.12. Visualization of Cl_2 evolution at a DSA sample polarized to E_s = 1400 mV by two different SECM modes. 3D image in the RC mode (E_t = 1360 mV) with a corresponding line scan at y = 300 µm; 3D image in the SG-TC mode (E_t = 950 mV) with a corresponding line scan at y = 300 µm. (5 M NaCl)

Obviously, similar information can be obtained about the local catalytic activity of the DSA sample for Cl_2 evolution. As a matter of fact, since the SG-TC mode and the RC mode of SECM are monitoring the same catalytic reaction at the sample with different reactions occurring at the tip they exhibit different distance dependence, resolution, dependence on the Cl^- concentration etc.

While Figure 6.12 shows the possibility to detect and visualize chlorine activity at DSA in two different SECM modes, it would be more convincing if a similar image of the same sector of the DSA surface consisting only from the catalyst layer could be visualized. Certainly,

resolution using a 25 μm microelectrode will provide an image that illustrates only fluctuations in the activity due to local surface inhomogeneities, but even in that case the SECM images in both modes should show a similar spatial distribution of activity.

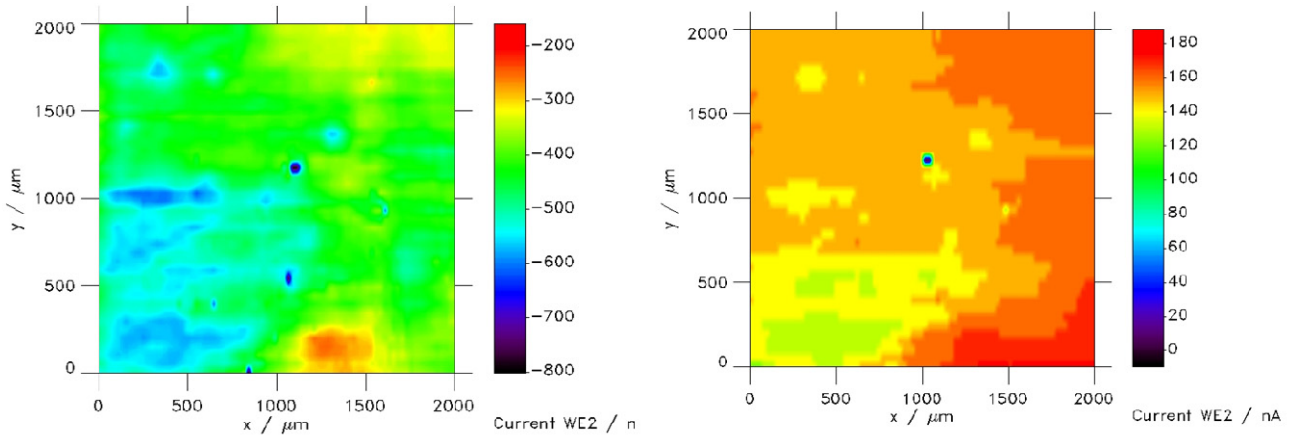

a) b)

Figure 6.13. SECM scanning of the DSA surface in: a) SG/TC mode and b) RC mode

From Figure 6.13 it is evident that the two different SECM modes give similar pattern in the distribution of activity. The catalytic activity for Cl_2 evolution at DSA using SECM can be visualized with both the SG-TC mode and the RC mode of SECM. The RC mode, which was previously restricted to diluted solutions, has been used to explore reactions in highly concentrated solutions. It provides information about the local catalytic activity of a DSA sample especially in the case of reversible reactions for which the equilibrium state can be affected by local changes in the educt of product concentrations. The possibility to visualize Cl_2 evolution at DSA opens the door for the more insightful evaluation of the local electrocatalytic activity by extending the SECM experiments to higher resolution by using smaller SECM tip electrodes and distance-independent positioning of SECM tips [124,125]. Further aim is directed to providing a more in depth insight into the catalytic reactions at the DSA samples, which may be the basis for optimization of the catalyst layer or for finding new improved catalysts for Cl_2 evolution.

6.3. Local morphology/conductivity/composition/activity relations

An initial hint on the nature of the relation between morphology and conductivity in case of DSA was already given previously (chapter 6.1.3.). However, the investigated region (Figure 6.6) was not a representative example of a “mud-crack” structure. In repeated experiments the local correlation between the morphological pattern and the electronic conductivity of the “cracked” DSA sample (Figure 6.14.) were examined by comparison of AFM micrographs made in tapping mode (topography and morphology pattern) and in conductive mode (spatial distribution of conductivity) over the same catalyst region

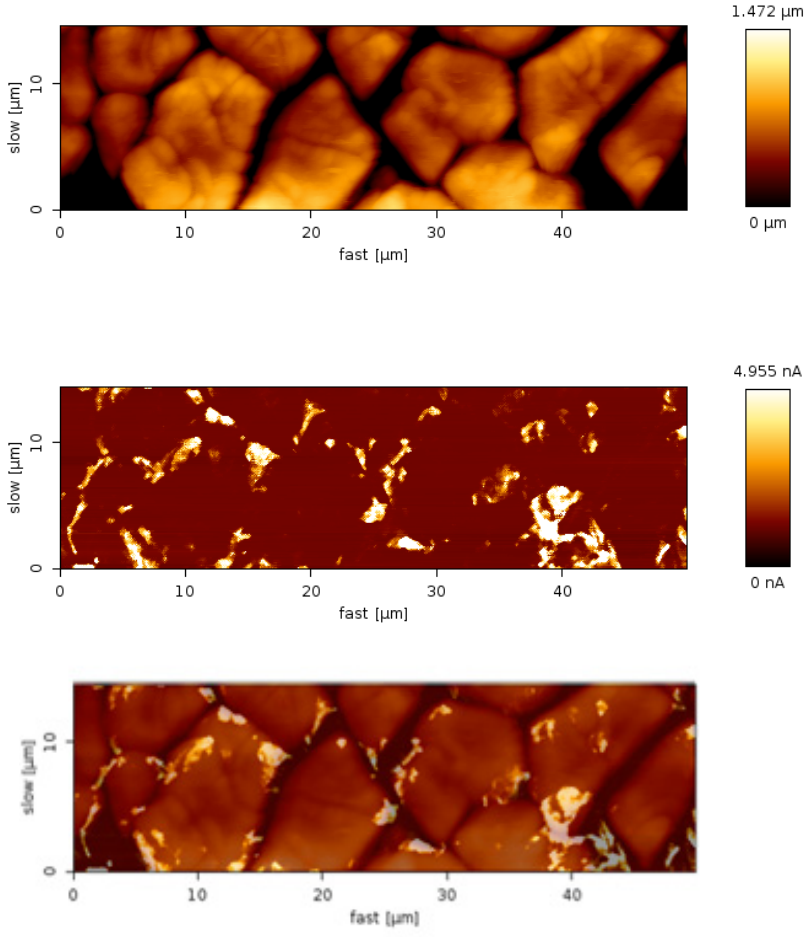

Figure 6.14. Linking morphological pattern with electronic conductivity; tapping mode AFM (µm scale), conductive mode AFM (nA scale) and micrograph in AFM tapping mode overlaid with transparent AFM micrograph in conductive mode

. Overlapping of AFM micrographs in tapping mode with the transparent micrograph made in the conductive mode strongly suggests that increased conductivity comes from the “cracked”

regions. As previously stated, enrichment with Ru is expected as we penetrate deeper in the catalyst layer.

Estimation of elemental distribution of Ru is made using SEM/EDX mapping before (Figure 6.15) and after the electrochemical test (Figure 6.17). The local enrichment in Ru can be easily detected as function of morphological features. Having in mind that EDX is not surface sensitive, the collected information includes also the composition of subsurface regions, what is essentially sufficient to confirm the assumption that Ru enrichment occurs in parts of the catalyst layers which are closer to Ti support. SEM/EDX mapping reveals a relatively homogenous surface composition, immediately after the synthesis (Figure 6.15). However, more careful inspection of the SEM/EDX micrograph shows that enrichment with elemental Ru (green color) in comparison to oxygen (red color) is seen in cracked regions. The assumption is that tensile stress induced during thermal treatment is leading to breaking of the layer in a way that in the vertical profile inside the “cracks” an enrichment with Ru occurs as compared with the terraces. This is most probably due to the higher affinity of Ti towards oxygen that will cause a more intensive formation of TiO_2 as compared with RuO_2 during thermal decomposition process.

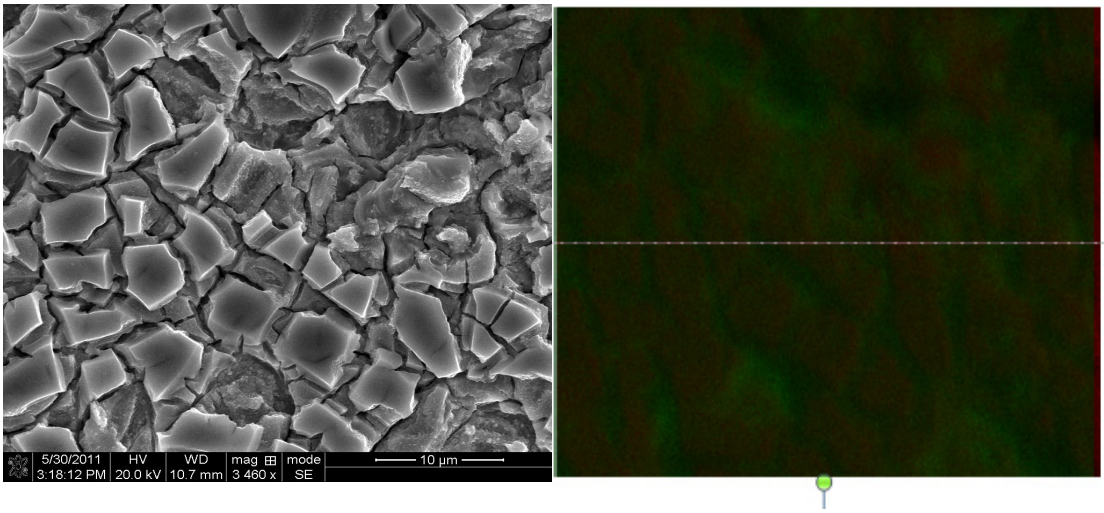

a) b)

Figure 6.15. a) SEM micrograph of “cracked” DSA electrodes and b) EDX mapping of Ru (green color) and oxygen (red color) of a “cracked” DSA electrode, before electrochemical testing

In this way, the metallic Ru represents a doping component for TiO_2. The conductivity of a doped semiconductors should essentially follow Fermi-Dirac statistics as it is shown in the histogram in Figure 6.16.

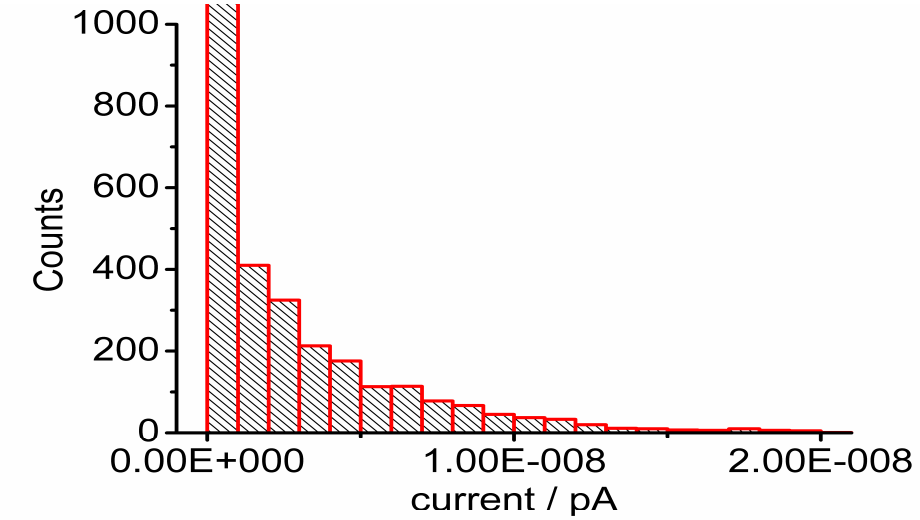

Figure 6.16. Histogram of conductivity distribution estimated with C-AFM

Distribution of conductivity suggests that the surface predominantly behaves as semiconductor with a relatively low number of conductive regions where the current can pass without significant resistance.

After intensive reaction during a so-called accelerated stability test [126], it an increased local concentration of oxygen in the region of the “cracks” can be noticed (Figure 6.17). Obviously, the reaction is locally promoted in the “cracked” regions suggesting that besides the impact of morphology and gas bubble detachment from the viewpoint of surface physics, there are local chemical effects, which are promoting activity. At regions where entire “islands” were removed a surface enrichment with Ru can be noticed proving the assumption of a vertical profiling of the Ru concentration caused by thermal treatment.

While high current densities were generally expected at the edges, the phenomenon of “island” detachment is surprising and illustrates the high local pressure at the triple phase boundary.

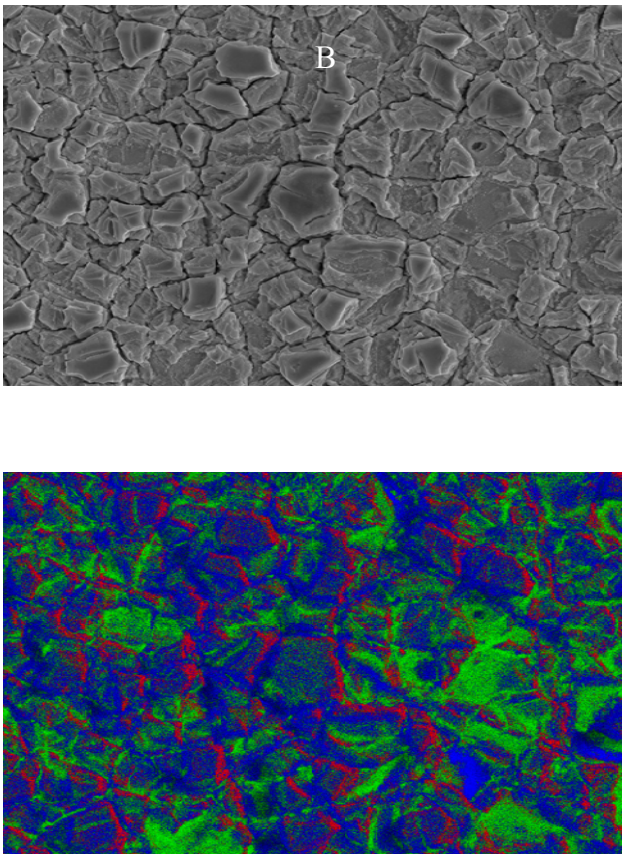

Figure 6.17. SEM/EDX mapping after an accelerated stability test during 1h in 1M H_2SO_4 at a current density of 10 kAm^{-2} (Ti - blue; Ru - green; oxygen - red). The white rectangular mark shows regions where an entire “islands” were removed

Knowing that a correlation between morphology, conductivity and chemical composition exists makes it necessary to localize the catalytic activity itself by means of electrochemical imaging based on the detection of concentration gradients. The concept was explained in a previous chapter (chapter 6.2), however, in this case it was necessary to use microelectrodes with adequate sizes. Taking into account the surface morphology of DSA (Fig. 6.17) a microelectrode of approximately 1 μm diameter should be sufficiently small to image local activity at least to an extend that the locally intensified production of Cl_2 in the “cracked” regions can be visualized.

The sizes of the microelectrodes were estimated using SEM (Figure 6.18a) and CV (Figure 6.18b).

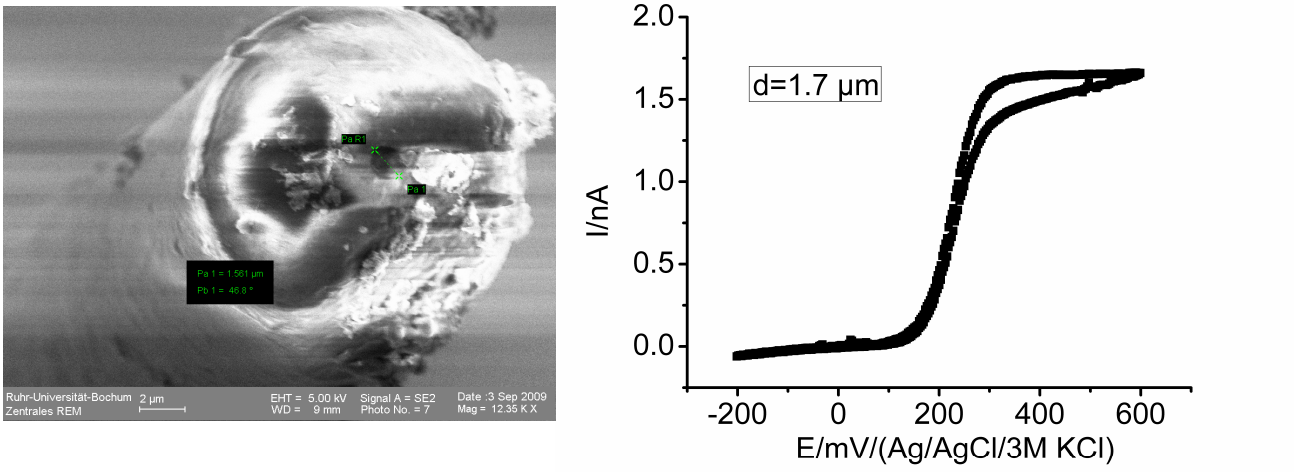

a) b)

Figure 6.18. a) The SEM micrograph reveals that the diameter of the shown microelectrode d = 1.57 µm. b) The electrode diameter estimated using CV is d = 1.7 µm

The produced microelectrodes had diameters between 110 nm and 3 µm. High resolution measurements with microelectrodes require a tip-to-sample distance of about the magnitude of the hemispherical diffusion profile which is about the diameter of the microelectrode. Due to the fact that gas evolution is coupled with significant convection, shear-force mode positioning for distance control becomes unreliable [124,125]. Consequently, a tip crash can be hardly avoided with microelectrodes smaller than 0.5 µm in diameter simply to the roughness of the catalyst layer. SECM scanning was done using an automated tilt control without additional constant-distance positioning. A SECM image of a DSA area of 25 x 20 μm^2 together with a line scan is shown in Figure 6.19

SECM image in Figure 6.19a resembles one of the “islands” from the “cracked” DSA electrode with surrounding “cracked” regions. Figure 6.19a suggests that the catalytic activity predominantly comes from the “cracked” regions what is illustrated additionally in the linescan given in Figure 6.19b. The current above the “cracked regions is around 40 nA while the current measured over the trapezoidal “island” is around 15 nA. The “cracked” region has a

more than 2.5 times higher activity than the plateau, despite “cracks” are topographically lower what may decrease the current due to the overlaid impact of distance on the SECM image.

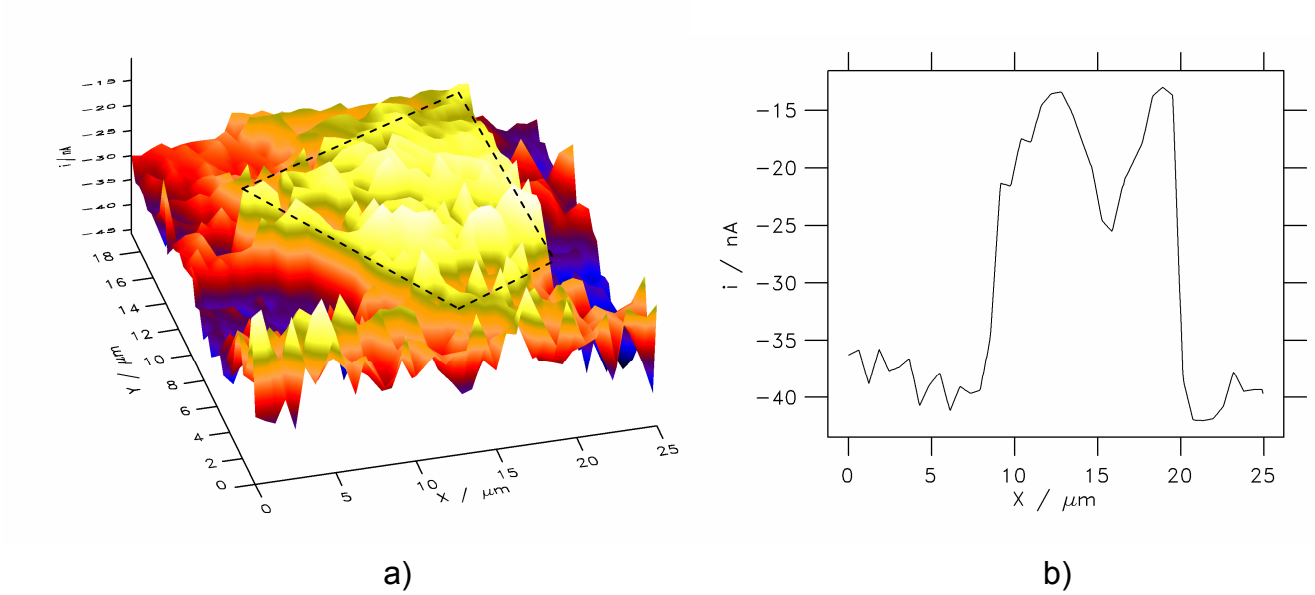

a) b)

Figure 6.19. a) 3D SECM image over a scanned area of 25 x 20 µm^2. b) SECM line scan over a “cracked” DSA electrode at coordinate y=7 µm

To evaluate the impact of the “cracked” morphology as a specific contribution to the overall performance, comparison between “cracked” and “crack-free” electrodes was made.

Figure 6.20a shows topography images of “crack-free” electrodes. Clusters detected at topographically higher regions are more conductive as depicted in Figure 6.20b. Finally, by SECM scanning over a 20 x 20 µm^2 region using a microelectrode of 1 µm diameter (Figure 6.20c) it was confirmed that clusters exhibiting a pronounced conductivity are active for Cl_2 evolution. The clusters are originating from “on-top” deposited RuO_2.

Local conductivity is a necessary but not sufficient condition for high local electrocatalytic activity. By coincidence in this particular case, regions with high local conductivity manifest at the same time high electrocatalytic activity, because RuO_2 has a metallic-type conductivity. Other materials with relatively low conductivity may exhibit higher activity in comparison with more conductive materials in dependence from the charge transfer resistance, adsorption

properties etc. For example, if conversion of free diffusing redox mediators like $[Fe(CN)_6]^{4-/3-}$ at boron doped diamond (BDD) shows a rate constant which is one order of magnitude higher in comparison with RuO_2 [53]. Hence, the overall measured catalytic activity is a consequence of several factors which always have to be analyzed separately.

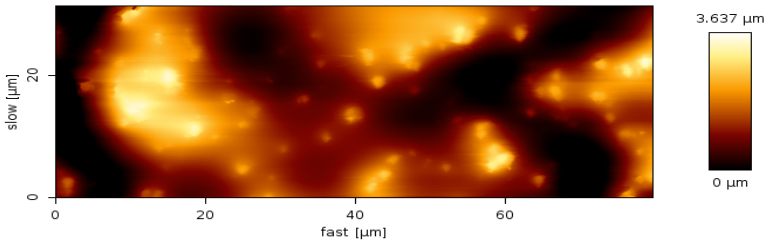

a)

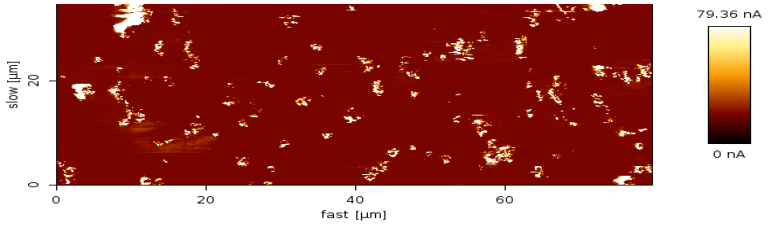

b)

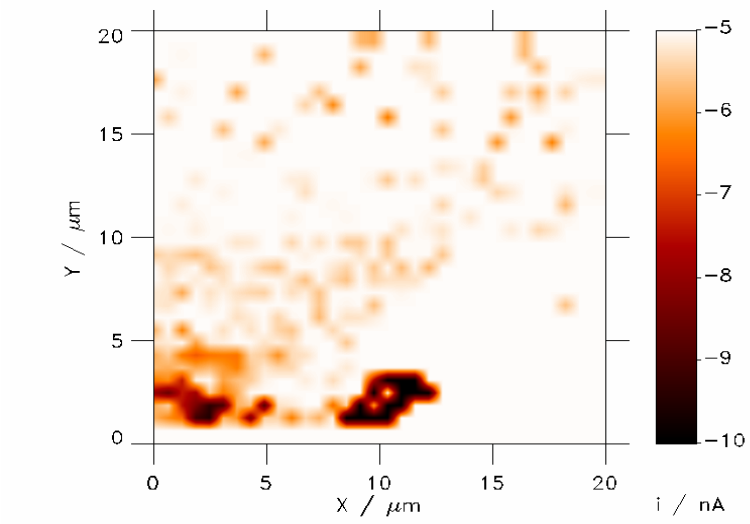

c)

Figure 6.20. a) Topography AFM micrograph and b) conductivity AFM micrograph over the same region and c) SECM image over a 20 x 20 µm^2 region of the “crack-free” DSA electrode.

Evaluation of catalytic activity in case of nanostructured materials is connected with serious technical limitations, considering electrode production, tip-to-sample distance control, noise etc… Therefore measurements at microscale resolution of 25 μm are often performed which are averaging information about the local activity in dependence from the achieved resolution. Thus, one has to question what can be learned from activity images that essentially show local fluctuations in activity.

6.4. Spatial distribution of electrocatalytic activity at gas evolving electrodes

Spatial distribution of activity (or active sites) is of high interest in (electro)catalysis [127-130]. However, till now no methodology was proposed to really estimate the distribution of activity. Distribution of active sites estimated with methods which provide information on structure and composition (SEM/EDX, TEM, etc.) represent an indirect approach lacking information about an adequate ohmic contact between catalyst and support. Additionally, some regions of the catalyst will be more favorable for the transport of reactants/products due to the morphological pattern, while at other regions the activity will be self-inhibited by the product despite the density of active sites may be very high. All this suggests that the local faradaic current as a measure of local catalytic activity is a result of several factors. Intuitively, it is assumed that a more uniform distribution of activity will contribute to an increased overall performance, but reasons for this and how to perform quantitative measurements are still without answer. For this purpose, SECM was used to determine the distribution of electrocatalytic activity during Cl_2 evolution at the solid/liquid interface of dimensionally stable anodes. Statistical interpretation of the local microscopic distribution of the electrocatalytic activity of dimensionally stable anodes was used as a basis for improved understanding of their overall electrocatalytic activity.

Based on previous considerations, it is supposed that the most straightforward approach to improve the performance of DSA is to improve the preparation procedures, keeping the

chemical composition of the coating constant. The improvement in preparation of the coating should involve minimization of surface segregation, attaining optimum porosity as a compromise between high surface area and a suitable morphology for effective Cl_2 bubble release, and a homogeneous coating over the entire surface area. Looking more closely into this, it becomes evident that these targets for improvement can be phenomenologically expressed by a homogeneous distribution of the local catalytic activity. Thus, we propose to perform an *in-situ* visualization of the local electrocatalytic activity of DSA samples for Cl_2 evolution using SECM [131-133], and to correlate the local catalytic activity with the overall activity of the DSA. The practical significance of the approach is demonstrated by the evaluation of the preparation procedure through comparative analysis of four DSA samples.

6.4.1. Sources of spatial fluctuations in activity

As previously stated, understanding a reaction at the molecular level (microkinetics) is not sufficient to evaluate the overall performance of a DSA catalyst coating. Mechanistic studies of the Cl_2 evolution reaction [41,134] are usually performed together with studies of mass transport induced by the presence of gas bubbles [135-137]. Thus, microkinetics together with the conditions of mass transport and spatial distribution of the potential and the current density determine the overall performance of a catalyst coating expressed as macrokinetics [38].

Since an electrocatalytic reaction takes place at a solid/electrolyte interface, the spatial distribution of activity is supposed to be probed from the local properties of the interface. The visual impression of the electrode surface as proposed previously [133] may provide first hints on the distribution of the local and the overall activity. Here, visual inspection of the electrode surface was combined with the visualization of locally resolved Cl_2 evolution by means of SECM in the sample-generation/tip-collection (SG-TC) mode (Cl_2 which is generated by anodic polarization of the sample is detected as a cathodic current at the tip due to Cl_2

reduction). From an idealized perspective, inactive spots on the sample should yield a negligible cathodic current at the tip. In reality, considering the resolution (25 µm diameter microelectrode) and diffusion of the generated Cl_2 in the electrolyte, the change in the current at the tip represents fluctuations of the local catalytic activity of the scanned area of the catalyst.

In Figure 6.21a 1000 x 1000 μm^2 SECM image of a DSA sample and the corresponding quasi-stationary potentiostatic polarization curve are shown.

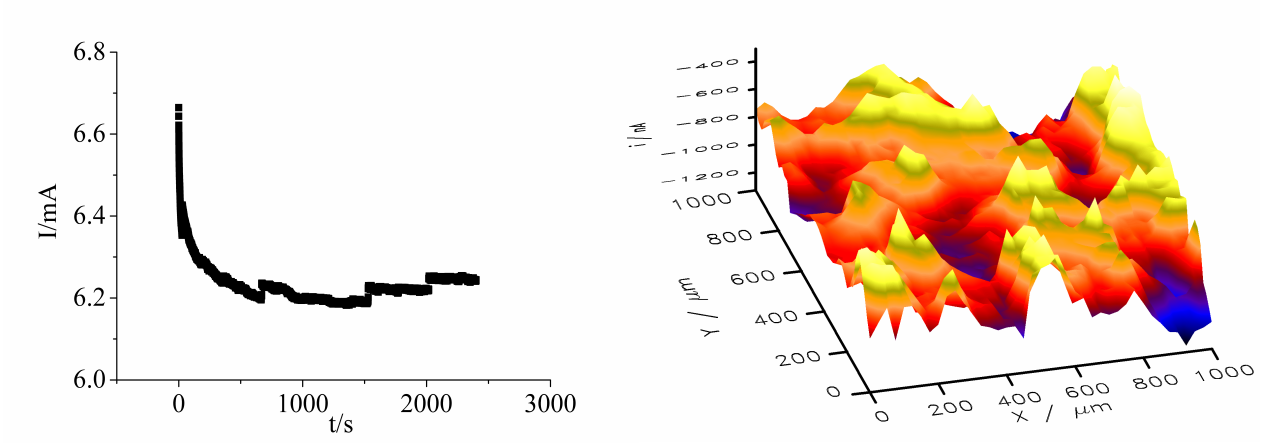

a) b)

Figure 6.21. a) Quasi-stationary potentiostatic curve measured at a DSA sample of 'd_s' 5 mm diameter, and b) SECM image of a scanned area of 1000 x 1000 μm^2. The current (i/nA) is a function of the tip position in the x-y plane.

The different colour codes represent different ranges of the cathodic current at the tip. The darker colours represent regions with the highest current and therefore the highest activity. When the sample was polarized at a constant potential of 1400 mV, the resulting current approached a pseudo-stationary state at a value of about 6.2 mA after approximately 900 s. By comparing the amperometric current at the sample and the current values as detected in the SECM scan, it is evident that the overall activity can be considered as the sum of the local activities. In fact, the local activities span over a wide range, from -400 to -1200 nA (Figure 6.21b). From the SECM image in Figure 6.21b two questions arise. On the one hand, it has to

be evaluated if the differences in the local current values are correlated with topographic features of the sample, and on the other hand, the reason(s) for the observed differences in the local activity manifested by the differences in the reduction currents at the SECM tip have to be elucidated. Considering that scanning was performed in a conventional constant-height mode, an impact of the sample topography cannot be excluded due to the dependence of the tip current on the tip-to-sample distance. To gain understanding of the impact of the sample topography on the activity imaging and to understand the reasons for the local fluctuations in the tip current, AFM and SEM measurements were done. In Figure 6.22 SEM micrographs and the topography profile recorded by an AFM line scan are shown.

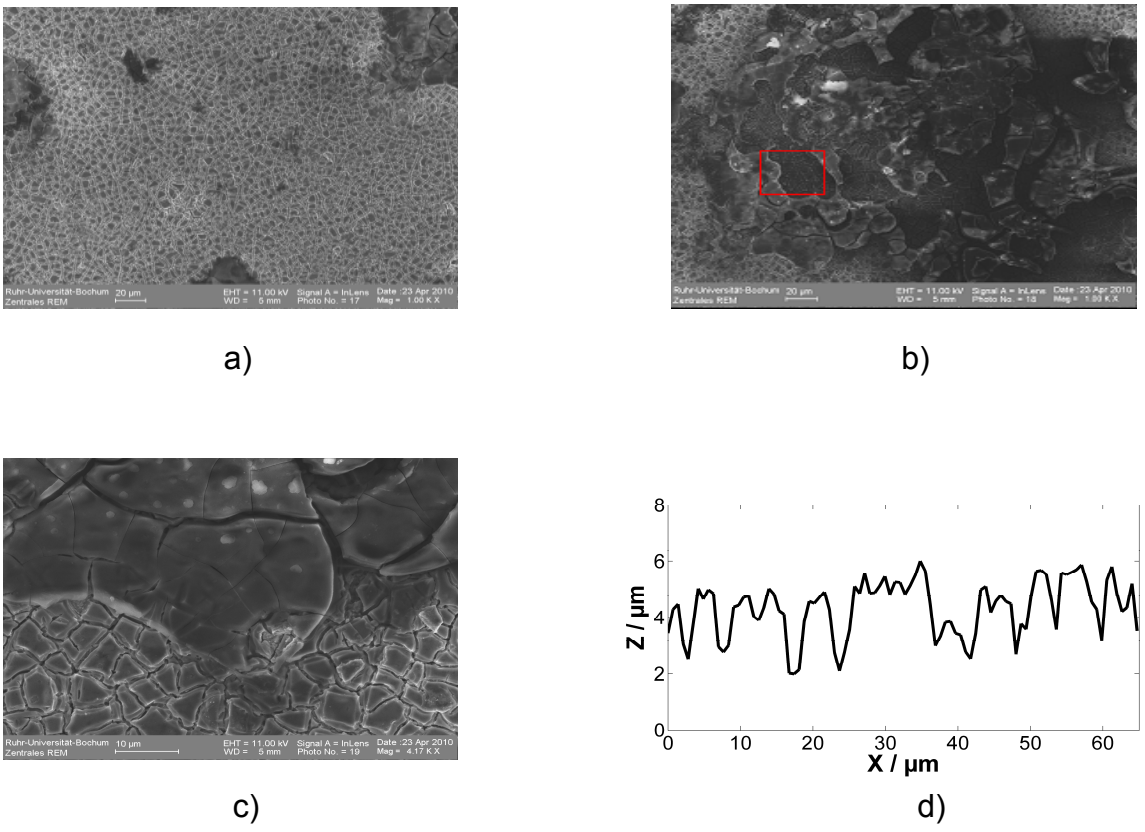

Figure 6.22. Morphology and topography of a DSA sample. a) SEM micrograph of a DSA with a fairly uniform morphology at the microscale. b) Catalyst surface with non-uniform morphology. c) Magnification of the area marked rectangularly in red from b). d) AFM line scan.

The SEM image (Figure 6.22a) reveals the expected uniform morphology of a DSA at the microscale. A detailed insight into the surface morphology revealed that besides the uniform regions the DSA consists of regions with non-uniform morphology (Figure 6.22b). A magnified view of the rectangular region marked in red (Figure 6.22b) is displayed in Figure 6.22c. Besides the expected “mud-crack” structures represented by “islands” and “cracks”, incompletely formed “mud-crack” structures are also visible. From the AFM line scan (Figure 6.22d) a height deviation in the range of 1 to 3 µm can be revealed. Taking this into consideration, the impact of the changes in height on the SECM tip current can be taken into account. The amount of Cl_2 produced over the area underneath the tip leading to the observed tip current can be calculated and correlated with the tip-to-sample distance (Figure 6.23).

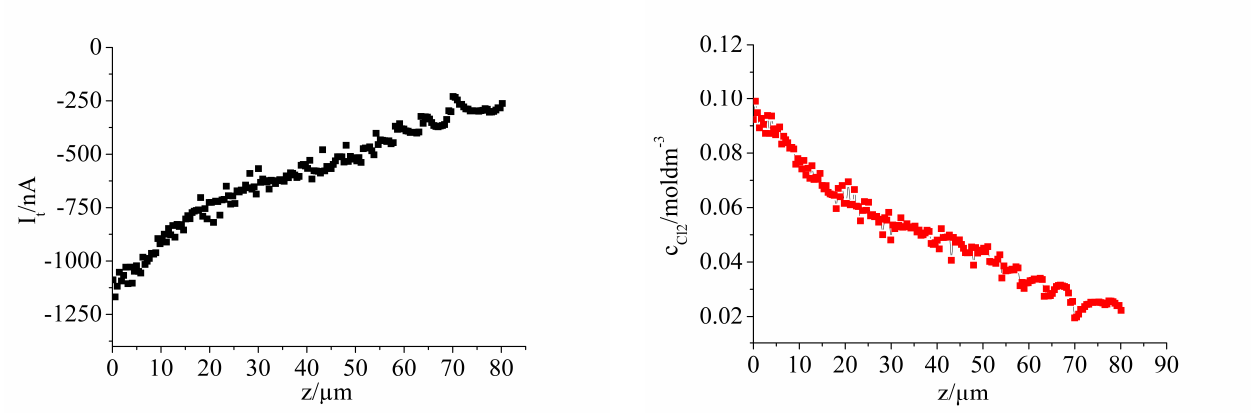

a) b)

Figure 6.23. Influence of the tip-to-sample distance on the tip current during SECM imaging expressed by a) the amperometric response at the tip as a function of the tip-to-sample distance and b) the concentration profile of the Cl_2 produced at the sample as a function of the tip-to-sample distance.

In Figure 6.23a the chronoamperometric response at the SECM tip is plotted as a function of the tip-to-sample distance. Starting from the sample surface currents were recorded at each point as the tip was retracted in increments of 1 µm to a height of 80 µm above the sample surface. The tip current decreases during the retraction due to a less intensive consumption

of the Cl_2 produced at the sample at the tip. By assuming steady state conditions at the tip, the concentration of Cl_2 can be extracted from the current at the tip using the equation for diffusion limited current for the case of hemispherical diffusion (chapter 4.1.2.). The Cl_2 concentration is expressed as a function of the tip-to-sample distance (Figure 6.23b). The measured solubility of Cl_2 in the electrolyte corresponded to previous observations [138]. The value of the diffusion coefficient of Cl_2 in brine was adopted from the literature [139]. It is obvious that the topography has an influence on the current signal at the tip, however, for deviations in topography in the range of 1-3 µm, which is typical for a “mud-crack” structure, changes in concentration are negligible, if the tip is positioned at a height of 20 µm above the sample. It is important to point out that fluctuations in tip current in the range of almost 300 % cannot be caused by topography (Figure 6.21b). Thus, the predominant cause of these fluctuations is attributed to changes in the local activity of the electrode.

There are two possible reasons that can contribute to an inhomogeneous distribution of activity on a catalyst surface: 1) surface segregation or 2) deviations from the standard “mud-crack” morphology.

The already shown EDX analysis (chapter 6.3.) explicitly reveals that all DSA samples have a uniform chemical composition after synthesis, however, a displacement of Ru can be noticed after use. Deviations from the expected “mud-crack” morphology exist as confirmed in Figure 6.22. Two zones can be distinguished from the SEM micrograph in Figure 6.22c, namely a “mud-crack” zone and a zone where “mud-crack” formation is incomplete. The “mud-crack” zones have higher roughness than the zones with incompletely formed “mud-crack” structures, which is expected to influence local activity. Indeed, it is known from the concept of voltammetric surface charge, that “cracked” electrodes have much higher active surface area than compact ones [66]. The “mud-crack” morphology based on “islands” and “cracks” is characterized by its edges. The local current density is expected to be highest at edges. Besides undesirable incomplete “mud-crack” formation the homogeneity of a coating can be

affected by variations in the size of the “islands” and “cracks” (channels). The sizes of the “cracks” can have a significant influence on the effectiveness of the process, influencing the size of the gas-bubbles evolved from the catalyst surface.

At the molecular level, a DSA catalyst coating is expected to produce Cl_2 at any RuO_2 center, but the efficiency of the entire process is limited by the frequency of detachment of the gas-bubbles [140] which is dependent on surface morphology [141-143]. The morphology of a catalysts coating influences the availability of its active sites and consequently its effective active surface area [99]. From this perspective, it can be concluded that fluctuations in the tip-currents are to a minor extent influenced by topography, but the main influence that defines the distribution of activity at the solid/liquid interface are compositional and morphological inhomogeneities or deviations from the expected “mud-crack” structure.

6.4.2. Statistical approach to SECM imaging

Although the distribution of activity caused by the non-uniform composition and morphology was monitored using SECM , the resolution of 25 μm was incapable to resolve activity differences caused by morphology variations. The “islands” and “channels” had average diameters of about 10 μm and 2 μm, respectively. In order to correlate the local distribution of activity with the overall activity of the DSA electrodes, the variation coefficient (C_v) was derived by a statistical treatment of SECM data. By recording all current values measured by means of SECM over three different regions of the same DSA sample, histograms with defined values of the mean (μ) and standard deviation (σ) were plotted to show the current distribution. The standard deviation describes how uniform the distribution of a given set of data is. However, when dealing with different data sets, which have different mean values, the standard deviation has to be normalized with respect to the mean values. Taking for example of two samples, 1 described by μ = -1000 nA and σ = -300 nA, and 2 described by μ = -500 nA and σ = -200 nA, the values of the standard deviationsuggest that sample 2 has a more

uniform current distribution. However, by taking into account the mean values, the standard deviation in case of sample 1 is only 30 % of the mean value while in case of sample 2 it is 40 %. In descriptive statistics, the standard deviation normalized by the mean value is called variation coefficient (C_v = σ/μ) which represents a dimensionless number that offers the possibility to compare data sets with different mean values.

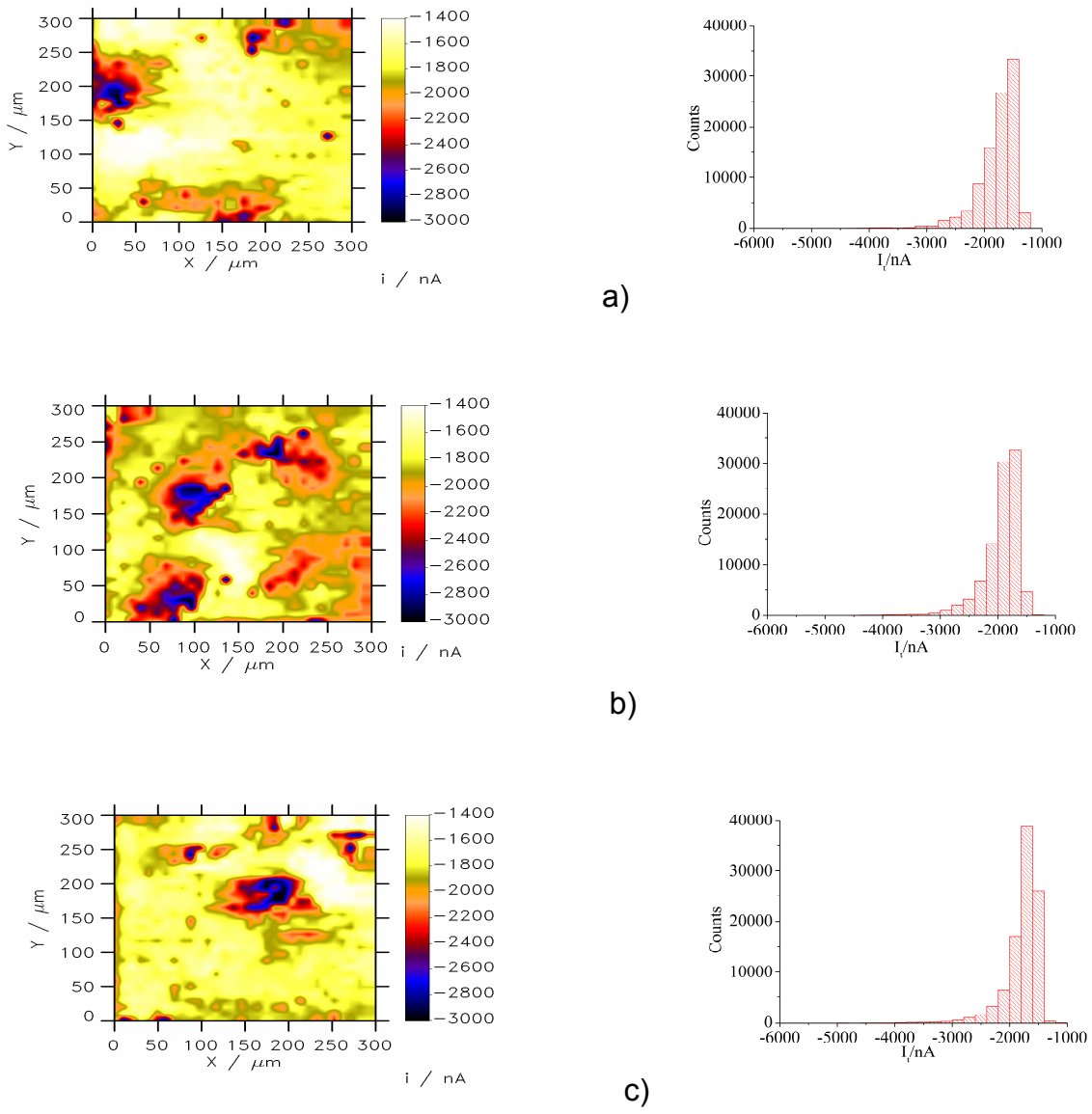

Figure 6.24. Distribution of activity at a DSA surface as expressed in SECM images of the scanned catalyst area (distribution of tip currents in the x, y-plane) and histograms of tip currents measured over the scanned areas with the corresponding values of the calculated variation coefficients for three different spots (for positions a, b, c the variation coefficients are 0.195, 0.171, 0.191, repectively).

To correlate the variation coefficient, extracted from a small section of the scanned catalyst surface, with the activity of the entire sample, it is essential that this small part of the catalyst surface is representative of the entire sample. Statistical evaluation of the distribution of currents over three different scanned regions for one of the tested samples is shown in Figure 6.24.

From the SECM images and the histograms in Figure 6.24 it seems that the scanned areas have very similar distribution of activity. The calculated values of the variation coefficients however reveal that slight variations exist which are spread by around 10 % of the average value for each of the three samples (for positions a, b, c variation coefficients are 0.195, 0.171, 0.191, respectively). This generally suggests that the local electrocatalytic properties of the catalyst layer including fluctuations in composition and morphology are periodically repeated over the entire surface. The local distribution of activity over the small scanned areas (300 x 300 μm^2) is thus representative for the entire sample.

6.4.3. Impact of the distribution of local activity on the overall DSA performance

Four samples of DSA made by the same preparation method having the same catalyst loading however with different number of layers were compared. The corresponding SECM images recorded over an area of 300 x 300 μm^2 are shown in Figure 6.25 representing differences in the local activity of the sample. Their activity trend, b-1 > b-3 > b-2 > b-4, is similar to that of the amperometric curves measured over the entire samples (sample 1 > sample 3 > sample 2 > sample 4). A quantitative correlation between the local distribution of activity and the overall activity was done using statistical and mathematical treatment of SECM data. The most important parameters of the analysis are summarized in Table 6.4.1.

Table 6.4.1. Parameters relevant for analysis of the correlation between macroscopic activity and local microscopic activity of DSA samples. The data were extracted from amperometric curves and SECM data measured for the different samples.

Sample	1	2	3	4
Current density at the sample/mAcm^{-2}	53.1	32.0	35.9	27.5
Current loss (%) at the sample after 900 s	0.255	0.322	0.312	0.455
Mean value/nA (average value of currents measured at the tip)	4507	2706	3095	2332
Standard deviation of currents measured at the tip/nA	735	685	604	700
Variation coefficient	0.163	0.253	0.186	0.300

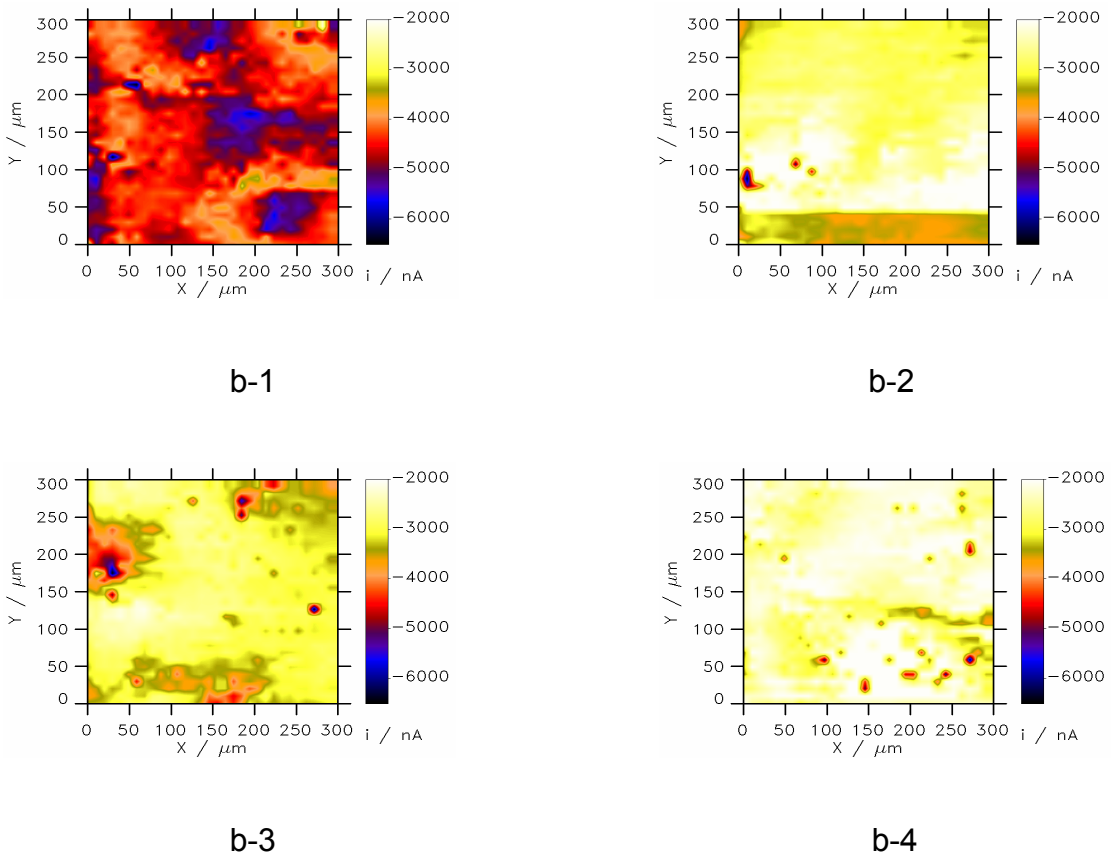

Figure 6.25. SECM images showing the distribution of activity corrected for the collection efficiency of four DSA samples prepared by the same preparation procedure. Sample potential was 1400 mV vs Ag/AgCl, tip potential was 950 mV vs Ag/AgCl. Scanning was performed with increment of 25 µm in 3.5 M NaCl having pH 3 (addition of HCl).

Besides measurement of the overall activity of the samples expressed by means of their current densities, the loss of activity with time of the samples was monitored using the above shown potentiostatic curves (chapter 6.1.1).

Considering the fact that Cl_2 evolution is self-inhibited by the product owing to supersaturation and partial coverage of the active surface area with gas bubbles, the current loss with time (in this case after 900 s), was used as a coarse measure of the stability of the DSA sample. The drop in activity was calculated according to $(I_{max} – I_{min})/I_{max}$, where I_{max} is the current measured at the time t = 0 and I_{min} is the current measured at t = 900 s (chapter 6.1.1). Finally, current density and the drop in current with time were plotted as functions of the variation coefficient. The overall activity of the sample and its activity loss with time are expressed as functions of the local distribution of activity as shown in Figure 6.26.

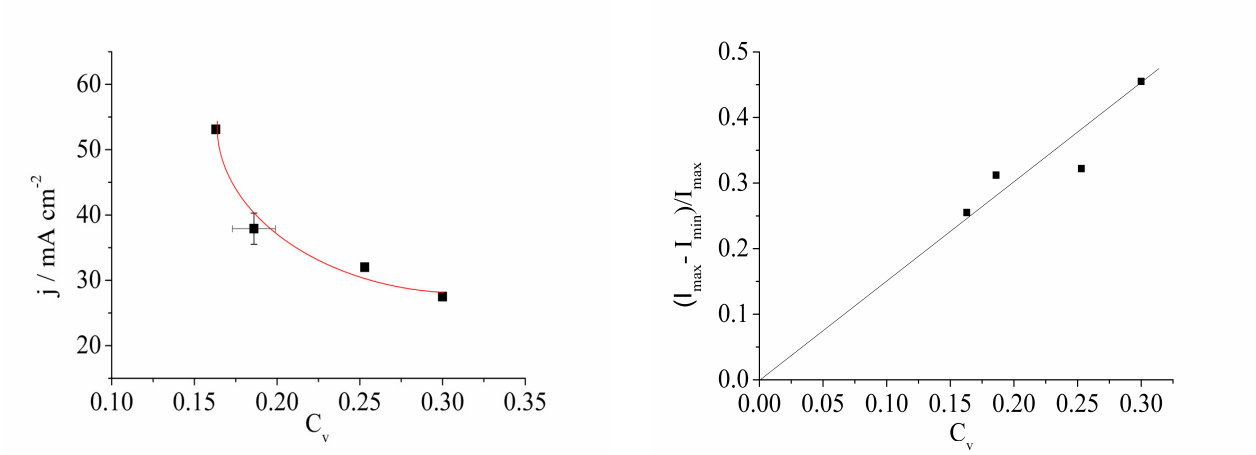

a) b)

Figure 6.26. a) Overall activity of DSA samples expressed as current density against variation coefficient, and b) activity loss with time as a function of homogeneity in activity distribution.

The graphs shown in Figure 6.25 highlight four important points, namely:

1) The intuitive assumption that the spatial distribution of activity influences the overall performance of a catalyst coating was confirmed experimentally by direct local imaging and measurement of activity.
2) The overall activity increases as the distribution of activity becomes more uniform. The dependence is nonlinear with a tendency of a sharp increase for apparently ideally uniform catalysts.
3) The activity loss with time becomes less pronounced when the distribution of activity is more uniform. The dependence is linear with quite an intriguing behaviour when the variation coefficient is extrapolated to zero. At this point the current decay is apparently equal to zero. Although we do not have experimental points in this region of extrapolation, the physical meaning of the dependence is discernible. From the point of distribution of activity, self-inhibition of the Cl_2 evolution reaction manifested through activity loss with time can only be eliminated in idealized cases when the distribution of activity is perfectly uniform.
4) If the sample with the lowest activity (4) is compared with the sample with the highest activity (1), the difference is almost 100 %. On the one hand, this indicates that reproducibility of the catalyst preparation is not straightforward. Control of the properties of the coating especially at the microscale is associated with substantial difficulties. On the other hand, perfect control of the parameters of synthesis reveals a significant potential for improvement of the performance of such coatings. Bearing in mind that the samples used for this study had the same loading and similar chemical composition, the difference in activity between sample 1 and sample 4 suggests that it is possible to increase the activity using the same loading or to achieve a higher activity for the same loading by improving synthesis.

5) A better performance induced by a more uniform detachment of gas-bubbles suggests that gas-evolving reactions are oscillatory systems highly dependent on a characteristic frequency of gas-bubble detachment.

Additionally, the long-term stability of DSA and optimization of their synthesis for better energy consumption was explained on the premise of the distribution of their activity. If it is assumed, arbitrarily, that a catalyst surface is comprised of three regions, '1', '2' and '3', and that the local currents in the three regions increase in the order; region '2' < region '1' < region '3', then the following three inferences arise. If the currents in region '1' fall in the range defined by the standard deviation, then the local currents in this range represent more or less the average activity of the sample. The rate of Cl_2 evolution in these regions is essentially determined by the time interval between the departures of two consecutive bubbles. If this time interval for the regions '1', '2' and '3' are denoted by t_1, t_2 and t_3, respectively, it is clear that this interval time increases in the order $t_3 < t_1 < t_2$.

According to Faraday's law, for a galvanostatic process in an electrochemical reactor the mass of Cl_2 produced with time is constant. The efficiency of the process is estimated by the energy consumed during electrolysis manifested through the operating voltage (or potential). In the region with an activity below the average one, bubbles will stay longer on the surface than on parts of the coating with higher activity. This means that, periodically, the effective surface area of the electrode will be smaller and therefore the current density will be higher. Consequently, the overpotential will be higher and by this the consumption of energy in the reactor is higher. For a region with an activity higher than average, it seems at first that this region may positively influence the overall efficiency. This is however not necessarily true. Based on the fact that the interval time for gas-bubble departure is smallest for this region, it is expected that at certain instants only this region will be active, while the other two will be covered by the gas phase. By this, the overall current will pass through only a small part of the entire surface leading to a locally very high current density. At very high current densities

corrosion of the catalyst coating is imminent. The fact that DSA lose activity with time by various mechanisms [126,144-148] and the fact that the overall current passes through very small elements of the surface (region '3') suggests that accelerated deterioration of the catalyst is expected at spots with higher local activity. From this perspective, it is clear that homogeneous distribution of activity should be strived for, not only for the benefit of improving the activity but also in the interest of energy savings and stability of the anode material.

6.5. Activity trends

6.5.1. Comparative analysis between "cracked and "crack free" electrodes

An important conclusion considering "cracked" DSA samples (chapter 6.1.1) is seen in the possibility to simultaneously decrease the number of active sites and increase the turnover frequency thus improving the overall performance of a DSA sample. By this, energy consumption could be reduced at the same time decreasing the catalyst loading. Thus, a comparative analysis of "cracked" and "crack" free electrodes has to be performed based on the evaluation of the active surface area, the overall activity, the activity normalized by the active surface area and the spatial distribution of the activity. In case of "cracked" electrodes the "crack" width has to be taken into consideration. Trends of such an analysis are shown in Figure 6.27. For the "crack-free" DSA electrodes an increase in the voltammetric surface charge will result in a more uniform distribution of activity, a higher measured current density, but a drop in the turnover frequency (Figure 6.27a).

In the case of "cracked" electrodes the current density and the turnover frequency are dropping with increasing voltammetric surface charge, while the latter one is anti-correlated with the size of the "cracks" (Figure 6.27b).

„Crack-free" electrodes show an improved performance predominantly following an increase in the active surface area. „Cracked" electrodes show an improvement in the performance even if the active surface area is decreasing due to the significant increase in turnover

frequency (dependent on the „crack“ size“). In both cases a more uniform distribution of activity is directly proportional to the current density and TOF is inversely proportional to q*.

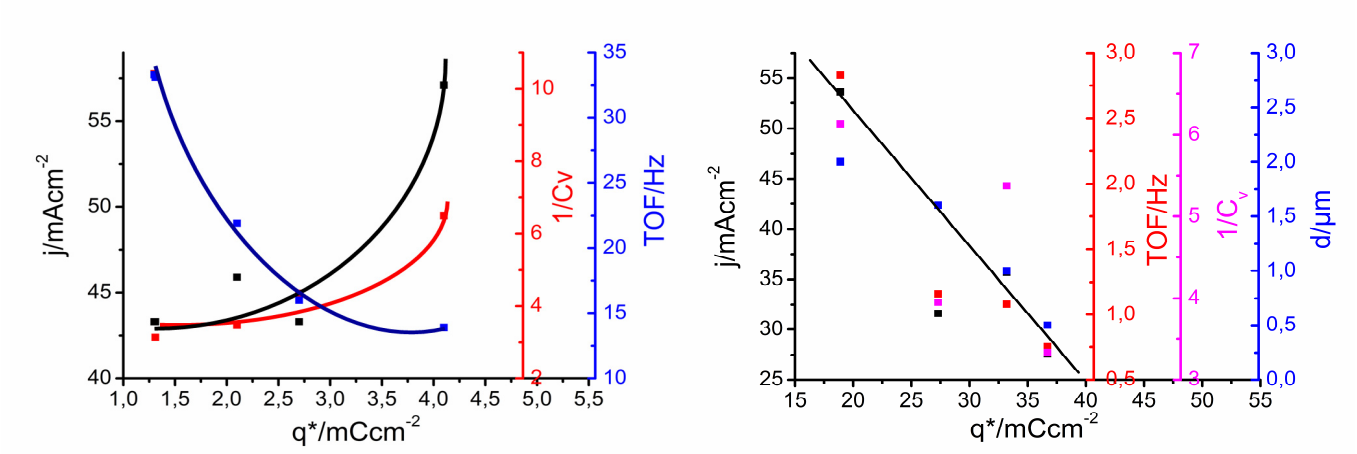

Figure 6.27. Current density, turnover frequency and inverse of variation coefficient expressed as a function of voltammetric surface charge for a) “crack-free” (BDD/RuO_x, FAU) and b) “cracked” DSA electrodes (KINT 710 Standard, BMS). For “cracked” DSA electrodes the voltammetric surface charge is additionally correlated with “crack” width.

By observing the general trends, it becomes more obvious that the most probable reason for a successful performance of “cracked” electrodes is due to the oscillatory behavior of the gas evolution reaction, where the morphological pattern can influence frequency of gas-bubble detachment. Nucleation of the gas-bubble inside the “cracks”, where growth and coalescence are limited allows the formation and departure of comparatively small gas bubbles coupled with a relatively higher gas-bubble detachment frequency.

Further confirmation of the influence of the surface morphology on the frequency of gas-bubble departure is derived from the analysis of morphological patterns of engineered surfaces gradually changing from “cracked” (maximal “crack width” around 0.5-0.7 µm “) towards “crack” free. The maximal “crack” width was substantially smaller than the radius of gas-bubble nucleation at standard conditions.

SEM micrographs of the designed electrodes are shown in Figure 6.28.

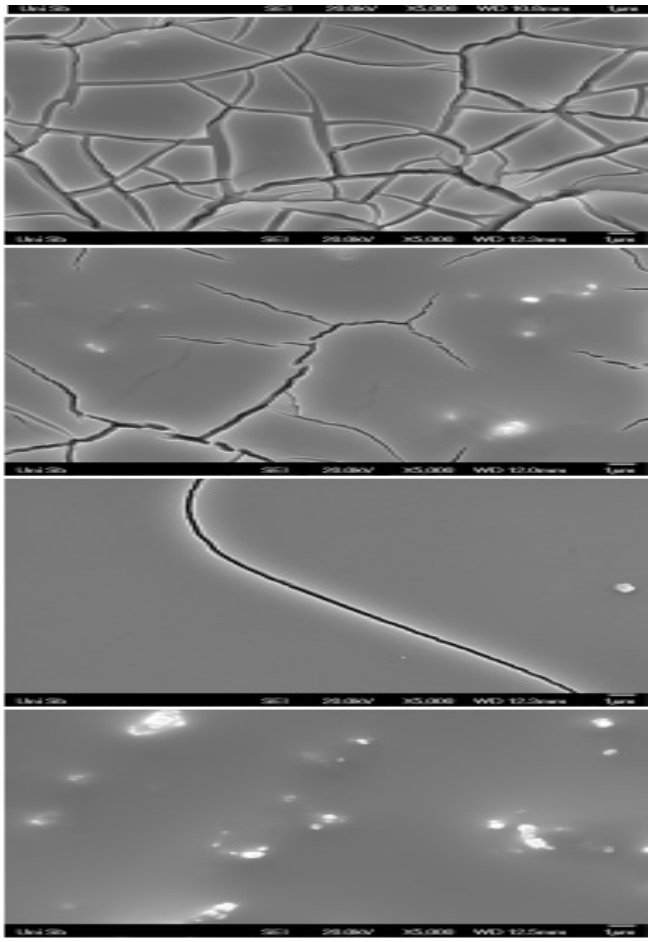

a)

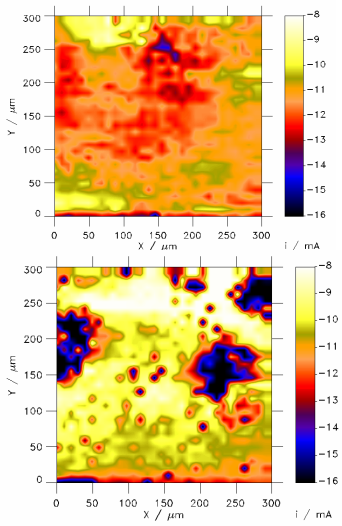

b)

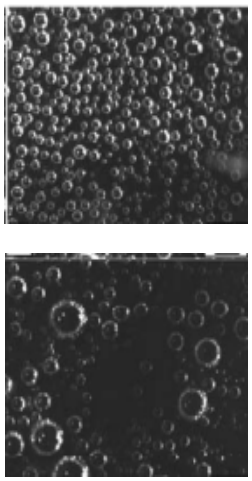

c)

		$(I_{max} - I_{min})$ / mA	C_v (from SECM)
P 164 2	mc	15.5	0.167
P 164 3	rc	17.3	0.184
P 164 4	lc	10.9	0.088
P 164 5	cf	19.9	0.218

d)

Figure 6.28. a) SEM micrographs of gradually changed morphology from “cracked” towards “crack”-free surfaces, b) SECM images of samples P164 4 and P164 5, c) video imaging of gas-bubble behaviour for the samples P164 4 and P164 5 and d) table with current drop and variation coefficents.

The electrodes shown in Figure 6.28 have an almost identical activity in potentiostatic measurements (which is lower than that of the previously studied “cracked” electrodes), while in the galvanostatic regime they slightly differ. In this case, the number of active sites (q*) could not be directly correlated with activity [11,149]. SECM imaging of the distribution of active sites and video imaging of gas-bubble detachment gave a similar picture demonstrating that a more uniform distribution of active sites allows for a more uniform distribution in the size of the gas-bubbles. At the same time, the sample with the most uniform distribution of active

sites (P164 4) had the smallest size of the bubbles. Sample P164 4 showed the lowest drop in activity in time in the potentiostatic regime as shown in the table in Figure 6.28d and at the same time it exhibited the best capability to sustain the potential with increasing current density [11]. This nicely illustrates that the spatial distribution of active sites plays an important role in the overall performance of gas-evolution reactions and that the oscillatory behavior of the bubbles has a strong connection with surface morphology.

6.5.2. Activity trends at semi-industrial conditions

The information gathered using standard electrochemical characterization can help to further improve the understanding of gas-evolution reactions. A comparative analysis of the samples was conducted galvanostatically at a current density of 5 kAm^{-2} and at a temperature of 55°C. Ohmic drop correction was performed using EIS at 100 kHz. The reference electrode in a form of a Luggin capillary was positioned in close proximity of the sample. Under these conditions, distortions of the impedance spectra are expected due to the intensive gas evolution and therefore only a qualitative activity trends were obtained. An example of establishing activity trends (for the KINT 710 samples) at conditions similar to industrial ones is shown in Figure 6.29.

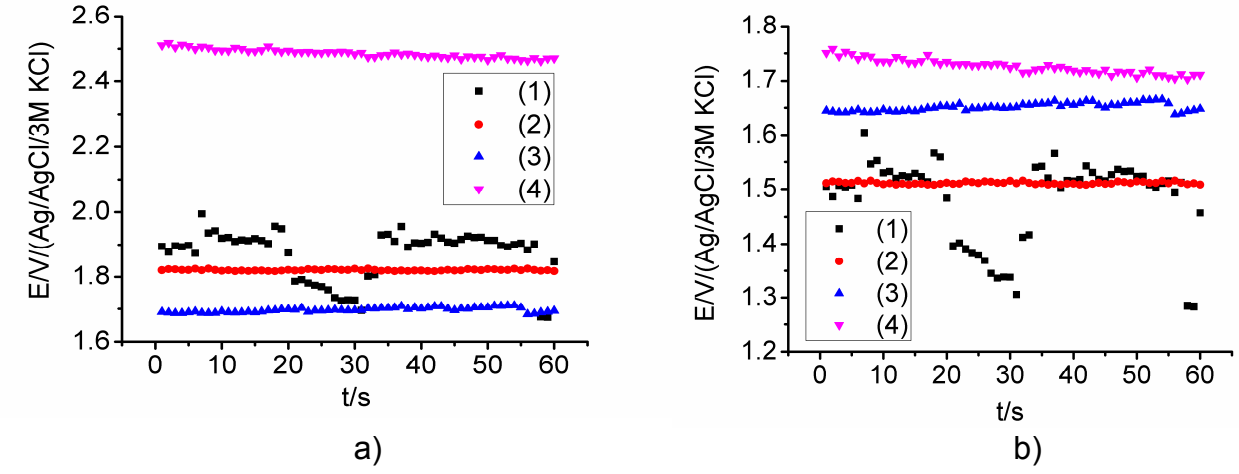

Figure 6.29. Activity trends for the KINT 710 samples in galvanostatic regime at 5 kAm^{-2} and 55°C a) with and b) without ohmic drop correction.

From Figure 6.29 one can see that the activity trend is changing after ohmic drop correction, despite the Luggin capillary was similarly positioned in close proximity of the DSA surface. Obviously, the gas-bubble behavior is different for the samples. Particularly interesting was the behavior of sample 1 (sample with “crack” width of around 2 μm). Fluctuations in activity of sample 1 were significant suggesting an oscillatory behavior. Data describing activity trends for KINT 710 samples are given in Table 6.5.1.

Table 6.5.1. Electrode potentials for the KINT 710 samples at semi-industrial conditions

$j = 5\ kAm^{-2}$	E/V/Ref	R/Ohm	(E-RI)/V/Ref
1	1.871	3.9	1.505
2	1.821	3.1	1.511
3	1.697	0.5	1.645
4	2.487	7.6	1.751

Additionally, impedance spectra were measured (for sample 1) galvanostatically at two different current densities as shown in Figure 6.30. With increasing current density the ohmic resistance is increasing due to the increase in the gas fraction in the electrolyte, which suggests that the ohmic drop correction for a kinetic analysis should be performed incrementally [150]. The polarization resistance is dropping according to the Butler-Volmer equation and the capacitance (with slight fluctuations) stays constant.

Impedance spectroscopy provides tendencies of the changes of the ohmic resistance, charge transfer resistance and capacitance with changing current density. This certainly is valid if there is no significant accumulation of the gas phase at the DSA surface. As shown in Figure 6.28. the EIS are distorted. Consequently, the ohmic drop correction should provide adequate, however, only qualitative activity trends. Furthermore, in real systems the ohmic drop contributes to the overall energy consumption. Therefore, besides comparison of the activities after ohmic drop correction which represents the evaluation of the electrocatalytic

behavior of DSA coatings, the samples were compared additionally without ohmic drop correction. A histogram of anode potentials for the different samples with and without ohmic drop correction is shown in Figure 6.31.

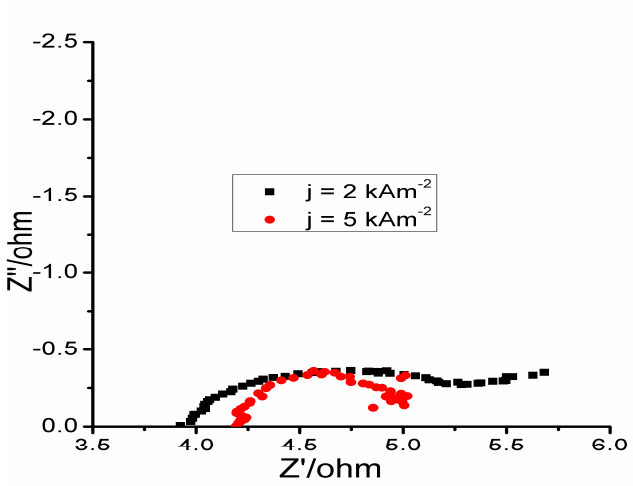

Figure 6.30. Impedance spectra of KINT 710 1 at two different current densities

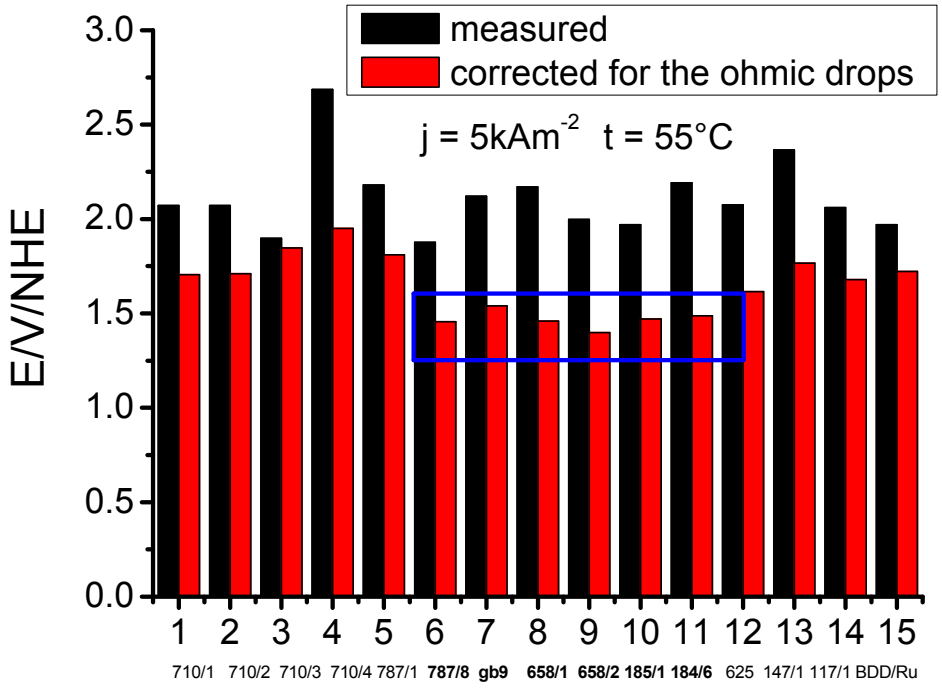

Figure 6.31. Anode potentials for tested DSA with (red bars) and without (black bars) ohmic drop correction given vs NHE

From the point of view of electrocatalysis, samples marked by the blue rectangular (Fig 6.31) are supposed to be the best, but for real applications the ohmic drop has to be taken into consideration.

In a galvanostatic regime the amount of produced Cl_2 is always the same including the gas fraction in the electrolyte. However, if the gas fraction starts to cover the surface of DSA the overpotential will increase due to the increasing current density (according to Tafel's approximation), but even more significant the ohmic resistance will increase. This is confirmed by EIS in which the ohmic resistance and capacitance (as analogue of the surface area) can be observed as function of overpotential (Figure 6.32).

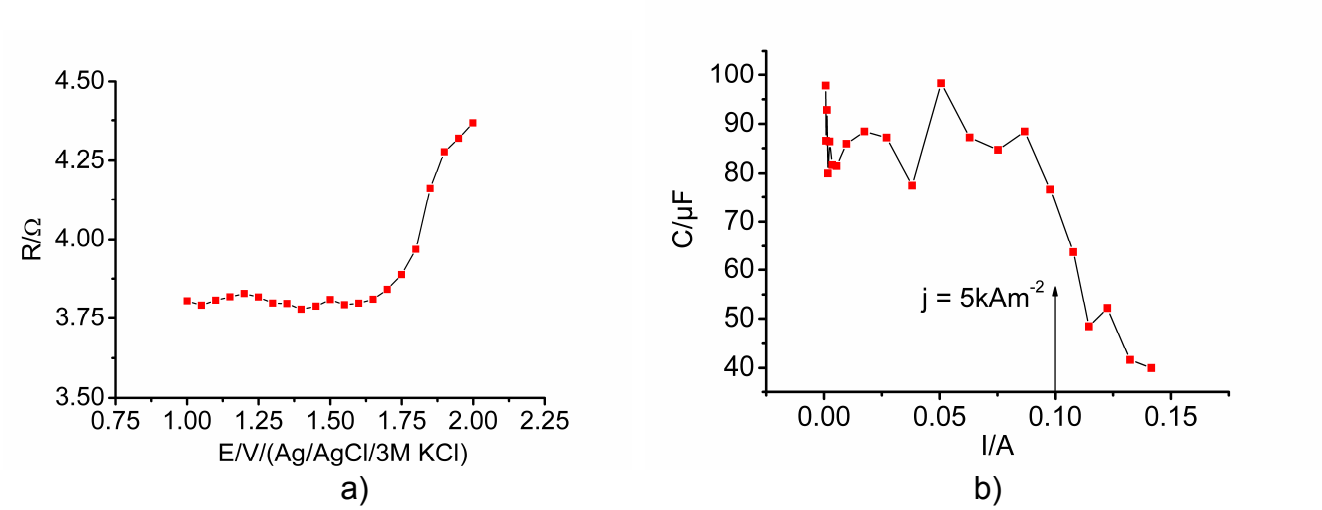

Figure 6.32. a) Ohmic resistance as a function of applied electrode potential, and b) capacitance of the double layer as a function of applied current intensity for defined geometric region of a DSA coating (A = 0.196 cm^{-2})

Figure 6.32 shows that the ohmic resistance starts to grow rapidly at a potential of higher than 1.75 V vs Ag/AgCl (without ohmic drop correction) while the capacitance of the double layer starts to drop at a current density higher than 4.5 kAm^{-2} (similar to the potential of 1.75 V vs Ag/AgCl). This clearly indicates that gas-bubbles are accumulating at the surface. In this sense it becomes even more clear that the frequency of gas-bubble detachment plays a crucial role in the description of gas-evolution reactions particularly at high current densities. The conventional approach is loosing a meaning because both, the ohmic resistance and the

active surface area are dynamically changing with the overpotential, what makes it impossible to estimate the exchange current densities but also the obtained Tafel's slopes due to serious errors in the ohmic drop correction.

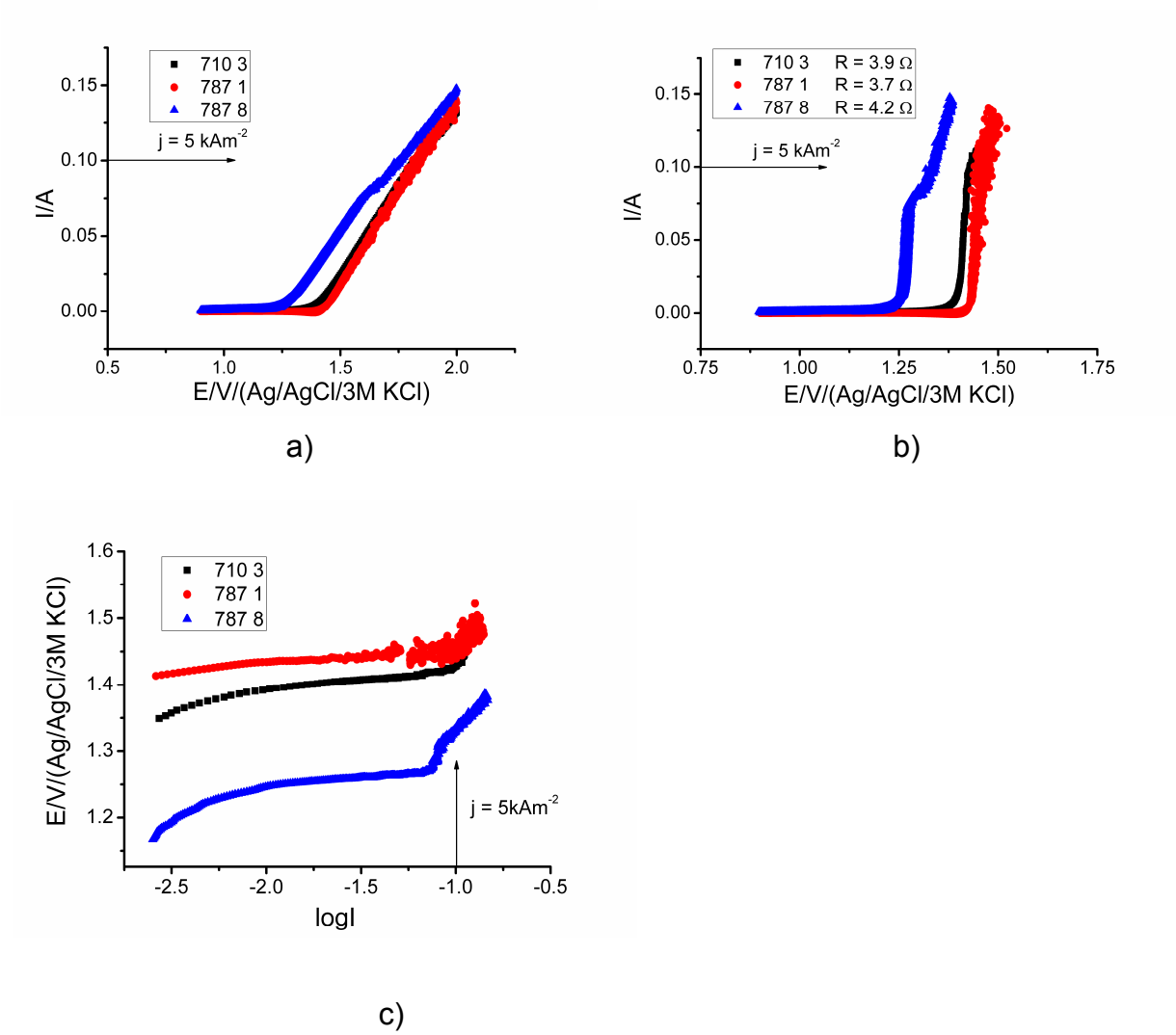

Figure 6.33. a) Potentiostatically conducted linear sweep voltammetry (LSV) with a sweep rate of 5 mV/s on three different DSA samples (at industrial current density). b) LSV corrected for the ohmic drop (ohmic resistances are denoted), and c) Tafel's plots.

In general, linearity of the Tafel's slope can be questioned in case of inner sphere reactions with adsorbed intermediates participating in the reaction [151,152]. In case of CER it is shown (Figure 6.33) that in dependence from the value of exchange current density the Tafel's slope deviates from linearity. In Figure 6.33a the potentiostatic polarization curves for three DSA samples are shown. In Figure 6.33b polarization curves are corrected for the individual ohmic

drops and hence a clear exponential dependence between the driving force (potential) and the rate of the reaction (current density) can be observed. Tafel's plots are displayed in Figure 6.33c.

The Tafel's slopes were around 40 mV/dec however the exact estimation is problematic. The better the catalyst is the more emphasized is the deviation from linearity. This is an additional proof that the usual approach based on extracting kinetic parameters from the Butler-Volmer's equation should be reconsidered for gas-evolution reactions especially at high current densities.

6.5.3. What is the missing parameter?

The intuitive hint that the spatial distribution of activity will influence the overall performance was confirmed above (chapter 6.4.3.). Furthermore, the comparative analysis of "cracked" and "crack-free" electrodes (chapter 6.5.1.) demonstrates that the conclusion about the importance of spatial distribution of activity was valid independently from the analyzed morphological pattern. However, the source of the interdependence between the spatial distribution of active sites and the overall performance are not yet clear.

Certainly there has to be a correlation between the spatial distribution of activity and the magnitude of the active surface area (Figure 6.34).

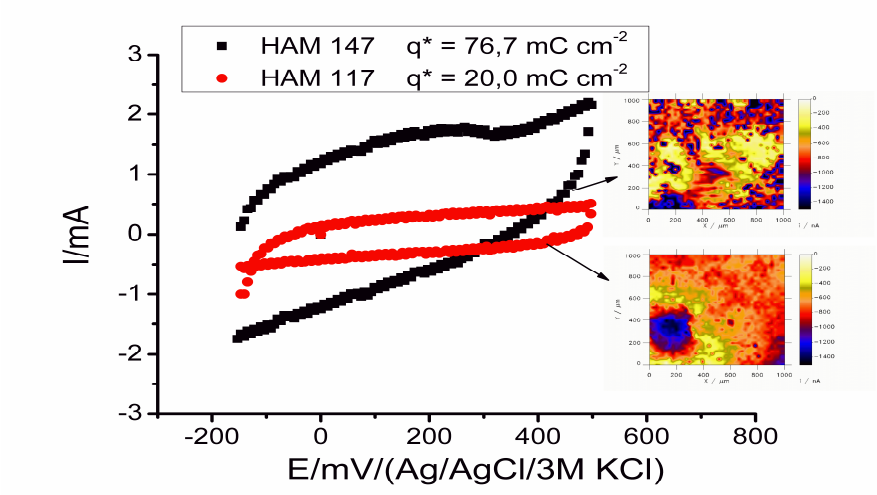

Figure 6.34. Active surface area as a function of spatial distribution of activity

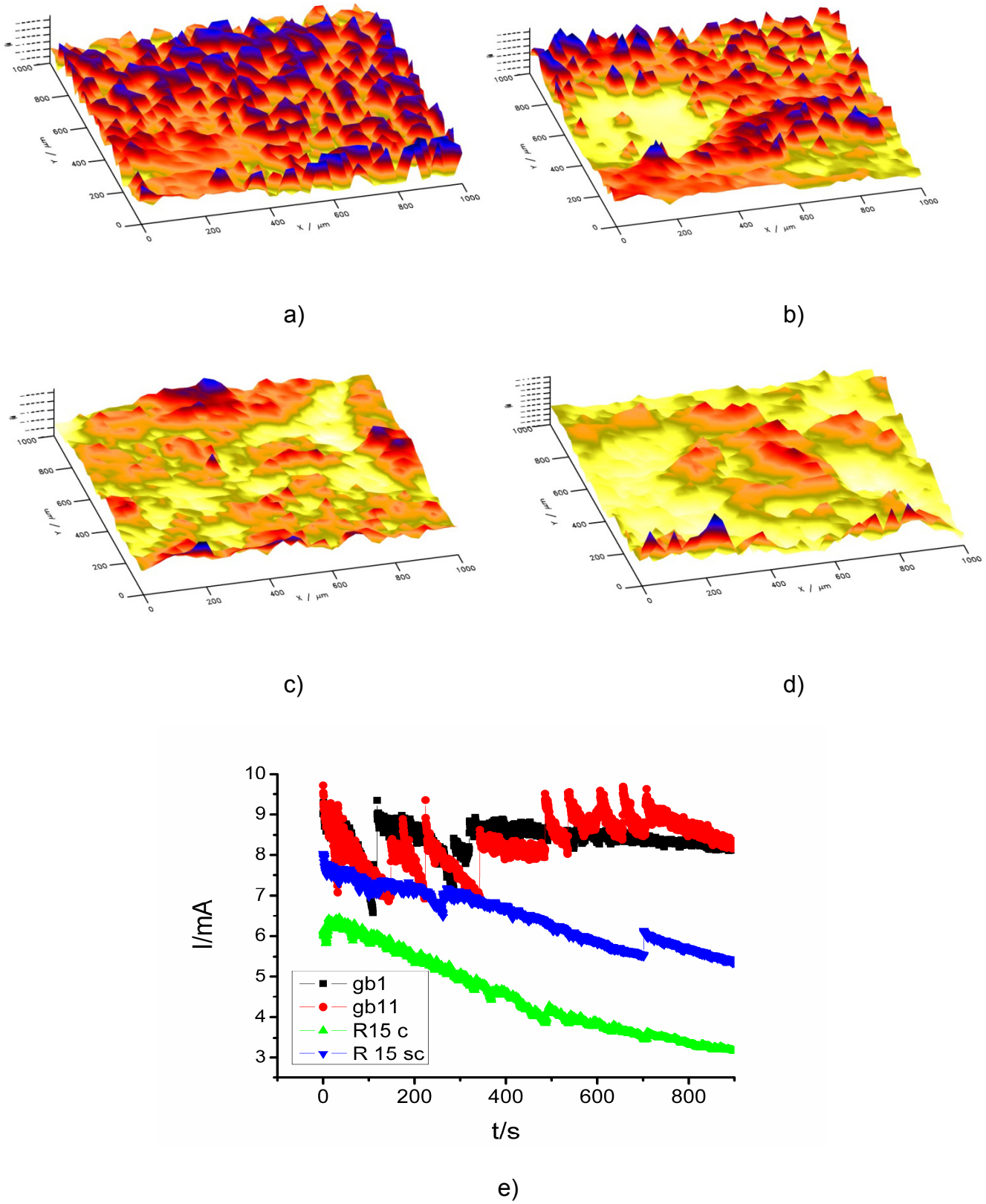

Figure 6.35. Simultaneous monitoring of the spatial distribution of active sites and the current decay in time; a) sample gb 11, b) sample gb 1, c) sample R 15 sc, d) sample R 15 c and e) current decay during 900 s.

From Figure 6.34 it is evident, that the magnitude of the surface area given by area of the CV depends on the distribution of active sites. Consequently,the magnitude of the active surface area influences the overall activity. However, the activity drop with time cannot be directly correlated with the magnitude of the active surface area. To put some light in this direction it is instructive to analyze simultaneously current response and local distribution of active sites of the 4 different samples (Figure 6.35.)

From Figure 6.35 one can observe that the sample with the most uniform distribution of activity (gb 11) has the best performance and does not show any current decay. Comparing further SECM images of individual samples with current responses in Figure 6.35e it is obvious that the less uniform the activity distribution becomes the more emphasized is the loss in the activity with time.

Probably the most adequate approach is to consider gas-evolution reactions as an oscilatorry reactions. Oscilatorry systems are characterized by a periodical transformation of potential into kinetic energy (and vice versa). During CER, electrical energy is transformed into chemical energy. The produced chemical species should periodically, with a characteristic frequency, leave the interface in form of a detached gas-bubble. The current response in Figure 6.35e suggests that the reaction at the samples with non-uniform distribution of activity behave like damped oscilations. The current signal fluctuates but with a constant decay (Figure 6.35 c,d)

In case of DSA samples with a uniform distribution of active sites the current also fluctuates but it stays at an almost constant mean value (Figure 6.35 a,b).

Introducing the time coordinate additionally increases the complexity of the analysis. It is necessary to find a method to extract the characteristic frequency of gas-bubble detachment at different electrode potentials. In case of reactions with distinct current decay it would be also important to obtain time resolved frequency spectra. However, following the experimental

fact that good coatings behave pseudostationary with no current decay it seems to be sufficient to find a modus to obtain a potential dependent frequency spectra.

6.6. Evaluation of catalytic performance of gas evolving electrodes using local electrochemical noise measurements

In this chapter, electrochemical noise measurements by means of SECM were used to characterize CER. All previously mentioned conclusions were in direction of the assumption that the frequency of gas-bubble detachment is a crucial parameter for the macrokinetics of gas-evolution electrodes (GEE). However, the frequency of gas-bubble detachment was not determined previously. Analysis of the electrochemical noise acquired using the SECM microelectrodes appeared to be a powerful method to evaluate the efficiency of the catalyst layer at GEE. High sensitivity (in the nA range) of the developed measurement system enables accurate monitoring of current fluctuations caused by gas bubble detachments from the electrode surface. Fourier transform analysis of the obtained current responses allows the determination of the characteristic frequency, Furthermore, the point of transition from an oscillatory towards a more stochastic performance was detected using potential dependent frequency spectra and finally the information about the characteristic frequency was used as a part of a methodology to evaluate the catalyst performance and, in particular, to estimate the fraction of the catalyst layer which is active during gas evolution.

6.6.1. Local electrochemical noise measurements

The choice of an in-situ technique, which is available to characterize gas-evolution process and evaluate the efficiency of the catalyst layer is very limited. Experiments based on classical electrochemical noise measurements [148] or electrochemical quartz crystal microbalance [154,155] do not allow a straightforward estimation of the characteristic

frequency. Although the introduction of a digital camera [142] allowed the observation of individual gas-bubbles directly, a quantification of the results appeared to be problematic.

Complexity is introduced to the analysis by a gas fraction at the electrode/electrolyte interface, which causes periodic or random changes in the number of the available active sites.

SECM-microelectrodes are proposed as a tool to monitor fluctuations of the current caused by the gas bubble evolution. Using SECM, the characteristic frequency can be easily extracted using fast Fourier transformation (FFT) of the noise signal.

If SECM microelectrodes are used to estimate the frequency of gas bubble detachment, a number of requirements should be taken into account. The first important requirement is that the microelectrode should be positioned close to the DSA surface, at a distance of approximately 1 µm. In this case, all current fluctuations caused by fluctuations of the electrolyte resistance (triggered by the gas bubbles) can be monitored. If a microelectrode is placed far away from the surface, the sensitivity decreases due to e.g. dissolution of the gas in the electrolyte during the convection from the solid/liquid interface towards the gas phase located above the electrolyte. A second important requirement is that the microelectrode should be located at a side of the sample which is opposite to the reference electrode as shown in Figure 6.36. In this case, the measured electrochemical noise is representative for the entire sample and and all spatial fluctuations in activity will be included into the analysis.

The SECM setup for electrochemical noise measurements (shown in Figure 6.36) uses detection principles described before (chapter 6.2.). Briefly, Cl_2 generated anodically at the sample is reduced cathodically at the tip. Mean values of the tip current as well as the current fluctuations are a function of both time and the potential of the sample (see examples in Figure 6.37). A general expectation is that with increasing potential at the sample, the frequency of gas bubble detachment and the radius of gas bubbles also increases. This can be recognized by an increasing mean value of the tip current and the corresponding residuals

of standard deviations. At the same time taking into account the experimental setup (Figure 6.36), it should be possible to extract the characteristic frequency of the gas bubble detachment from the signal recorded at the microelectrode tip rather than at the sample itself. This is due to the fact that tip current values are rather small and hence very sensitive to fluctuations of the ohmic resistance caused by gas bubbles leaving the surface.

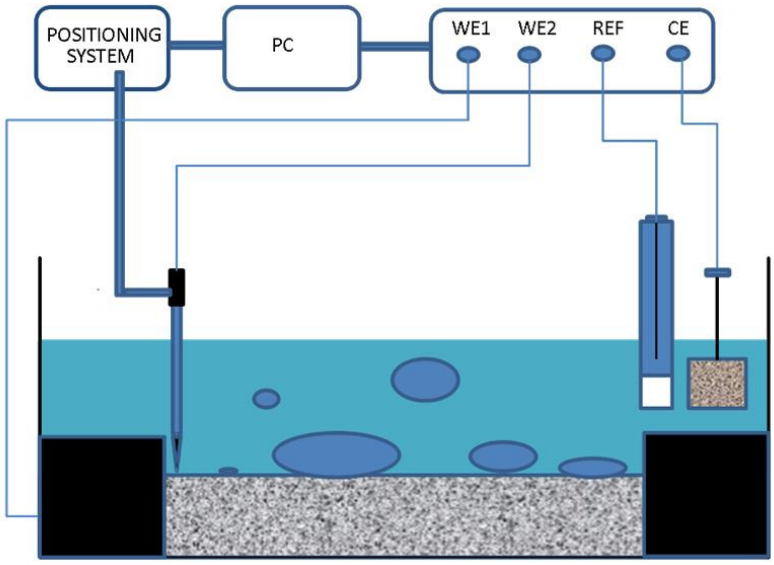

Figure 6.36. SECM setup used for electrochemical noise measurements

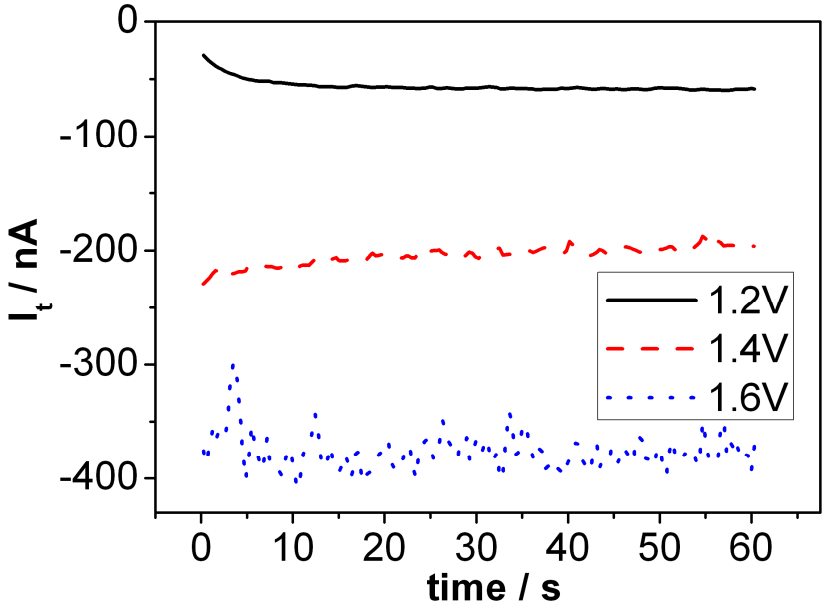

Figure 6.37. Examples of the electrochemical noise measured using the SECM setup at a microelectrode at different potentials applied to the DSA. The potential of the tip was 0.95 V *vs* Ag/AgCl/3M KCl reference electrode.

In the potentiostatic regime, the electrode potential is a sum of the reversible potential, overpotentials and ohmic drops as given by equation 6.6.1:

$$E = E_{rev} + \eta + RI \qquad \textit{Equation 6.6.1.}$$

As a first approximation, it can be assumed that the reversible potential (E_{rev}) and the overpotential (η) are constant due to the fact that they originate from thermodynamics and kinetics of the reaction itself. To sustain the constant potential conditions, the term which describes the ohmic drops has to stay constant as well. The gas bubble detachment would increase the amount of gas in the electrolyte and consequently, the ohmic resistance between the microelectrode and the reference electrode will fluctuate, depending on the frequency of bubble release and the amount of gas. The equation which describes the dependence of the resistivity (ρ) from the gas fraction in the electrolyte (ε_g) is given in equation 6.6.2 [37]:

$$\rho = \rho_o (1 - \varepsilon_g)^{-3/2} \qquad \textit{Equation 6.6.2.}$$

All changes in the electrolyte resistance will be compensated proportionally by the current and hence the term RI in Equation 6.6.2 remains constant. Figure 6.37 illustrates the fact that the increase in the overpotential of the sample leads to an increase of mean values and corresponding deviations of the tip current leading to a higher supersaturation and a more intensive gas bubble evolution from the DSA surface. To extract the characteristic frequency of the gas bubble detachment from the DSAs, it is necessary to transform the current signal of the tip into a frequency spectra using e.g. a fast Fourier transform (FFT) algorithm.

6.6.2. Linking surface morphology with potential dependent frequency spectra

Considering electrochemical Cl_2 evolution from highly concentrated chloride solutions, super-saturation of the electrolyte layer at the electrode surface with the product is a prerequisite to form gas bubbles. On the other hand, the time which is necessary to reach supersaturation, depends on intrinsic electrocatalytic properties of the electrode material as well as on the number of active sites exposed to the electrolyte.

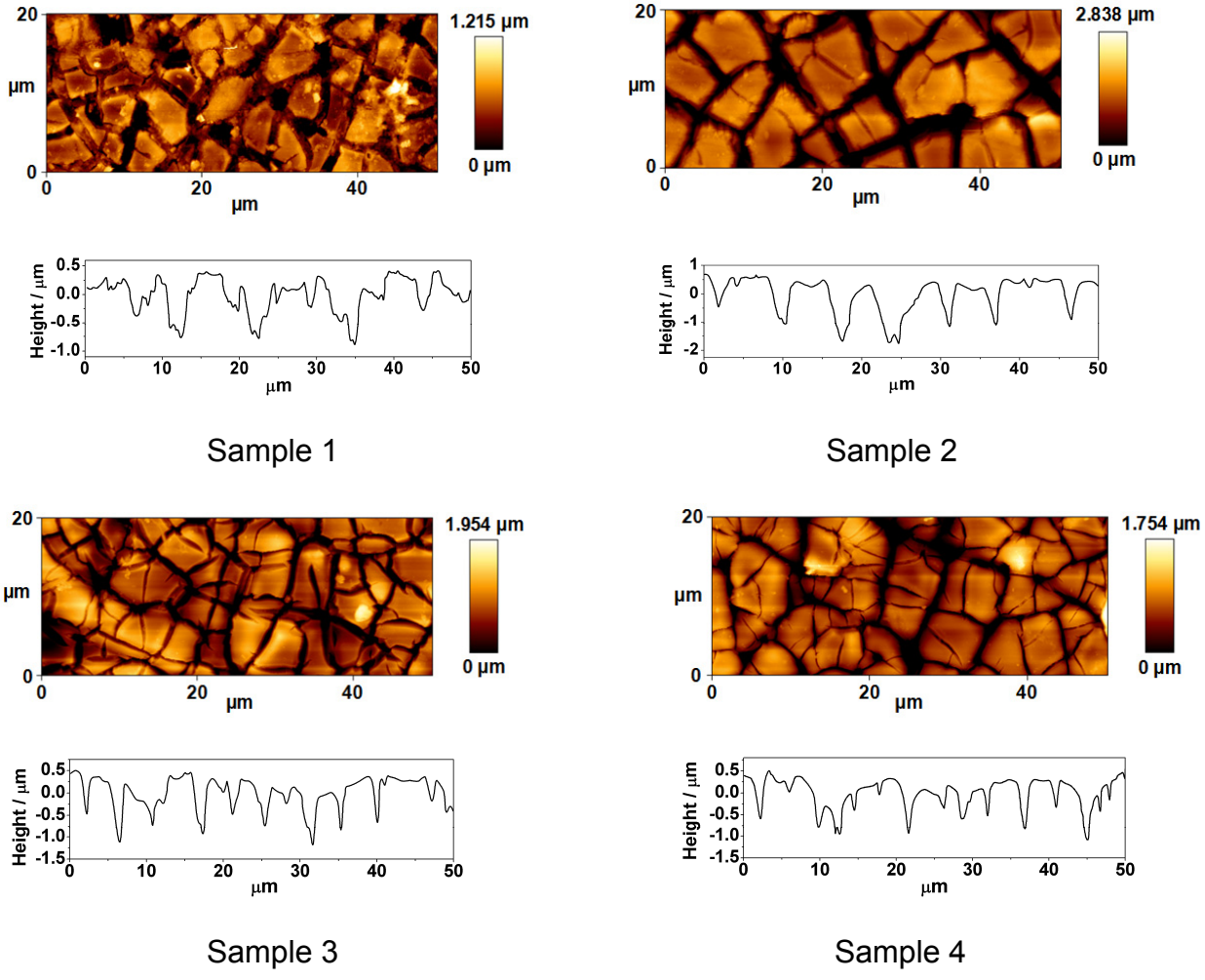

Figure 6.38. AFM micrographs with cross sections of four commercial DSA samples made from the same material.

After reaching supersaturation at a constant overpotential, nucleation starts followed by the growth and finally detachment of the gas bubble. If we accept that (i) the material of DSAs, (ii) chemical composition and (iii) thermo-physical properties of the electrolyte do not change and

are determined by the experimental conditions, an efficient removal of the gas bubbles from the electrode surface would depend predominantly on the contact angle.

Figure 6.38 shows morphological features of the surfaces of four commercial DSA samples developed for Cl_2 evolution in aqueous electrolytes. Surfaces of all these samples demonstrate so-called “mud-crack” morphological patterns consisted of “islands” and “cracks”. The difference in the thickness of the catalyst layers can be compared using cross sections of AFM pictures (also shown in Figure 6.38). It is evident from Figure 6.38 that the DSA samples have different size of “cracks” which can be interpreted as a sort of macro-porosity.

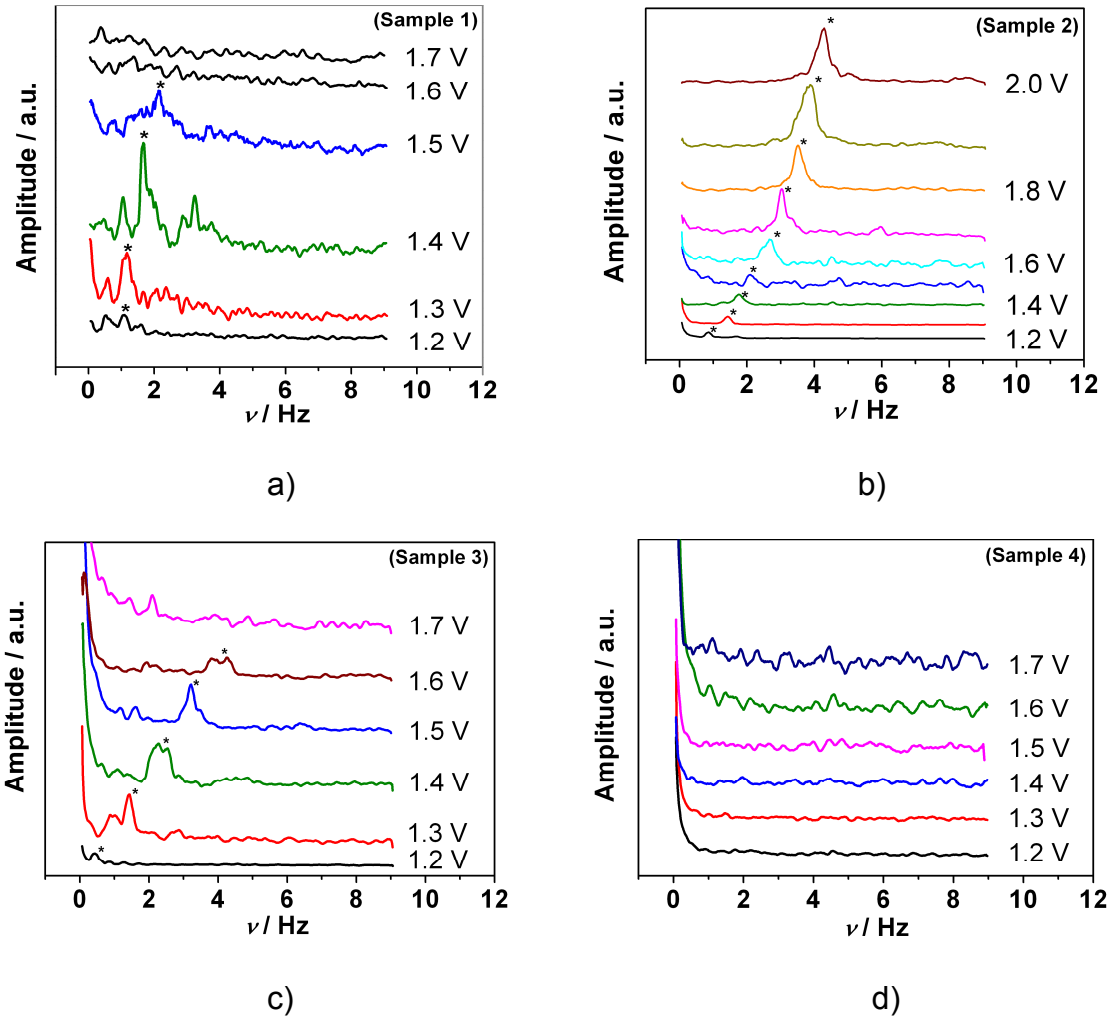

Figure 6.39. FFT amplitude spectra for four DSA samples at different electrode potentials. FFT was applied to the amperometric responses recorded at the SECM microelectrode (the duration of the measurements was 60 s in each case).

Each of the samples was characterized using local electrochemical noise measurements in the SECM setup with intention of recording potential dependent frequency spectra. Figure 6.39 shows the amplitude spectra obtained from FFT of the corresponding electrochemical noise signals for the four DSA samples prepared from the same catalytic material. *A priori* expectations about the electrochemical Cl_2 evolution suggest that the increase of the electrode potential would shift the characteristic frequency of gas-bubble detachment towards higher values. In addition, the potential range in which this frequency shift can be detected is different for different samples (Figure 6.39). For sample 4, it was not possible to extract a characteristic frequency at all. In the case of sample 3, the characteristic frequency shifts towards higher frequencies in the potential range between 1.2 V and 1.6 V, while for the sample 1 the frequency shift is observed between 1.2 V and 1.5 V. For the samples 1 and 3 the transition from a “quasi-periodic” towards a “non-periodic” behavior occurs at around 1.6 V and 1.7 V, respectively (Figure 6.39a and 6.39c). It was previously observed that at a certain overpotential a quasi-periodic mode of the electrode performance disappeared [155-157]. This phenomenon reflects the importance of choosing an adequate operational regime, where the system functions at the highest possible characteristic frequency before the transition to a more stochastic regime. If the operational mode is defined, optimization of surface morphology would provide an opportunity to achieve the appropriate characteristic frequency.

In case of sample 2, the characteristic frequency was observed between 1.2 V and 2.0 V (Figure 6.39b). It is worth to notice that in case of sample 2 the peaks at the characteristic frequency are very pronounced and indicate a very uniform dynamic behavior of the surface in comparison with the samples 1, 3 and 4.

To finally prove that the frequency of the gas bubble evolution is the crucial parameter of macrokinetics of gas-evolving electrodes, the overall activities of the samples were correlated with the corresponding characteristic frequencies. It is important to emphasize that the microelectrodes were positioned randomly over the sample surface in the region, which is

opposite to the reference electrode, as shown in Figure 6.35. Figure 6.40a compares the overall and some local activities of the four commercial DSA samples at a sample potential of 1.4 V. The following ranking for the overall activities of the samples is: sample 3 > sample 2 > sample 1 > sample 4. Figure 6.40b shows the corresponding FFT amplitude spectra of the current recorded at the SECM tip at a sample potential of 1.4 V. Changes in the characteristic frequencies correlate with the *overall* activities of the samples (Figure 6.38) despite the fact that the local currents measured at the tip were not representative for the overall sample currents. This is a clear sign that the determined characteristic frequency originated from fluctuations caused by gas-bubble departure at the sample surface which was not significantly influenced by the mean value of the tip current itself.

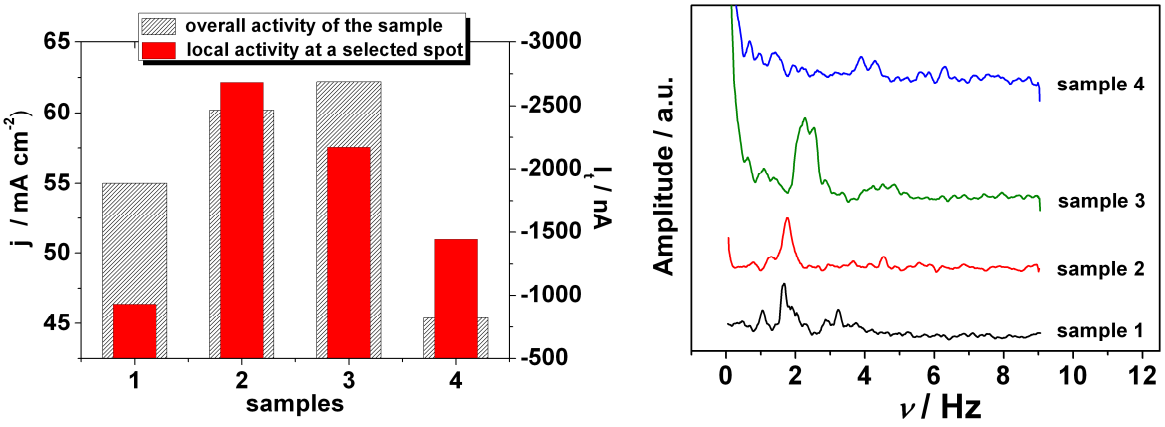

a) b)

Figure 6.40. (a) The overall activity for the four commercial DSA samples (grey bars) compared with the corresponding local activities at random spots evaluated using the current recorded at the SECM tip (red bars). (b) Corresponding FFT amplitude spectra of the currents recorded at the SECM tip for the four samples (potential of the samples 1.4 V). Notice the absence of a pronounced characteristic frequency for sample 4 in (b).

Different activities of the four DSA samples made from the same material suggest that geometrical effects, namely morphology and active surface area, have a significant influence on the performance of the GEEs.

The impact of macropores as well as the possible impact of the thickness of the catalytic layer on the gas evolution at the electrode surface was previously analyzed [92,93,103,143].

According to [143], the size of “cracks” (or macropores) significantly influences the turnover of gas bubble removal from the surface. The size of the macropores, which is similar to the critical size of the gas bubble formation, promotes the efficiency of DSA. At the same time, the thickness of the catalyst coating influences both the critical potential for the gas bubble nucleation and the ohmic drop in the anode itself [103]. Both parameters are equally important for the overall catalyst performance. The influence of the thickness of the coating on the ohmic drop is the reason why the standard procedure for ohmic drop correction was not applied. The approach was to position the reference electrode always at the same distance from the DSA and from the tip to assure that the ohmic drop through the gas-free electrolyte was the same. At operational conditions the resulting signal would be influenced by both the ohmic drop through the electrolyte in presence of gas bubbles and through the anode itself.

6.6.3. Functionality of the oxide catalyst layer

The information about the characteristic frequency is used for the estimation of the catalyst coating efficiency. The evaluation of the GEE catalyst efficiency was only attempted in few studies [99-101]. While in [99] an accurate estimation of kinetic rate constants was difficult, [100,101] presented some results (for example calculation of the roughness factor) based on the results from [99]. Both approaches used Zn^{2+} adsorption for the estimation of the electrochemically active surface area. As the nature of the active sites for Zn^{2+} adsorption at the surface of the DSA is questionable this technique was not applied here.

Essentially, if the intention is to estimate which part of the catalyst coating participates in the reaction at a constant overpotential, a reasonable reference point is needed. As already shown above voltammetric surface charge was used as a measure of the electrochemically active surface area using the concept based on protonation/deprotonation of RuO_2, as deprotonation of water, most probably, is a first step in the reaction path of Cl_2 evolution. The

concept is explained elsewhere in details [96,97]. Briefly, the reversible exchange of protons with the solution allows an indirect estimation of the number of Ru centers (Reaction 15). Partially hydrated Ru-oxide consists of a non-stoichiometric rutile phase which allows a transition towards the higher oxidation state of Ru (and *vice versa*) releasing protons into the solution.

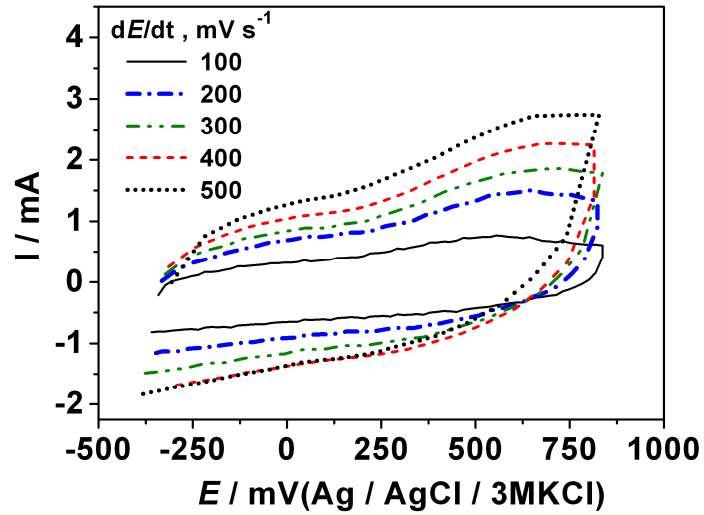

a)

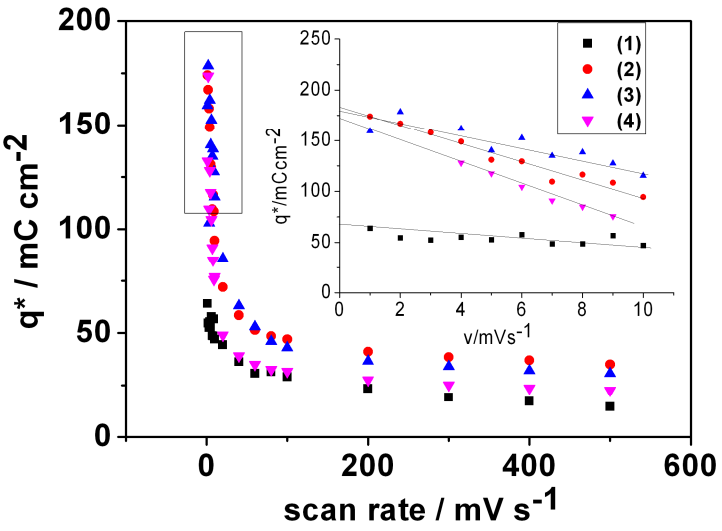

b)

Figure 6.41. (a) Examples of cyclic voltammograms of a DSA samples in 5 M NaCl at pH = 2 (HCl is added) at different scan rates. (b) Voltammetric surface charge as a function of the scan rate for the DSA samples. Inset: Dependence of the voltammetric surface charge on the scan rate for small d*E*/dt values.

The charge which is necessary to conduct this kind of process is proportional to the applied potential. In this work, the potential was cycled within the water stability region at different scan rates to obtain the dependence between the voltammetric surface charge and the scan rate. Extrapolating the voltammetric surface charge to the scan rate d*E*/dt = 0 represents a situation at which protons could diffuse from (or into) inner parts of the coating. The extrapolated surface charge would then be representative, with a reasonable approximation, for the entire electrochemically active surface.

Figure 6.41a presents examples of cyclic voltammograms taken to estimate the electrochemically active surface area of the DSA samples.

The voltammetric surface charge was estimated by taking half of the value of the integral under the voltammograms divided by the corresponding scan rate and geometric surface area. The dependence of the voltammetric surface charge on the scan rate is plotted in Figure 6.41b. The shape of the curves corresponds to those previously reported [96]. For the extrapolation the linear parts of the at lower scan rates as shown in Figure 6.41b were used. The values of the overall voltammetric surface charge were used as the reference points for further estimations of the efficiency of the catalyst coating.

The following questions arise: (i) What is the effective charge passing through the interface at the active sites during the average bubble turnover at a certain overpotential. (ii) What is the fraction of the surface which is responsible for the major catalyst activity? A realistic approach should consider the situation that the current density, which is measured at a certain overpotential, depends on the frequency of the gas bubble detachment from the catalyst surface. One has to take into consideration that bubble formation/detachment can proceed with different frequencies at different active centers. From this point of view, it would be more reasonable to normalize the measured current density by the characteristic frequency of gas-bubble detachment. The approach can be described using Equation 6.6.3:

$q_v = j/v_b$ *Equation 6.6.3.*

where j is the current density at the sample at the applied potential and v_b is the frequency of gas-bubble detachment at the applied potential. Therefore, q_v represents the normalized charge which is involved into the bubble turnover under the assumption that the measured overall sample current mainly originates from the active sites operating at the characteristic frequency only.

This normalization takes into account that the measured current density (calculated with respect to the geometrical area of the sample) can originate either from the high frequency of gas bubble detachment at few active sites or from highly effective surface areas where the active sites are evenly distributed. The increase in the current density can be proportional to or faster than the increase in the frequency of gas-bubble detachment. If the increase in current density is faster than the increase in frequency of the gas-bubble detachment, it is likely that the effective surface area increased too. The effect of enlargement of the effective surface area is typical for GEEs [141]. When the overpotential increases, inner parts of the catalyst coating start to participate in the reaction (this is opposite to gas consuming electrodes, where inner parts of the coating are gradually excluded from the reaction when the overpotential increases). A theoretical background for this experimental fact is derived from surface physics namely the Young-Laplace equation (Equation 6.6.4):

$\Delta p = (2\sigma \cdot \cos\theta)/r$ *Equation 6.6.4.*

where Δp is the pressure difference across the electrolyte interface, σ is the surface tension of the electrolyte, r is the radius of the pore, and θ is the contact angle.

If an electrolyte wets the surface completely ($\cos\theta = 1$), the pore size depends on the pressure difference across the electrolyte interface. For gas evolving electrodes this difference increases with increasing overpotential (while for the gas consuming electrodes it is opposite). These simple considerations confirm a big importance of the porosity for utilization of the catalyst coating.

Arbitrarily assuming that each Ru catalytic centre should contribute equally to the gas evolution, it is possible to estimate the part of the layer which is actively involved into the reaction. This can be done by comparing the normalized turnover charge, q_v, which passes through the interface at a certain overpotential, with the overall voltammetric surface charge, q*. The corresponding parameters are given in Table 6.6.1.

Table 6.6.1. Estimated utility of the layer (q/q*) at the potential of the samples of 1.4 V

Samples	q*/ mC·cm^{-2}	*j* / mA·cm^{-2}	*v* / Hz	q_v / mC·cm^{-2}	utility,%
1	68.1	55.1	1.68	32.8	48.0
2	182.8	60.2	1.77	34.0	18.6
3	179.1	62.2	2.30	27.0	15.1
4	172.5	45.4	-	-	-

As was previously mentioned, it was not possible to extract a characteristic frequency for sample 4. Consequently, this sample was excluded from further analysis.

Figure 6.42 shows the estimated utilisation of the DSA catalyst coating as a function of the applied potential for the three DSA samples.

The samples demonstrate different utilization of the surface area as a function of the electrode potential (Figure 6.42). For samples 1 and 2 an increase in the potential causes the reaction to penetrate into the inner parts of the coating, while for sample 3 the utilisation of the coating remains the same in a wide potential range.

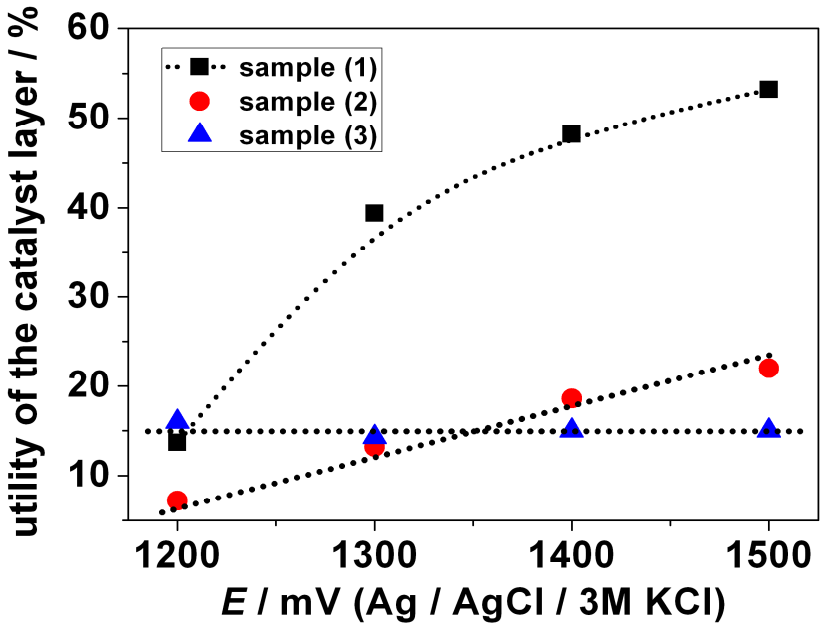

Figure 6.42. Estimated utilisation of the catalyst layer as a function of the applied potential for DSA samples

From AFM measurements (Figure 6.38) one can notice that samples 1 and 2 had larger "cracks" sizes (macropores) as compared with sample 3. If one compares samples 1 and 2, despite the fact that sample 2 has larger macropores, the utilisation of the sample 1 is better. This can be attributed to the smaller thickness of the layer, as also shown by AFM in Figure 6.38. Sample 2 shows an increase in the utilisation while the utilisation of sample 3 is constant despite sample 2 has a larger layer thickness as compared with sample 3. This suggests the possibility for optimization of the catalytic activity based on the pore size and the thickness of the catalyst layer. The AFM images ((Figure 6.38) together with the potential dependent FFT amplitude spectra (Figure 6.39) strongly suggest that adaptation of the morphology offers a great potential for the improvement of the efficiency of GEEs. Proper structuring of the surface of GEEs results in an increase in the effective surface area, and correspondingly, in smaller overpotentials. In this way, it is possible to increase the amount of product with disproportionally smaller consumption of energy in electrochemical reactors.

The developed methodology provides an opportunity to monitor changes in the characteristic frequency and establishes links between surface morphology and the overall catalytic

performance of GEEs. Achieving the highest possible characteristic frequency by designing the morphological patterns is essential for industrial applications. From a fundamental point of view, monitoring the characteristic frequency and linking this parameter with the surface morphology would be beneficial to understand the impact of the gas phase formation at the electrode surface on the overall kinetics of gas evolution reactions.

In summary SECM tips were advantageously used as tool to determining the characteristic frequency of gas-bubble detachment.. The size of the macropores influences the magnitude, potential dependence and uniformity of the observed characteristic frequencies for gas-bubble detachment. The size of the macropores determines whether the reaction penetrates into inner parts of the coating, while the thickness of the layer influences the degree of penetration. It is important to notice that the developed methodology is principally suitable to investigate other GEE such as water electrolysis due to a great similarity between Cl_2 evolution and O_2 evolution. Geometrical factors are very important to improve the efficiency of GEEs. This is especially significant when classical electrocatalysis cannot offer improved materials and compounds that are superior to the state-of-the-art ones.

However, despite electrocatalysis in case of CER can provide a modest reduction in overpotential, selectivity of CER is of mayor importance. It could be demonstrated that it is possible to gain insight into the functionality of the catalyst layer at different working regimes and moreover that very often parts of the catalyst layer are not in use. The reason why coatings are sometimes very thick (close to 5 µm) is due to the oxidation of RuO_2 into nonstable higher oxidation states caused by anodic activation of water which is an integral part of OER. Deterioriation of the catalyst layer due to intensive oxidation processes is the reason why thick coatings, despite their low effectiveness, are produced. Interesting is that according to [8] selectivity should be at least 97 %. Practically, very selective DSA coatings collapse because of only a few percents of charge are consumed for OER. From this point of view, it is worth to perform an in-depth analysis of the electrocatalytic properties of RuO_2

based DSA. Understanding of the reaction path of CER can be helpful for improving the electrocatalytic properties of DSA.

6.7. Role of water in CER at RuO_2 based electrodes – understanding electrocatalysis as a resonance phenomena

The reaction path of the Cl_2 evolution reaction (CER) was investigated by combining electrochemical and spectroscopic methods. The state of the RuO_2 surface during the electrochemical reaction was analyzed *in situ* with Raman spectroscopy, by monitoring vibrations of the crystal lattice of RuO_2 and changes in the surface concentration of adsorbed species as a function of the electrode potential.

Within this chapter, some new insights are shown to enable a better general understanding of electrocatalysis. Instead of using thermodynamic catalytic descriptors in the form of adsorption energy of intermediates, the vibration frequencies of the crystal lattice were utilized as a dynamic catalytic descriptor. Interpretation of the newly constructed “volcano”- curve requires conceptually different view on (electro)catalytic reactions.

6.7.1. Some general remarks on electrocatalysis

Electrocatalytic gas-evolving reactions (GER), namely chlorine, hydrogen and oxygen evolution reactions, have been a matter of continuous investigation for decades [158,159]. At the same time their enormous technical significance is coupled with an insufficient fundamental understanding. This was motivation to expand existing knowledge with the intention of establishing adequate unifying concepts in surface science that could bridge electrochemistry with heterogeneous catalysis and surface physics [1,143]. Particularly complicated for analysis are anodic GER, chlorine evolution reaction (CER) and oxygen evolution reaction (OER), where electron transfer proceeds at a reconstructed, oxidized

surface, which has properties that are quite different from those observed at open circuit conditions.

The conventional interpretation of electrocatalysis (the effect of electrode material on the electrode reaction rate) [8] does not specify the impact of the solvent on faradaic process at the electrode/electrolyte interface, whereas the theory of electron transfer postulates the importance of the solvent [61]. However, it is not really clear how the solvent contributes to the rate of an electrode reaction [19,33] especially if the reaction proceeds through adsorbed intermediates. In the seminal papers of Trasatti [24,160] it was demonstrated that the work functions of metals in a solution are practically the same as those of metals in vacuum. At the same time it was assumed that the solvent behaved like a dielectric continuum that shifts the absolute scale of reactivity to the same extent for all metals due to the water dipoles that alter the surface potential at solid/liquid interface.

A new point of view is proposed based on spectro-electrochemical measurements, in which the solvent (water) is crucial in the oxidation of Cl^- ions at RuO_2 based electrodes, not only as reaction medium but also as an integral part of intermediates that allow electron transfer which is necessary for the electrocatalytic reaction. Of particular importance is the observation that the electrocatalytic reaction is strongly dependent on the characteristic vibrations of chemical bonds in the crystals used as catalyst, where the main accent is on a resonance phenomenon established between the electrode surface and intermediates in the electrochemical double layer.

6.7.2. Acid-base properties of RuO_2 as the basis of electrocatalytic activity.

An important characteristic of some transition-metal oxides, including RuO_2, are their acid-base properties. A versatile tool for the analysis of surface properties of RuO_2 is CV [161]. In a range of electrode potentials where water is thermodynamically stable, the hydrated form of RuO_2 can reversibly exchange protons with the electrolyte due to characteristic redox

transitions (Reaction 15). In Figure 6.43 it is shown that inside the potential range from -0.150 to 1.050 V/(Ag/AgCl/3M KCl) the only relevant process is protonation/deprotonation. This behavior is reversible, with the charge for deprotonation in the anodic sweep being approximately equal to the charge for protonation in the cathodic sweep.

If the anodic polarization is extended above 1.05 V vs. Ag/AgCl the process exits the region of thermodynamic stability of the solvent (water) and it is reasonable to assume that deprotonation of the solvent starts (Reaction 12), consuming an additional amount of charge

The process is hence no longer reversible. Further, the formed non-stoichiometric hydrated oxide can be deprotonated to form stoichiometric RuO_2 or even higher oxidation states depending on the applied polarization.

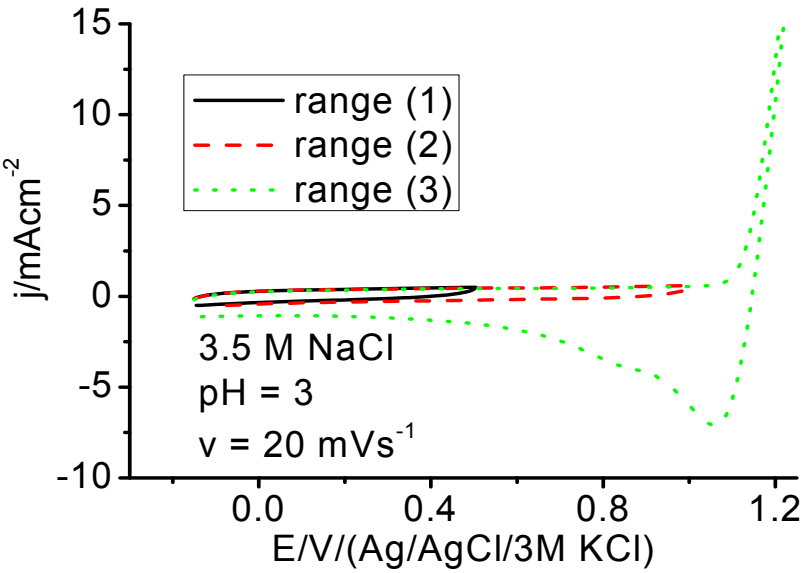

Figure 6.43. Cyclic voltammograms of RuO_2 electrodes in 3.5 M NaCl for three different anodic potential limits.

Besides deprotonation of water, according to a Brönsted-Lowry concept of acid-base behavior, it is also possible to cause acidification of the electrolyte near the electrode surface through acceptance of an electron pair from the Cl^- ion, according to the Lewis concept of acid-base behavior. (Reaction 7)

Knowing the initial reaction during CER is important due to two reasons: 1) if CER starts with discharging of Cl^- then discharging of water will be an obstacle for selectivity as it can proceed towards OER. However, 2) if CER starts with discharging of water than discharging of Cl^- can block active sites.

6.7.3. Selectivity of RuO_2 based catalyst

In a concentrated aqueous solution of NaCl during the anodic polarization above 1.05 V vs. Ag/AgCl simultaneous OER and CER are expected. The fact that OER is thermodynamically more favored as compared with CER (Reaction 6.7.4), naturally questions arise about the selectivity of CER, simply due to the fact that CER proceeds at potentials above the positive limit of thermodynamic stability of water.

$2Cl^- \rightleftharpoons Cl_2 + 2e^-$ $E° = 1.15$ V/(Ag/AgCl/3M KCl) ($t = 25°C$ $a(Cl^-) = 1$ $p = 1$ bar)

Reaction 6.7.4a

$H_2O \rightleftharpoons O_2 + 4H^+ + 4e^-$ $E° = 1.02$ V /(Ag/AgCl/3M KCl) ($t = 25°C$ $a(H^+) = 1$ $p = 1$ bar)

Reaction 6.7.4b

To quantify the charge used for each of these two processes, differential electrochemical mass spectrometry (DEMS) was utilized (chapter 6.7.5). According to the literature oxygen evolution should already be negligible in 0.1 M NaCl [66].

From DEMS measurements it can be concluded that the selectivity for CER is dependent on the concentration of Cl^- ions and in a 5 M NaCl it is approximately 98 %. However, a small part of the charge is continuously consumed for the OER. Anodic water activation, as a main source of corrosion of DSA [144-147] essentially causes further oxidation of the oxide surface and the formation of unstable higher oxidation states of RuO_x [148]. From this point of view both selectivity of CER and oxidation of the surface should be a function of the concentration

of Cl^- ions in the used electrolyte. However, with an observed faradaic efficiency of around 88 %, it seems that besides the charge consumed for oxidation of the surface additional parasitic process is continuously consuming electricity.

6.7.4. Oxidation of the surface during the reaction - reconstruction of the surface as prerequisite for CER.

CV was employed to estimate the level of oxidation of the surface during CER. The approach used to estimate the charge necessary for oxidation of the surface during the CER can be observed in Figure 6.44. CVs were recorded with the same scan rate, in the same potential range, pH and ionic strength for different concentrations of NaCl (Figure 6.44a). As expected higher currents are observed as the concentration of Cl^- ions increases. In the next step the recorded CVs are transformed into the time domain (inset of Figure 6.44a) showing that the charge consumed during the anodic sweep increases with the concentration of Cl^- ions while the charge during the cathodic sweep is almost constant.

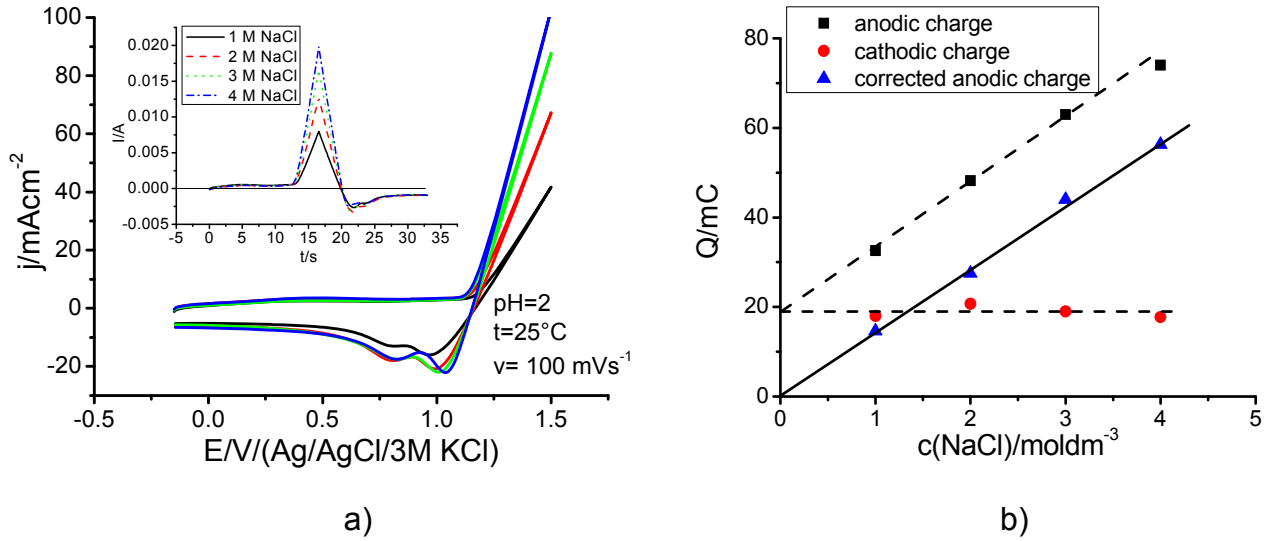

Figure 6.44. a) Cyclic voltammograms of RuO_2 in 1, 2, 3 and 4 M aqueous solution of NaCl at a scan rate of 100 mV/s and pH 2 maintained using HCl. The ionic strength was maintained using $NaNO_3$. The inset shows the cyclic voltammograms transformed into the time domain. b) Charge during the anodic sweep (black cubes) and charge during cathodic sweep (red circles) and anodic charge after subtraction of the cathodic charge (blue triangles).

After integration of the current-time dependence from the time-resolved CV (inset of Figure 6.44a) it can be observed (Figure 6.44b) that the charge consumed in the anodic sweep increases linearly with the increase in concentration of Cl^- ions. This corresponds to the amount of Cl_2 produced. From this perspective it is expected that extrapolation of the dependence between anodic charge and concentration of Cl^- ions should pass through the origin. However, this was not the case and the extrapolation yielded a charge of around 20 mC for zero concentration of Cl^- ions. It was expected that CER proceeds in parallel with the oxidation of the surface during the anodic sweep and that reduction of Cl_2 proceeds during the cathodic sweep concomitantly with the reduction of the previously oxidized surface.

However, the charge during the cathodic sweep is identical for all four concentrations of NaCl. One possible explanation is that the reduction of Cl_2 is almost negligible, due to the fact that Cl_2 (produced at relatively low current density) escapes rapidly from the solid/liquid interface towards the gas phase. This suggests that during the cathodic sweep the observed charge arises predominantly from the reduction of the oxide formed in the anodic sweep during the CER. Further arguments for this are found in [42]. When the cathodic charge (reduction of the formed oxide) was subtracted from the anodic charge (combined CER and oxidation of the surface) the dependence with respect to the concentration of Cl^- ions starts as expected from the origin (see subtracted net anodic charge in Fig. 6.44b).

The comparison of results from DEMS with transient measurements obtained by CV is illustrative. To quantify the charge used for CER and OER DEMS was utilized [162,163] for the four concentrations of aqueous NaCl solution at a current density of 400 $mAcm^{-2}$ and a temperature 25°C.

The volumetric flows were calculated using the measured volume fractions and the flow of nitrogen according to Equation 6.7.1:

$$V_{ml/\min,x} = \frac{V_{vol\%x}}{V_{vol\%N_2}} \bullet V_{ml/\min,N_2}$$ *Equation 6.7.1.*

From the calculated flows for Cl_2 and O_2, the selectivity for CER was calculated as a ratio between the flow of Cl_2 and the sum of the flows for Cl_2 and O_2. The efficiency was estimated by comparison of the measured flows of Cl_2 and O_2 with theoretically expected flows calculated from the Faraday's law assuming an ideal gas behavior and taking into account the selectivity at given concentrations of the electrolyte.

Table 6.7.1. Data extracted from DEMS measurements (TU Berlin) relevant for estimation of selectivity and faradaic efficiency.

c [mol/l]	$V_{measured}$ [vol%]			$V_{calculated}$ [ml/min]		Selectivity	Current efficiency	Current efficiency
NaCl	N_2	O_2	Cl_2	O_2	Cl_2	Cl_2	Cl_2	$Cl_2 + O_2$
1	97.08	0.58	2.34	0.60	2.41	0.80	0.49	0.61
2	96.15	0.19	3.66	0.20	3.81	0.95	0.72	0.75
3	95.84	0.10	4.06	0.10	4.24	0.98	0.79	0.80
4	95.48	0.15	4.35	0.16	4.56	0.97	0.85	0.88

As shown in Figure 6.45. the tendency in the change of the faradaic efficiency with concentration of Cl- ions is very similar for DEMS (used data from TU Berlin) and CV. While CV measurements suffer from influence of hydrogen and hydroxyl ions produced at the counter electrode what partially influences current efficiency, DEMS experiments are more accurate. The current efficiency in case of CV measurements was estimated by comparison of corrected anodic charge with the overall anodic charge from Figure 6.44b. Despite CV was not accurate in giving absolute values of the current efficiency, the obtained trend strikingly resembles the results from DEMS measurements. This was taken as a hint that the constant cathodic charge as shown in Figure 6.44b has to be due to a particular physical meaning.

One of the intriguing aspects of CER and OER is the phenomenon of surface reconstruction. Catalytically active layers are usually non-stoichiometric oxides with coordinately unsaturated sites (CUS) playing a crucial role in the formation of intermediates [58]. Considering the

general understanding of anodic electrocatalytic reactions it is expected that the anion (Cl^-) or molecule with free electron pair(s) (H_2O) will be located in the inner Helmholtz plane where the electronic density from an anion or molecule can be partially delivered to the d-orbitals of the transition metal. Either of these two possibilities will cause the existing RuO_x to be transformed into a higher oxidation state during the applied anodic polarization.

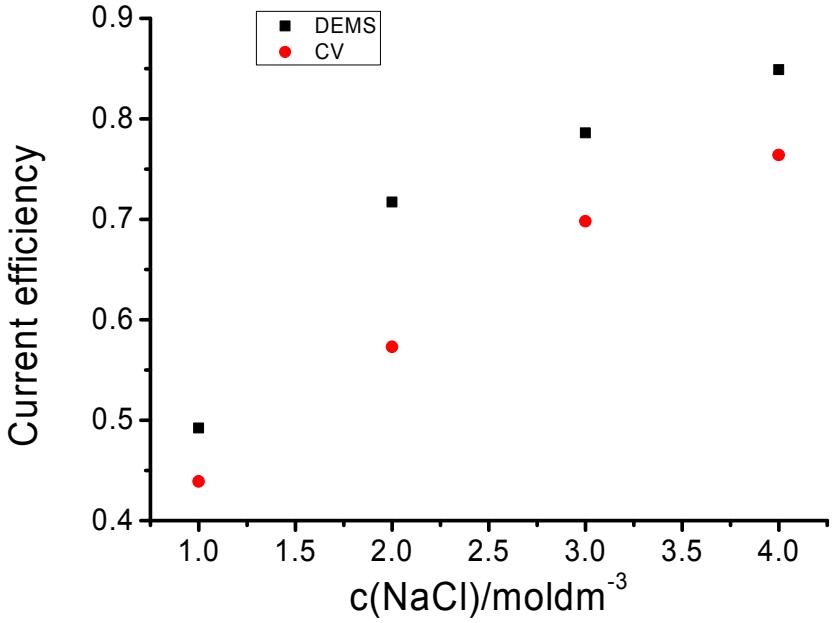

Figure 6.45. Comparison of current efficiency obtained by two different methods: 1) DEMS (black cubes) and 2) CV (red cirlces) for several concentrations of Cl^- ions.

The enthalpy of the bulk transition from lower to higher oxides is correlated with the kinetics of OER and CER [184] as well as the binding energy between the oxide and the adsorbed oxygen species (a relic of the doubly deprotonated water molecule) [58]. However, a more detailed insight reveals that for facilitating electrocatalytic reactions it is important that the redox potential of the transition from the lower to the higher oxidation state of the used oxide catalyst is close to the redox potential of the catalyzed reaction [81,164], in this case CER. If the redox transition from the lower towards the higher oxidation state starts too early (e.g. in the case of metal-centers with large d-band vacancy the redox potential of this transition is

too negative as compared with the redox potential of the catalyzed reaction) the surface is oxididized with higher intensity during the reaction.

If water was not important for CER it would be possible to obtain respectable kinetics for CER in Cl^- containing non-aqueous solutions, if the catalytic material has a redox potential for transition from the lower to the higher oxidation state of the oxide similar to the redox potential for CER.

However, this is not the case. According to previous work in organic solvents, for example trifluoroacetic acid (TFA) [58], CER proceeds at a much lower rate derived from the measured anodic current as compared with the current in aqueous solution without employing any other analytical techniques. Experiments were conducted in several ionic liquids, but no Cl_2 could be detected by means of DEMS despite anodic currents were measured as a response to the polarization of the electrode. The anodic currents originated from the formation of chloro-organic compounds with no production of molecular Cl_2. Although most of the ionic liquids have lower dielectric constants than water [165-168] a certain amount of Cl_2 should be produced in non-aqueous media if the contribution of the media is based only on electric field effects. This was an important proof that water has a specific role in CER that is beyond a media with high dielectric constant.

6.7.5. Impact of local equilibriums on selectivity and efficiency of CER

Some strategies were already proposed considering an improvement of stability or activity [169] or even selectivity of oxide electrodes during CER and/or OER based on ternary oxides [40,83,84]. However, while it is usually assumed that a homogenous mixing of oxides at the atomic level occurs [43,170], in reality there are regions at the catalyst surface which are enriched with one of the components what will certainly change local activity [11,143].

As said previously, nonstoichiometric oxides with coordinately unsaturated sites (CUS) are catalytically active as main active centers [58]. During the applied anodic polarization, RuO_x

will be converted into higher oxidation states. Simultaneously, anions (Cl^-) or molecules with free electron pair(s) (H_2O), located in the inner Helmholtz plane, will partially deliver electronic density to the d-orbitals of the transition metal and cause that RuO_x into higher oxidation state returns into its initial state.

The fact that CER is a $2e^-$ transfer process while OER is a $4e^-$ transfer process can be helpful in adressing selectivity issues. If redox the potentials for the transition from the lower towards the higher oxidation state allows the exchange of $2e^-$ slightly before the reversible potential for CER is reached, while the redox potentials for the exchange of two additional electrons are much more positive, it can be expected that CER will be promoted and OER inhibited. Certainly, this point of view is based on the assumption that OER follows a reaction path with a stoichiometric number equal 1 or in other words that the rate determining step will happen ones in order to produce one molecule of oxygen (peroxo-pathway). If OER follows a reaction path with a stoichiometric number equal 2 (recombination pathway), the problem of selectivity of CER in presence of OER gains additional complexity. However, while oxidation and reconstruction of the surface during the CER can be in relation with the intrinsic catalytic properties, it cannot be used at the same time as an explanation for the measured faradaic efficiency. While the capacitance current is negligible and no leakage of gases occurs (the DEMS setup was calibrated with N_2 flow), the maximal faradaic efficiency of 88 % suggests that parasitic chemical reactions continuously consume electricity, what certainly cannot be the oxidation process due to the requirement of equivalence between the generated mass of the product and the charge passing through the electrochemical interface. The oxide thickness should grow progressively with time what is not the case as shown in Figure 6.44b. Thus, the issue of faradaic efficiency is still not clear and very often disregarded in studies concerning the selectivity of CER and OER. Fractions of Cl_2 and O_2 are usually compared as function of different kinetic parameters, but without comments on the faradaic efficiency of

reactions [40,83,84,171]. In an attempt to better comprehend the catalytic performance of oxides for CER and OER, it is instructive to analyze local properties of the catalyst coatings.

It was previously reported that the selectivity of CER is dropping if the percentage of RuO_2 becomes too high. In case of Ti/(TiO_2+RuO_2) with more than 40 % of RuO_2 the fraction of OER becomes significant [43,48]. Having this in mind, the question is how the local surface enrichement with RuO_2 manifests in the performance of the DSA.

In Figure 6.46a the morphological pattern of the analyzed DSA catalyst coating can be observed. EDX mapping over the same catalyst region (Figure 6.44b) illustrates a surface enrichment with Ru in some of the subregions of the coating.

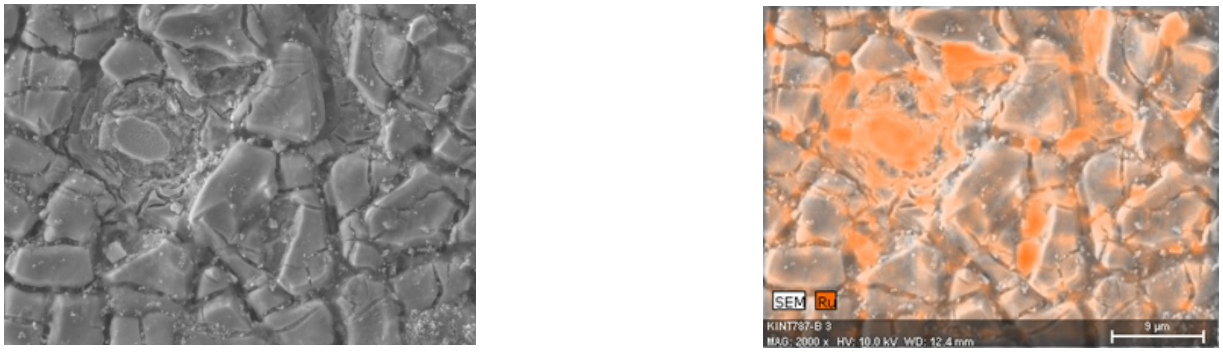

a) b)

Figure 6.46. a) SEM micrograph of the morphological pattern of electrode DSA b) EDX mapping of Ru displacement at the electrode surface.

Instead of the expected amount of around 15 % of RuO_2 locally significantly higher amounts of RuO_2 are visible which promote OER. Promotion of OER is partially based on a change of the equilibrium state (increase in % of RuO_2 will cause a drop in the OCP for OER while the OCP for CER stays constant [171]) but also in kinetics (increase of density of Ru centers makes the recombination step more probable which is possibly important for OER). A local increase in kinetics of OER will cause acidification of electrode/electrolyte subregion and additionally inhibit CER (partial order of CER in respect to [H^+] is -1).

Moreover, the local enrichment with RuO_2 will cause a nonuniform distribution of overpotentials and current densities at the electrode surface, what will in consequence cause

different concentration profiles over different subregions of the DSA coating. During the experimental protocol rotation was employed to minimize concentration gradients, but in case of a “cracked” DSA electrode where the inner part of the porous layer participates in the reaction, it is almost impossible to control the surface concentration. Knowing that a nonuniform distribution of the overpotential is established at the electrode surface and that the Cl^-/Cl_2 redox pair is moderately reversible (much less reversible than typical redox mediators but much more reversible than the H_2O/O_2 redox couple [53]) the question is what portion of the produced Cl_2 is reduced at the electrode itself and if this can be an explanation for the previously mentioned unusual faradaic efficiency. This is hard to proof by any experimental procedure, but one result that was obtained certainly is important.

Investigation of the local electrochemistry of CER was already initiated by developing a concept for detection and visualization of Cl_2 on DSA. It was assumed that the efficiency and the selectivity of CER and OER could be due to a spatial distribution of active sites or a matter of the homogeneity of the surface [11,40].

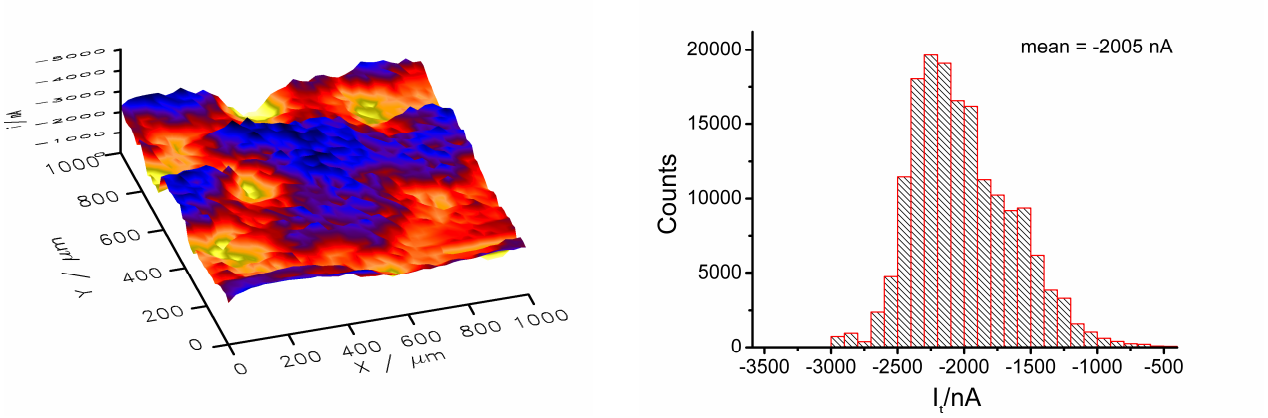

a) b)

Figure 6.47. a) SECM image showing the spatial distribution of the activity of a 1000 x 1000 μm^2 region of DSA in a sample-generator/tip-collector mode; potentials at the sample and tip were E_s = 1400 mV and E_t = 950 mV, respectively. b) Current distribution histogram derived from the tip currents collected during the scanning of the DSA surface; data points were collected every 10 ms during stationary polarization.

The SECM image in Figure 6.47 shows one section of the catalyst layer. Despite the resolution is determined by the use of a microelectrode with a diameter of 25 µm, the image realistically illustrates fluctuations caused by inhomogeneities in the surface composition. Chlorine generated at the sample is reduced at the microelectrode tip causing variations in the cathodic current at the tip. The SECM image in Figure 6.47a essentially fits to expectations based on EDX mapping as shown in Figure 6.46b and allows to conclude that nanostructured materials, usually with homogenous properties after synthesis, are passing through a metamorphosis and surface reconstruction during the electrochemical reaction and loose their initial properties rapidly.

The current distribution histogram is illustrating that minimal and maximal values of tip currents differ by almost 6 times (from -500 to -3000 nA), suggesting that local fluctuations in the concentration of the produced Cl_2 are significant. Concentration gradients caused by the accumulation of Cl_2 are always coupled with concentration gradients of Cl^-. This will certainly induce diffusional overpotentials as a kinetic effect but it is also interesting to observe possible thermodynamic effects. Possible changes in the equilibrium potential of CER, due to the supersaturation with the product opened discussions in this direction [172].

In case of the microelectrode tip, the reversible potential of the Cl^-/Cl_2 redox couple can change due to the fact that for the microelectrode “bulk” values of $[Cl^-]$ and $[Cl_2]$ are those from the surroundings of the hemispherical diffusion zone of the microelectrode itself.

The possibility of changing the equlibrium potential at the microelectrode tip as a function of the local activity at the sample can be helpful to understand the possibility of a simultaneous reduction of Cl_2 produced at the DSA and the faradaic efficiency. The observed spatial distribution of the activity as shown in Figure 6.47, displays two characteristic subregions, one with a very low activity (coordinate x = 450 µm, y = 950 µm) and one with a very high activity (coordinate x = 500 µm, y = 750 µm). Positioning the microelectrode at these spots and performing experiments in the redox competition mode of SECM (tip polarized at 1400 mV is

competing with the sample for Cl^- ions) illustrative results were obtained. In the redox competition mode more active sites are recognized by a higher decrease of the anodic current at the tip (reaction at the tip is inhibited due to the reaction at the sample). By increasing the potential at the sample the tip current was decreasing till a certain value was reached. Then, surprisingly the previously anodic current at the tip is changed into a cathodic current despite the potential at the tip was 1400 mV vs. Ag/AgCl. It becomes obvious that at certain potential value at the sample it is possible to reduce Cl_2 at the tip at a potential of 1400 mV vs Ag/AgCl.

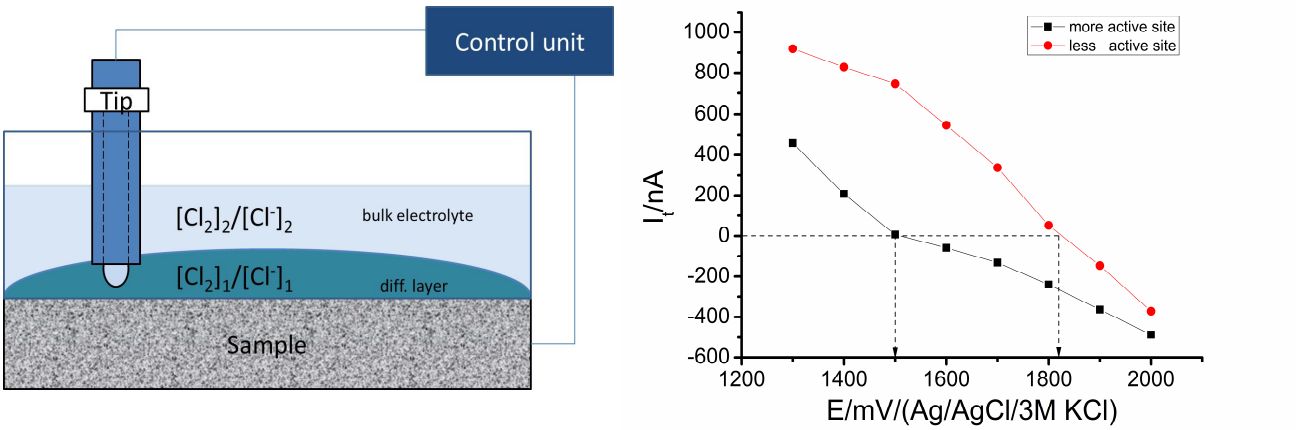

a) b)

Figure 6.48. a) Scheme of a section of the DSA sample under investigation with the SECM tip. The microelectrode tip senses the concentration ratio of $[Cl_2]/[Cl^-]$ near the electrode surface which differs from the one in the bulk of the electrolyte. b) Amperometric response at the tip polarized at E = 1400 mV/(Ag/AgCl/3M KCl) in proximity of the sample as a function of the sample potential. The point of transformation from anodic to cathodic current at the tip is referring to the equilibrium between the potential at the tip and the potential at the local area of the sample.

A scheme of the section of the DSA sample under investigation with the SECM tip is shown in Figure 6.48a. The microelectrode tip senses the concentration ratio of $[Cl_2]/[Cl^-]$ near the electrode surface which differs from the one in the bulk of the electrolyte. Figure 6.48b shows the amperometric response at the tip polarized at E = 1400 mV/(Ag/AgCl/3M KCl) in proximity of the sample as a function of the sample potential. The point of transformation from anodic to cathodic current at the tip is referring to the equilibrium point between the potential at the tip

and the potential at the local area of the sample. In case of a less active site the initial anodic current is higher (less intensive inhibition from by the sample) as compared with a more active site. With increasing of the anodic polarization at the sample, a less active site influences the anodic behavior of the tip which sustains its potential in a larger interval before it starts to behave cathodically. In opposite to that, a more active site induces an anodic behavior at the tip sustaining a much smaller interval of the sample potential.

If we shift from the idealized image of a macroelectrode as homogenous system with a uniform diffusion layer and with equal size at all points of the coating, the properties of a macroelectrode can be treated as a sum of microelectrodes which have their local diffusional zones which overlap and form a large diffusion layer over the entire sample. Wherein this case, the exchange current density and equilibrium potential can be influenced by supersaturation [172] and hence local supersaturation may influence the local exchange current densities and hence the local equilibrium potentials. As already stated, areas with local enrichment with RuO_2 will have a lower OCP for OER, while the OCP for CER stays constant. Knowing that always a mixed OCP based on OER and CER is measured it is expected that different equilibrium potentials at different spots of the sample are detected. For example, if enrichment with RuO_2 changes from 10 % to 50 % the equilibrium potential drops by approximately 100 mV [171].

While the ohmic drop at the tip are negligible due to small currents, the exact local value of the potential at the sample depends on the ohmic drops. The ohmic resistance was estimated by means of impedance spectroscopy with the sample and the reference electrode kept always at the distance of 1 cm. The obtained value of 15 Ω is representative for both spots because the distance between them is negligible in comparison to the distance from the reference electrode knowing that main contribution to the ohmic resistance comes from the electrolyte containing the gas fraction. At potentials of 1.5 V and 1.8 V vs. Ag/AgCl (points where anodic tip currents are transformed into cathodic ones) the measured currents were

6.1 mA and 12.8 mA, respectively, and the ohmic drops were 92 mV and 192 mV. This suggests that local electrode potential at a highly active site was around 1.41 V vs. Ag/AgCl while at a low active site it was around 1.61 V vs. Ag/AgCl. The potential difference between the two sites is around 200 mV.

Obviously, it is possible to simultaneously reduce Cl_2 produced at the DSA in dependence on the uniformity of the distribution of active sites. In other words, the efficiency and selectivity of CER and OER strongly depends on the control of the local properties of the macroelectrode, in particular from the spatial distribution of active sites.

As stated at the beginning, it is considered to be relevant to perform analysis predominantly on polycrystalline materials. One of the reasons is that the approach based on DFT calculations is restricted to single crystals [58] and excludes the impact of structural phenomena like edges, defects or vertices which are important in real nanocrystalline materials [84]. While the size of the nanoparticles was already proven to play a role in the electrocatalysis of some other reactions by influencing the potential of zero charge [67], it is assumed that the size and the shape of nanoparticles can play a role in the selectivity of OER and CER [83]. In this sense it is important to emphasize some facts considering electrocatalysis of CER and OER.

The application of single crystals in electrocatalysis was usually performed with the clear intention of distinguishing electronic from geometric properties. This approach is generally accepted despite the fact that the density of active sites (usually dependent on the loading) can substantially influence the Tafel's slope [52], illustrating that the geometric property (active surface area) can influence the electronic property (Tafel's slope). At atomic scale, the analysis of single crystals of RuO_2 and IrO_2 [58] suggests CUS sites as the active ones for the both, CER and OER, where the pH and the electrode potential determines the nature of adsorbed species at the catalyst surface. DFT suggests, in case of (110) facets, that CER is thermodynamically favoured on IrO_2 by more than 50 mV. At the same time the pH value at

which CER starts, is 5 and below in case of IrO_2 while it is 2 and below in case of RuO_2. In the light of polycrystalline materials, CER is possible on RuO_2 at pH values higher than 2 while the kinetics of CER is slightly better on RuO_2 than on IrO_2 [13]. Furthermore, in case of OER, the lowest Tafel's slopes measured for different single crystals was at least 60 mV/dec while at the same time the Tafel's slope for polycrystalline RuO_2 can be less than 40 mV/dec [52,81]. This is of mayor importance because the Tafel's slope is an intensive catalytic property which is assumed to be independent from the surface area.

While the term synergy was used before to explain other phenomena in electrochemistry (for example the spilover on PtRu alloy during methanol oxidation [173] for which the use of the term bifunctional catalyst would be more appropriate), the meaning of a synergetic effect in case of electrocatalysis on oxide surfaces is seen as achieving of new superior properties based on an intimate mixing of components at an atomic level under formation of a solid solution [170]. The formation of a solid solution from different transition-metal oxides can be problematic due to surface segregation and incomplete formation of the crystalline phase during the thermal treatment [51,96,117,161,] leading to a rather additive than synergetic behavior. However, the unique performance of polycristalline RuO_2 in comparison to single crystals of RuO_2 [81] is an example for the appearance of a new quality. Superior properties, unpredictable by any of the individual constituents are a proof of a synergy effect.

Still, one question remains open. The main strategy for tuning of the selectivity was doping or mixing of oxides [83,84] assuming that changes in the crystal structure should induce changes in the catalytic activity. However, in case of rutiles, the main oxides used for CER and OER, the parameters of the crystal lattice of RuO_2, the most active oxide, are very similar to TiO_2, an almost completely inactive oxide [82]. At the same time RuO_2 (rutile type structure) and Co_3O_4 (spinel type structure) have comparable activity for OER and CER [13] while the parameters of their crystal lattices are significantly different [56,82]. This suggests that the usual understanding of (electro)catalytic activity as a consequence of a specific crystal

structure is oversimplified and probably incorrect. Electrocatalytic activity is clearly governed by additional unknown phenomena.

6.7.6. Solvent induced reaction pathway

Observing that CER is kinetically superior in comparison to OER, one can easily conclude that in concentrated NaCl solutions discharging of Cl^- ion is a process that will dominate over discharging of water molecules. However, the reality is much more complex.

To understand the possible influence of water it is instructive to analyze one of the reaction pathways for the CER proposed by Erenburg [41] :

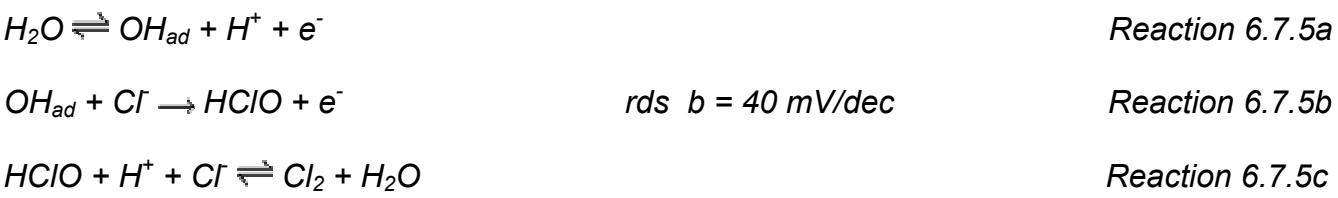

This reaction pathway fulfills several important requirements (or discriminatory criteria):

1) water has to participate in the reaction

2) CER has to be pH dependent with a partial order of the reaction with respect to the concentration of protons of -1 [79].

3) the partial order of reaction with respect to Cl^- ions has to be 1 [79].

4) according to the value of the Tafel's slope of 40 mV/decthe exchange of the second electron is the rate determining step (rds).

If these requirements are put into the context of the usually assumed Volmer-Heyrovsky pathway [33,41] practically none of them, except the last one is fulfilled, while the pathway of Erenburg fulfills all the requirements. Worth to mention is that any kind of assumption where CER should start with Cl^- discharging cannot explain the pH dependence of CER. Knowing that any kind of mechanicistic analysis is, essentially, discriminatory it is not claimed that the

proposed pathway is the absolute truth, but closer to the truth than any other of the proposed pathways. Certainly, it is realistic that the active sites for both CER and OER are identical (CUS sites), while only the activation energies of the individual processes differ, based on pH, applied potential and spatial separation between active sites (if OER requires two active sites for recombination, while CER does not). At the same time the possibility of the existence of two types of active sites should be further considered.

Intuitively, it is proposed that both types of active sites contribute to the formation of molecular Cl_2 in the presence of Cl^- ions, where the one that behaves only as a Brönsted type acid also contributes to OER:

$H_2O \rightleftharpoons OH_{ad} + H^+ + e^-$ *Reaction 6.7.6a*

$(1-x)\ OH_{ad} \longrightarrow (1-x)\ O_{ad} + (1-x)\ H^+ + (1-x)\ e^-$ *(on some active sites)* *Reaction 6.7.6b*

$x\ OH_{ad} + x\ Cl^- \longrightarrow x\ OHCl + x\ e^-$ *(on other active sites)* *Reaction 6.7.6c*

$x\ OHCl + (2-x)\ H^+ + (2-x)\ Cl^- + (1-x)\ O_{ad} \rightleftharpoons Cl_2 + H_2O$ *Reaction 6.7.6d*

A Lewis type acid site can be distinguished from a Brönsted type acid using IR spectroscopy and this is one of the directions of the future work [174]. To strengthen this point of view and considering the proposed reaction pathway it was necessary to observe: 1) which adsorbed species (OH_{ad} or Cl_{ad}) is present at the surface of RuO_2 and 2) how the surface coverage with the adsorbed species varies with the electrode potential.

6.7.7. *In situ* spectroscopic surface study of RuO_2 during CER

For a more sophisticated analysis of the catalyst surface during the CER, Raman spectroscopy was coupled with an electrochemical cell. In Figure 6.49. the Raman spectra of a RuO_2 based DSA in electrolyte solution for different values of applied electrode potential is

shown. The frequency range of the Raman spectra corresponds to the O-H stretching mode (O-H bond from surface water molecules or OH adsorbed at the electrode surface).

The predominant peak around 3470 cm^{-1} has usually a shoulder at 3240 cm^{-1}. The shoulder becomes less intense with increasing ionic strength in the solution [175]. The intensity of the peak corresponding to the O-H stretching mode decreases as the electrode potential becomes more positive or, in other words, during acceleration of CER water molecules or even OH_{ad} at the solid/liquid interface are intensively deprotonated (Figure 6.47). It is worth mentioning that the peak of Cl_{ad} at RuO_2 is absent in the Raman spectra in the entire range between 200 and 4000 cm^{-1}. Experiments were conducted at different concentrations of Cl^-, from very dilute to highly concentrated, and the only relevant change in the Raman spectra was the shape of the peak of the O-H stretching mode in agreement with previous reports [175]. The only relevant change in the surface concentration of the adsorbed species at the electrode-electrolyte interface during CER is obviously connected with the solvent. This suggests that proposed reaction pathway is quite likely.

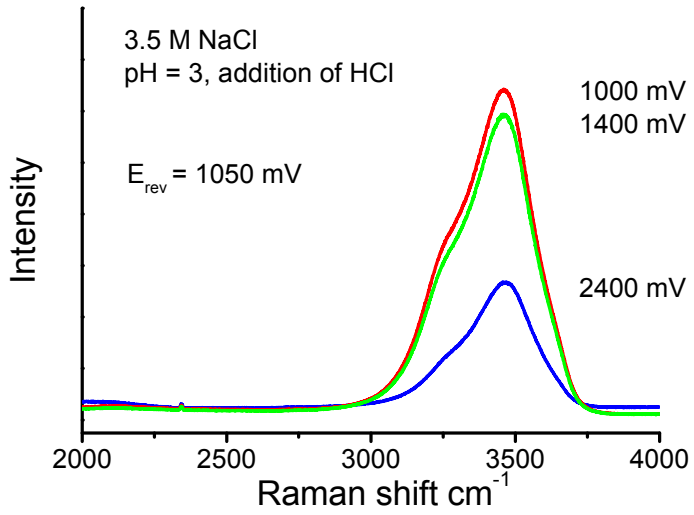

Figure 6.49. Raman spectra of TiO_2/RuO_2 in 3.5 M NaCl, pH 3 (addition of HCl) at varying electrode potentials; peak for O-H stretching mode around 3470 cm^{-1}; shoulder of O-H stretching mode around 3240 cm^{-1}.

The role of Cl^- ions can be only seen in the formation of a HClO complex through bonding with O while simultaneously weakening the oxide – OH bond. The change in the intensity of the Raman spectra corresponds to a change in the coverage of the adsorbed species and reflects deprotonation of water moleculs (or OH_{ad}). According to the proposed reaction pathway, upon anodic polarization the concentration of OH_{ad} increases due to the fact that Reaction 5b becomes rate determining, i.e. relatively sluggish in comparison with Reaction 5a. With acceleration of CER by increasing the potential from 1 V to 2.4 V vs. Ag/AgCl/3M KCl the intensity of the band of the O-H stretching mode is decreasing. Possibly, already at open circuit conditions water is substantially deprotonated suggesting that the reaction starts probably with deprotonation of OH_{ad} under formation of O_{ad}, while in a second step HClO is formed as an intermediate as shown in Reactions 6.7.7a and 6.7.7b:

$$OH_{ad} = O_{ad} + H^+ + e^- \qquad \textit{Reaction 6.7.7a}$$

$$O_{ad} + Cl^- + H^+ = HClO \qquad \textit{Reaction 6.7.7b}$$

Certainly Reaction 6.7.7b is proceeding towards Reaction 6.7.5c, while Reaction 6.7.7a can proceed towards OER. The pathway defined by Reactions 6.7.7 fulfills all four previously mentioned discriminatory criteria used to evaluate the pathway of Erenburg.

Experimentally it was easier to monitor the drop in OH_{ad} surface concentration during OER due to a significantly lower reaction rate. By this, the interference of the produced gas was minimal as shown in Figure 6.50. Figure 6.50 looks very similar to the Raman spectra made in aqueous NaCl solutions, except the shoulder at around 3240 cm^{-1} which is more pronounced. From the reaction pathway for OER as proposed in literature [176], it can be deduced that the final reaction is the recombination of two O_{ad} thus requiring two neighboring active sites. In case of CER, if the reaction proceeds through a HClO intermediate, only one active site is

necessary to produce one Cl_2 molecule. This can be a potential reason for the facilitated kinetics of CER in comparison to OER.

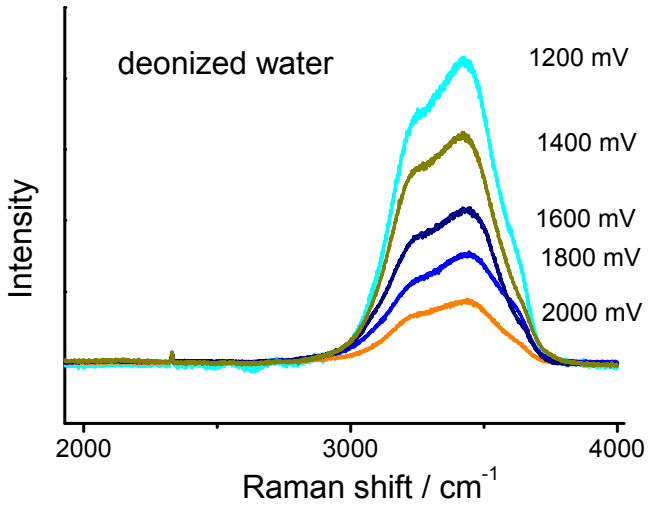

Figure 6.50. Raman spectra of water for different electrode potentials; O-H stretching mode

To distinguish CER from OER in Raman spectra, despite differences in the shape of the shoulder at 3240 cm^{-1}, it was necessary to detect HClO as intermediate during the CER.

6.7.8. Matching of characteristic vibrations – electrocatalysis as a resonance phenomena.

One of the fingerprints of the RuO_2 in Raman spectra is a peak around 716 cm^{-1} which responds to the B_{2g} vibration mode of RuO_2 [177,178], a characteristic vibration of the crystal lattice of RuO_2. This part of the spectrum in an electrolyte with or without Cl^- ions shows distinct changes with increasing the polarization potential (Figure 6.51).

In Figure 6.51a one can see that in the case of water, a peak around 716 cm^{-1} is slowly developing with increasing electrode potential. In presence of Cl^- ions in the electrolyte a substantial change in the spectra is observed as shown in Figure 6.51b and the B_{2g} vibration mode of RuO_2 becomes more emphasized during CER as compared with OER.

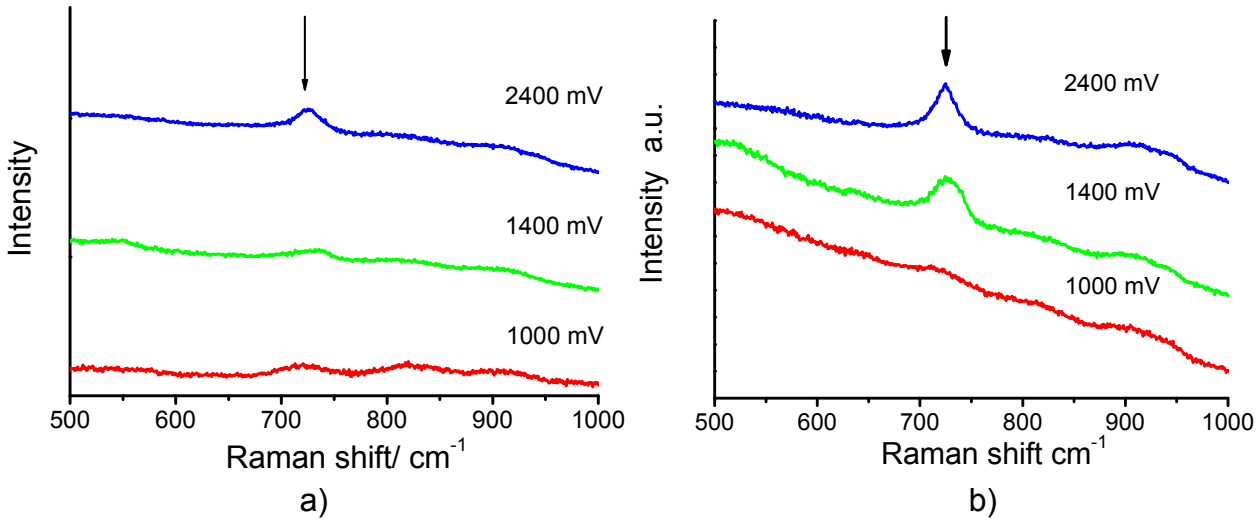

Figure 6.51. Raman spectra of DSA in a) water and b) 3.5 M NaCl, pH 3 (addition of HCl); applied potentials are 1000, 1400 and 2400 mV vs Ag/AgCl/3M KCl.

The main question is: what will allow fast heterogeneous electron transfer in the case of inner sphere reactions which require the existence of adsorbed intermediates? A “volcano” curve as the main predictive basis on which electrocatalysis rests [8] usually expresses the kinetics of the electrode reaction as a function of a catalytic descriptor, where the highest kinetics is a function of the optimal value of the chosen catalytic descriptor. Usual electrocatalytic descriptors are in the form of a binding energy between the electrode surface and the adsorbed chemical species which behave as intermediates in the rds [58]. In this way, kinetics of the reaction are expressed as a function of thermodynamic parameters. In other words, the physico-chemical quantity of the process is expressed as a function of the physico-chemical quantity of the state. Even if the observations of Schmickler and Trasatti [30] is disregarded and DFT predictions of electrocatalytic trends are considered [31,58,179] intuitively it is problematic to comprehend how one thermodynamic parameter can be sufficient to explain the dynamics of electron transfer at the electrode/electrolyte interface.

An electrochemical reaction as a process means that a chemical energy of an electron defined by the Schrödinger equation as a tridimensional standing wave, is transformed into electric energy (or *vice versa*). An electron understood as a tridimensional standing wave represents a vibration in resonance. This can also describe the behavior of electrons when

they are part of a chemical bond. Transfer of the vibrational energy of electrons into electric current (or *vice versa*) proceeds through the electric double layer. Knowing that the timescale of electron transfer and molecular vibrations is very similar, 10^{12}-10^{14} Hz, it is intriguing to try to comprehend the role of vibrational energy in electrocatalysis of CER.

Keeping in mind the previous conclusions about the activity trends for CER [13] the intention is to provide some additional insight why RuO_2 is an almost perfect catalyst for this specific reaction. Upon analysis of the existing data gathered from Raman spectroscopy experiments for the used catalyst material RuO_2, there are 4 characteristic vibration modes that are "fingerprints" of rutile RuO_2 [177,178]: B_{1g} (97 cm^{-1}), E_g (528 cm^{-1}), A_{1g} (646 cm^{-1}), B_{2g} (716 cm^{-1}). The first one, around 97 cm^{-1} is in the section of the spectra (below 200 cm^{-1}) that is usually disregarded from analysis. The fourth, around 716 cm^{-1} can be observed in Figure 6.51, however the second and third were not clearly visible. Consequently, the experiments were repeated in a chloride containing solution with a thinner layer of the liquid over the sample. The result is shown in Figure 6.52.

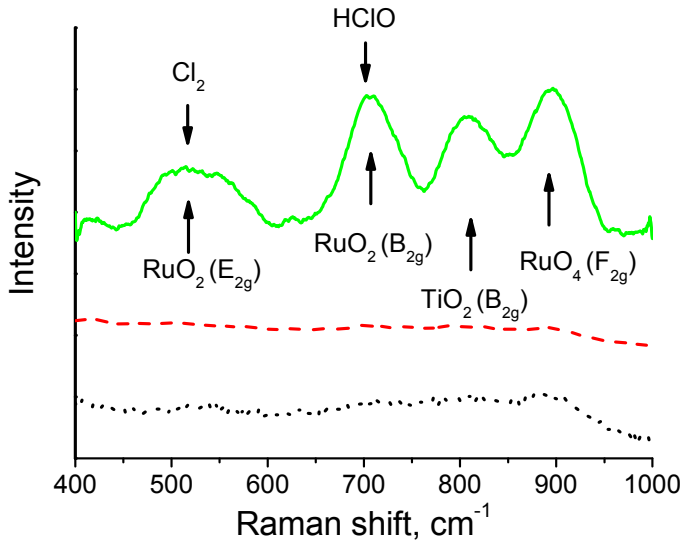

Figure 6.52. Raman spectra of RuO_2 in: a) air (black dotted line) b) in chloride containing electrolyte without polarization (red dashed line), c) sample polarized at a potential of 1.5 V vs. Ag/AgCl/3M KCl in chloride containing electrolyte (full green line. The peaks of the characteristic vibrations of RuO_2 are overlapping with characteristic vibrations of chemical species (Cl_2 and HClO) in solution.

In Figure 6.52 the following characteristic peaks are observed: RuO_2 (E_g) at 528 cm^{-1}, RuO_2 (B_{2g}) at 716 cm^{-1}, TiO_2 (B_{2g}) at 826 cm^{-1} [178] and RuO_4 (F_{2g}) 906 cm^{-1} [180]. In air, the DSA shows characteristic peaks for RuO_2 but also for TiO_2. They can also be observed in water and in chloride containing electrolyte. However, when an electrode potential is applied all peaks become more emphasized (surprisingly, also the one for TiO_2). Considering the value of the potential of zero charge of the RuO_2/TiO_2 mixed oxide [116], at open circuit potential the water molecules in the double layer are oriented with the oxygen towards the electrode. Dependent on the binding energy between the electrode and oxygen from water, a certain potential difference at the observed solid/liquid interface will be established, which can be altered by applying an external potential. The presence of RuO_4 during the reaction can be interpreted as a strong proof for the oxidation of the surface during CER, but also as proof for the reconstruction of the surface during CER. This means that the redox transition of RuO_2 into a higher oxidation state happens simultaneously with the catalytic reaction. Practically, for a succesfull inner sphere electron transfer, the redox transition from a lower to a higher oxidation state of the oxide should proceed at a potential slightly more negative than the potential at which oxidation of the reactants into products occurs [81,164].

A surprising observation was that the Raman shifts of HClO and Cl_2 in aqueous solution are 728 and 540 cm^{-1}, respectively [181], frequencies which are very similar to the Raman peaks of RuO_2 shown in Figure 6.52. Notable is the matching of the Raman shifts of HClO, the potential intermediate in the rate determining step (according to Erenburg), and the B_{2g} vibration mode of RuO_2. Additionally, the Raman shift of the product Cl_2 itself is matching with the E_g vibration mode of RuO_2.

The matching of Raman shifts and evidently more emphasized vibration mode peaks during CER gives an indication to a deeper physical meaning. To confirm the link between the observed matching of vibration modes of the crystals with vibration modes of species that are

intermediates during the reaction the Raman spectra of a range of oxides that are used or tested for CER were analyzed.

Some of the oxides that exhibit good electrocatalytic activity for CER have a similar “fingerprint” in their Raman spectra as RuO_2. The closer the vibrational modes are to that observed for RuO_2, which is known to be the best catalyst for CER, the better the catalytic performance of the oxide is. This suggests that it would be possible to consider the dependence of the kinetics of CER as a function of the characteristic Raman shifts as an electrocatalytic descriptor.

The lack of accurate experimental data for overpotentials or exchange current densities in the case of CER can be overcome by rationalization of the existing data gathered for OER as the general activity trend for CER and OER is almost identical for a number of transition metal-oxides (such as rutiles, spinels and perovskites). When the potential for OER is plotted as a function of the potential for CER, for the same current density, a slope equal to one is observed [13]. This suggests that the use of kinetic data collected for OER [13] would have a more general validity in the case of CER if the intention was to analyze only qualitative activity trends for a range of oxides. Certainly, the overpotential for CER is always lower than for OER on the entire series of tested oxides. The “volcano”- curve in the case of OER is constructed from the dependence of the overpotential, at a defined current density, on the enthalpy of transition from the lower to the higher oxidation state of the oxide [13]. Connecting the property of the bulk material with surface activity should not be problematic as such a connection has been shown previously in the case of sp metals for the H_2 evolution reaction [24]. In fact, a positive linear dependence between the surface potential of water at an electrode and the enthalpy of formation of the metal oxide is already established for several (mostly sp) metals [182]. This implicitly means that the rate of reaction for CER is connected with the enthalpy of the lower/higher oxide transition of RuO_2 which is then directly connected with the nature and strength of the interaction between oxide and oxygen from the water

molecule. Theoretical calculations confirm this in general. According to Rossmeisl et al. [58] the binding energy between oxide and O_{ad} is a universal catalytic descriptor for CER and OER.

Finally, the overpotentials for several transition-metal oxides with the same current density [13] are expressed as a function of the characteristic Raman shifts (Figure 6.53.).

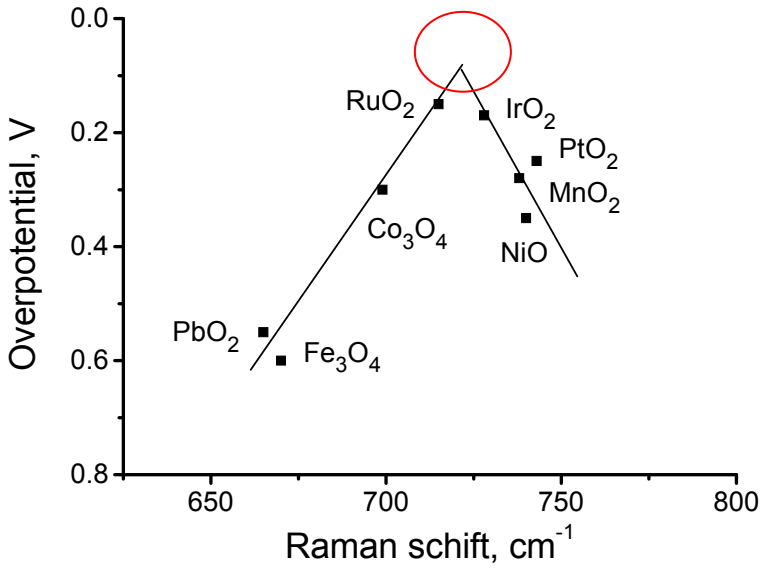

Figure 6.53. Overpotential of CER as function of the characteristic Raman shifts. The top of the volcano curve marked with a red circle corresponds to the Raman shift of vibration of the Cl-O bond in aqueous solution of HClO, a possible intermediate during CER. Values of the overpotential for CER are taken from [13] while values for Raman shifts of RuO_2, IrO_2, PtO_2, MnO_2, Co_3O_4, NiO, PbO_2 and Fe_3O_4 are taken from the references [178,183-189], respectively.

As can be observed in Figure 6.53 the kinetics of CER exhibit a “volcano”- type dependence from the characteristic Raman shifts. This is qualitatively a different “volcano”- curve than those previously plotted for OER (or any other electrode reaction) due to the fact that the catalytic descriptor is the Raman shift, a dynamic property based on vibrations of chemical bonds. Additionally, what provides a qualitative difference to this volcano curve is the peak of the volcano dependence. This peak at around 725 cm^{-1} corresponds to the vibration of the Cl-O bond in an aqueous solution of HClO, being the proposed intermediate during CER. This confirms not only that most probably HClO is an intermediate in CER but also, more

importantly, that the optimal catalyst should exhibit a vibration of the M-O bond in the oxide identical to the vibration of Cl-O bonding in the HClO intermediate. Obviously, the reaction has to be in resonance with the catalyst surface. A hint to a similar conclusion was given by Koper et al. who suggested that, assuming a Volmer-Heyrovsky reaction pathway for CER, for an ideal catalyst, the intermediate Cl_{ad} is just as strongly bound to the catalyst surface as it is in the Cl_2 molecule [33]. This is seen as aconnection between the surface binding energy and free energy in molecule.

It can be stated that Raman spectroscopy gives strong arguments to understanding of why CER starts with water discharging. Instead of replacing of adsorbed water molecules with Cl_{ad} it is much more probable that Cl^- is attached to an oxygen from an oriented water dipol or OH_{ad} because the Cl-O bond is stronger than the M-Cl bond. From Raman spectra it is known that the Cl-O bond is stronger than the Cl-Cl bond which is according to Koper [33] approximately two times than a M-Cl_{ad} bond.

Of general importance is that the length of the M-O bond is inversely proportional to the Raman stretching frequency. Excellent agreement can be achieved between Raman spectroscopy and XANES (X-ray absorption near edge spectroscopy) for the estimation of the M-O bond lengths [174]. Besides identifying the best materials that will catalyze a tested reaction, it should be possible to calculate, using characteristic vibrational frequencies, the optimal interatomic distance, M-O, whose vibration will match the vibration of the intermediate allowing a facilitated electron transfer.

6.7.9. Qualitative relation between resonance and binding energy during an electro-catalytic reaction.

It is illustrative to analyze the “volcano”-curve of the most studied reaction in electrochemistry, the hydrogen evolution reaction (HER). Top of the “volcano” curve [24,31] corresponds to $\Delta G = 0$ or in other words, for the optimal catalyst the change in the free energy during

establishing or breaking of the M-H bond is equal zero. This suggests that the binding energy, which is essentially the enthalpy of the bond between surface and intermediate is defined by changes in entropy, suggesting a strong influence of the solvent on the rate of reaction. It is worth to mention that the core of the observations by Marcus was the influence of the solvent on the rate of electron transfer where the reorganization energy of the solvent was a crucial factor that determines the activation energy for outer sphere reactions. For the inner sphere reactions, like HER, in case of the optimal catalyst corresponding to the top of “volcano”-curve, the solvent also plays a mayor role. The entire process of adsorption of an ion (or a proton) from solution consists of 3 steps: 1) desolvation of the ion (increase of entropy). 2) desorption of water molecules (increase of entropy), and 3) adsorption of ions (decrease of entropy). The change of degrees of freedom during adsorption is given by 3n-3 (three translational degrees of freedom are lost), where n is the number of molecules of the solvent replaced by one ion during the adsorption. If in ideal case (n = 1), the increase in entropy during desorption of a water molecule is equal to the decrease in entropy during the ion adsorption. In this case, the entire process would be driven by the entropy of the desolvation of the ion. This suggests and at least qualitative link between the optimal binding energy of the formed intermediate and the energy of the reorganization of the solvent.

If these observations are applied to CER, the question remains why the top of the “volcano”-curve, constructed using characteristic Raman vibrations, corresponds to the Cl-O vibration in solution instead of the vibration at the surface ? The top of the “volcano” curve should correspond to the optimal binding energy (or optimal vibrational frequency from Raman spectroscopy) of the adsorbed intermediate in the rate determening step. Plotting the correlation betweeen the overpotential for CER and the characteristic vibrations of transition metal oxides, the top of the “volcano” curve is at about 725 cm^{-1}. It was expected that the top of the “volcano” curve corresponds to either a) the optimal OM----intermediate vibrational

frequency or b) the optimal vibrational frequency of another chemical bond in the intermediate itself. The value surprisingly is the one of the vibration of the Cl-O bond in HClO in solution

The real question is how the Cl-O vibration frequency of HClO in solution differs from the vibration frequency of Cl-O in HClO attached to the surface? An optimal catalyst which is located at the top of the “volcano” curve is considered to exhibit a $\Delta G_r = 0$. Thus, no work was invested in the formation or breaking of the OM---OCl bond or no free energy was consumed for establishing or breaking of this bond. Hence, the establishing or breaking of the OM---OCl bond is exclusively entropy driven and consequently the vibrational frequency which originates in the chemical energy stored in the chemical bond should be unchanged.

It is supposed that under these conditions the exchange of electrons through the O-M---O-Cl is most efficient according to to Frank-Condon principle. During an electronic transition a change from one vibrational energy to another will be more likely to happen if the two vibrational wave functions overlap more significantly. The equation for the reaction rate of Levich and Dogonadze is derived from the Frank-Condon principle [81]. Furthermore, during the formation of the OM--OCl bond and the subsequent exchange of electrons resonance will be established in the OM---OCl bond due to the fact that the O-M is oscillating with a similar frequency as the Cl-O bond. The bond vibration will become very intensive until the bond is broken or weak enough that HClO can be replaced by a new water molecule (or OH_{ad}). This corresponds to a change in entropy necessary for binding of a water molecul at the catalyst surface. For the optimal catalyst the difference in the characteristic vibration frequency of the Cl-O bond in solution and the characteristic vibration frequency at the surface should be close to zero.

How general is the discussed resonance principle? Is it possible to discuss cathodic reactions such as HER or ORR in a similar way? HER or ORR proceed at pure metal surfaces which are not covered by an oxide. Since Raman active species have vibration modes that result in a change of polarizability it is difficult to assume such an effect for metals which are almost

infinitely polarizable. This is the reason for a lack of data for the pure metals. Certainly, this is only an approximation. Small clusters or thin metal films may be Raman active at least to some extent.

Finally, while for outer sphere reactions the reorganization energy of the solvent is crucial for the electron transfer, in case of inner sphere reactions like CER the degree of overlapping of the orbitals of the active site and the adsorbed species is additionally important. The overlapping of orbitals between the active site and an adsorbed species is expressed by an exchange integral between the wave functions of the electrons in the reactant and the electrode illustrating theFranck-Condon principle. Thus, the observation of electrocatalytic CER as a resonance phenomena is important for an overall understanding of electrocatalytic reactions.

To further comprehend electrocatalysis from a fundamental point of view the following questions have to be considered:

1) What is the connection between the resonance at the surface during an electrocatalytic reaction and the redox potentials that describe the transition from lower to higher oxidation states of the used oxide catalyst.

2) How does the difference between E_{pzc} and OCP influence the reorganization energy of the solvent considering the fact that with changing the applied potential from E_{pzc}, which is considered to be the point of maximum entropy in the double layer, towards OCP is connected with a continuous reduction of the entropy of the double layer..

3) Is it possible to extend the concept to other important reactions such as oxygen reduction/evolution and hydrogen evolution/oxidation.

6.8. Note on corrosion and stability

The corrosion stability of DSA is an important factor for their industrial application. The expected service time of DSA is at least 3 years. In the case of “cracked” electrodes, the

critical stability point is the penetration of the electrolyte (through the “cracks”) to the titanium support. This causes growth of TiO_2 which in turn induces an additional ohmic drop in the anode ultimately deactivating it [146]. However, this phenomenon is more characteristic for HCl electrolysis where the pH of the electrolyte is around zero. In the case of NaCl electrolysis, the pH value of the electrolyte is between 2 and 3. This makes the titanium support to be under less serious risk of corrosion. This is an experimental fact although some authors have reported severe corrosion of the catalyst layer when the pH was between 2 and 4 [147]. It is known that during NaCl electrolysis the catalytic layer gradually corrodes through dissolution of Ru [144]. The oxygen evolution reaction (OER), which is thermodynamically more favorable as compared with the chlorine evolution reaction, is seen as the primary reason for corrosion in this case. Anodic activation of water causes RuO_2 to be transformed into its higher oxidation states which are less stable [148].

For the investigated DSA samples it was illustrated that the more active electrodes do not necessarily corrode faster. Under galvanostatic operation conditions, when constant current is forced through the electrolyzer, the resulting overpotential is strongly dependent on the effective surface area. In case of a DSA with a desirable “crack” geometry, the effective surface area is relatively high causing a lower real current density and consequently a lower local overpotential. Having in mind that high current densities or correspondingly high overpotentials are one of the main reasons for corrosion of DSA [145], it is clear why DSA with a relatively low non-effective surface area are corroding faster.

7. SUMMARY

- Analyzing “state-of-the-art” in chlor-alkali technology we concluded that the greatest potential for efficiency improvement of CER on DSA lies in reducing of energy loss connected with so called “gas-bubble” effect
- Designing of adequate morphological pattern requires coupling of knowledge of electrochemistry and surface physics where GEE are observed as oscillatory systems
- Calculated turnover frequency of the DSA catalyst layer was correlated with geometry of the “cracks” (pores)
- “Cracks” width was recognized as parameter that can promote gas-nucleation with limited growth and coalescence; smaller radii of detached gas-bubble responds to higher detachment frequency
- “Cracks” induced by the tensile stress are locally enriched with RuO_x, active component of DSA
- CER can be locally detected and visualized
- Local morphology/conductivity/composition/activity relations are proving that “mud-crack” structure is desired morphological pattern
- More uniform spatial distribution of active sites promotes more efficient CER and allows for longer life time of DSA
- Local electrochemical noise measurements allow for obtaining of potential-dependent frequency spectra as function of surface morphology what was clear indicator of structure/activity relation
- Fraction of the catalyst layer that will be functional during the GER is determined by the morphological pattern and applied regime of current density
- While activity can be improved (including energy efficiency), stability depends strongly from the selectivity what requires further fundamental study on electrocatalysis

- Investigation of reaction path of CER suggests crucial role of the solvent in formation of adsorbed intermediates and reconstruction of the surface
- Experimental results suggests that (electro)catalysis can be understood as a resonance phenomena, where efficiency of (electro)catalytic process depends strongly from characteristic vibrations of crystals used as a catalyst and characteristic vibrations of bonds in chemical species which participate in the reaction
- Newly constructed “volcano” - curve based on characteristic vibrations (Raman shifts) allows for establishing of qualitative relation between resonance and optimal binding energies

8. REFERENCES

1) C.G. Vayenas, J. Solid State Electrochem. 15 (2011) 1425-1435
2) J.O'M. Bockris, J. Serb. Chem. Soc. 70 (2005) 789-790
3) S. Trasatti, Russ. J. Electrochem+ 41 (2005) 1255-1264
4) M. Redclift, Global Environ. Change 2 (1992) 32-42
5) W.M. Addams, Report of the IUCN Renowned Thinkers Meeting (2006)
6) N.S. Lewis, D.G. Nocera, Proc. Natl. Acad. Sci USA 103 (2006) 15729-15735
7) Eurochlor, Chlorine Industry Review, 2007/2008
8) S. Trasatti, Electrochim. Acta 45 (2000) 2377-2385
9) P. Patnaik, .Handbook of Inorganic Chemicals, McGrow-Hill New York (2003) p.208
10) M.J. Prather, R.T. Watson, Nature 344 (1990) 729-734
11) R. Chen, V. Trieu, A.R. Zeradjanin, H. Natter, D. Teschner, J. Kintrup, A. Bulan, W. Schuhmann, R. Hempelmann, Phys. Chem. Chem. Phys. DOI: 10.1039/c0xx00000x
12) J. Pérez-Ramírez, C. Mondelli, T. Schmidt, O. F.-K. Schlüter, A. Wolf, L. Mleczko, T. Dreier, Energy Environ. Sci. 4 (2011) 4786-4799
13) S. Trasatti, Electrochim. Acta 29 (1984) 1503-1512.
14) E. Santos, W. Schmickler, in *Recent Advances in Theoretical Aspects of Electrocatalysis* from *Modern Aspects of Electrochemistry,* Vol 50*,* (2010) Springer, New York, p. 25-88.
15) F. Studt, F. Abild-Pedersen, H. A. Hansen, I. C. Man, J. Rossmeisl, T. Bligaard,ChemCatChem 2 (2010) 98-102
16) D. Crihan, M. Knapp, S. Zweidinger, E. Lundgren, C. J. Weststrate, J. N. Andersen, A. P. Seitsonen, H. Over, Angew. Chem. 120 (2008) 2161-2164
17) J. P. Hofmann, S. Zweidinger, A. P. Seitsonen, A. Farkas, M. Knapp, O. Balmes, E. Lundgren, J. N. Andersen, H. Over Phys. Chem. Chem. Phys. 12 (2010) 15358-15366
18) F. Federico, G.N. Martelli, D. Pinter, in *Modern chlor-alkali technology: Gas-diffusion electrodes for chlorine related (production) technologies*, (2001) Blackwell Science: London
19) H.B. Beer, J. Electrochem. Soc. 127 (1980) 303-307
20) J.O'M. Bockris, Nature, 158 (1946**)** 584
21) J.O'M. Bockris, Nature 159 (1947) 539-540
22) B.E. Conway, B.V. Tilak, Electrochim. Acta 47 (2002) 3571-3594
23) R. Parsons, Trans. Faraday Soc. 54 (1958) 1053-1064
24) S. Trasatti S. J. Electroanal. Chem. 39 (1972) 163-184
25) A.T. Kuhn, C.J. Mortimer, G.C. Bond, J. Lindley, J. Electroanal. Chem. 34 (1972) 1-14
26) J.M. Jaksic, M.V. Vojnovic, N.V. Krstajic, Electrochim. Acta 45 (2000) 4151-4158
27) M.M. Jaksic, J.M. Jaksic, Electrochim. Acta 39 (1994) 1695–1714
28) J.M. Jaksic, V.R. Radmilovic, N.V. Krstajic, C.M. Lacnjevac, M.M. Jaksic, Maced. J. Chem. Chem. En. 30 (2011) 3-18

29) E. Santos, P. Hindelang, P. Quaino, E.N. Schulz, G. Soldano, W. Schmickler, ChemPhysChem 12 (2011) 2274-2279.

30) W. Schmickler, S. Trasatti, J. Electrochem. Soc. 153 (2006) L31-L32

31) J.K. Norskow, T. Bliigard, A. Logadottir, J.R. Kitchin, J.G. Chen, S. Pandelov, U. Stimming, J. Electrochem. Soc. 152 (2005) J23-J26

32) R. Subbaraman, D. Tripkovic, D. Strmcnik, K-C. Chang, M. Uchimura, A. P. Paulikas, V. Stamenkovic, N. M. Markovic, Science 334 (2011) 1256-1260

33) M.T.M. Koper, J. Electroanal. Chem. 660 (2011) 254-260

34) S. Zecevic, S.LJ. Gojkovic, B. Nikolic, in Elektrohemijsko Inzenjerstvo, TMF Beograd (2001)

35) S.LJ. Gojkovic, in Elektrohemijska Kinetika, interna skripta, TMF Beograd (2005)

36) A. J. Bard, L. R. Faulkner, Electrochemical methods – Fundamentals and applications, Wiley-VCH, New York, (2001).

37) H.P. Hack, P.J. Moran, J.R. Scully in Measurements and Correction of Electrolyte Resistance in Electrochemical Tests, (Eds.: L.L. Scribner, S.R. Taylor), ASTM International, Baltimore MD, (1990), pp. 23

38) K. Juttner, in Technical Scale of Electrochemistry, from Encyclopedia of Electrochemistry. Edited by A.J. Bard and M. Stratmann Vol. 5 Electrochemical Engineering. Edited by Digby D. Macdonald and Patrik Schmuki (2007) Wiley-VCH Verlag GmbH & Co. KGaA, Weinheim

39) C. Wagner, J. Electrochem. Soc. 98 (1951) 116-128

40) K. Macounova, M. Makarova, J. Jirkovsky, J. Franc, P. Krtil, Electrochim. Acta 53 (2008) 6126-6134.

41) S. Trasatti, Electrochim. Acta 32 (1987) 369-382.

42) P. Gu, Doctoral thesis, University of Otawa, Canada (1990)

43) M.D. Spasojevic, N.V. Krstajic, M.M. Jaksic, J. Res. Inst. Catalysis, Hokkaido Univ.,31 (1983) 77-94

44) A. Daghetti, G. Lodi, S. Trasatti Mater. Chem. Phys. 8 (1983) l-90

45) N. Takeno, Atlas of Eh-pH diagrams, Geological Survey of Japan Open File Report No.419, (2005)

46) Natl. Bur. Stand. (U.S.) Monogr. 25, 7, 83 (1969)

47) D. Grier, G. McCarthy, North Dakota State University, Fargo, North Dakota, USA, ICDD Grant-in-Aid, (1991)

48) L.D. Burke, O. J. Murphy J. Electroanal. Chem. 112 (1980) 39-50

49) H. Kim, B.N. Popov, J. Power Sources, 104 (2002) 52-61

50) S. Trasatti, Elektrochimica Acta, 36 (1991) 225-241

51) Yu.E. Roginskaya, I.D. Belova, B.Sh. Galyamov, F.Kh. Chibirova, R.R. Shifrina, Mater. Chem. Phys. 22 (1989) 203-229

52) G. Lodi, E. Sivieri, A. De Batisti, S. Trasatti, J. Appl. Electrochem. 8 (1978) 135-143

53) E. Guerrini, S. Trasatti, Russ. J. Electrochem+ 42 (2006) 1017-1025

54) S. Ardizzone, M. Falciola, S. Trasatti, J. Electrochem. Soc. 136 (1989) 1545-1550

55) J.O'M. Bockris, T. Otagawa, J. Electrochem. Soc. 131 (1984) 290-302.

56) S.C. Petitto, M.A. Langell, J. Vac. Sci. Technol. A 22 (2004) 1690-1696

57) A.N. Frumkin, J. Electroanal. Chem. 9 (1965) 173-183

58) H.A. Hansen H.A, I.C. Man, F. Studt, F. Abild-Pedersen, T. Bligaard, J. Rossmeisl, Phys. Chem. Chem. Phys. 12 (2010) 283-290

59) S.G. Bratsch, J. Phys. Chem. Ref. Data 18 (1989) 1-21.

60) R.A. Marcus, Nobel Lecture, Chemistry (1992)

61) R.A. Marcus, Annu. Rev. Phys. Chem. 15 (1964) 155-196.

62) L.D. Burke, O.J. Murphy, J.F O Neill, J. Electroanal. Chem. 81 (1977) 391-394

63) L.D. Burke, O.J. Murphy, J. Electroanal. Chem. 96 (1979) 19-27

64) L.D. Burke, J.F O Neill, J. Electroanal. Chem. 101 (1979) 341-349

65) G. Lodi, G. Zucchini, A. DE Battisti, E. Sivieri, S. Trasatti, Mater. Chem. 3 (1978) 179-188

66) Ardizzone, S.; Carugati, A.; Lodi, G.; Trasatti, S. J. Electrochem. Soc. 129 (1982), 1689-1693

67) K.J.J. Mayrhofer, B.B Blizanac, M. Arenz, V.R. Stamenkovic, P.N. Ross, N.M. Markovic, J. Phys. Chem. B 109 (2005) 14433-14440

68) A.J. Appleby, J. Electroanal. Chem. 357 (1993) 117-179

69) N. Ramaswamy, S. Mukerjee, J. Phys. Chem. C 115 (2011) 18015-18026

70) T. Arikado, C. Iwakura, H. Tamura, Electrochim. Acta 23 (1978) 9-15

71) T. Arikado, C. Iwakura, H. Tamura, Electrochim. Acta 23 (1978) 799-801

72) J. Suntivich, K.J. May, H.A. Gasteiger, J.B. Goodenough, Y. Shao-Horn, Science 334 (2011) 1383-1385

73) J. Suntivich, H.A. Gasteiger, N. Yabuuchi, H. Nakanishi, J.B. Goodenough, Y. Shao-Horn, Nature Chemistry 3 (2011) 546-550

74) I.C. Man, H.Y. Su, F. Calle-Vallejo, H.A. Hansen, J.I. Martínez, N.G. Inoglu, J. Kitchin, T.J. Jaramillo, J.K. Nørskov, J. Rossmeisl, *Chem. Cat. Chem.* 3 (2011) 1159-1165.

75) B.E. Conway, D.M. Novak, J. Electroanal. Chem. 99 (1979) 133-156

76) B.V. Tilak, D.M. Novak, B.E. Conway, J. Electrochem. Soc. 128 (1981) 1933-1936

77) B.V. Tilak, J. Electrochem. Soc. 126 (1979) 1343-1348

78) E. Gileadi, Multistep Electrode Reactions, in *Physical Electrochemistry*; Wiley – VCH Weinheim, (2011)

79) V. Consonni, S. Trasatti, F. Pollak, W.E. O'Grady, J. Electroanal. Chem. 228 (1987) 393-406

80) B.E. Conway, E. Gileadi, Can. J. Chem. 42 (1964) 90-106

81) Y. Matsumoto, E. Sato, Mater. Chem. Phys. 14 (1986) 397-426

82) R.D. Shanon, Solid State Commun. 6 (1968) 139-143

83) V. Petrykin, K. Macounova, O.A. Shlyakhtin, P. Krtil. Angew. Chem. 122 (2010) 4923-4925.

84) V. Petrykin, K. Macounova, J. Franc, O. Shlyakhtin, M. Klementova, S. Mukerjee, P. Krtil, Chem. Mater. 23 (2011) 200-207.

85) A.T. Kuhn, C.J. Mortimer, J. Electrochem. Soc. 120 (1973) 231-236

86) A. Dobrzeniecka, A.R. Zeradjanin, J. Masa, A. Puschhof, J. Stroka, P. J. Kulesza, W. Schuhmann, Cat. Today; accepted

87) B.V. Tilak, P.J. Orosz, E.A. Sokol, ESTIR Electrochemistry Enciclopedia, http://electrochem.cwru.edu/encycl/art-b01-brine.htm

88) J. Mozota, M. Vukovic, B.E. Conway, J. Electroanal. Chem. 114 (1980) 153-157

89) A. J. Bard, M. V. Mirkin, Scanning Electrochemical Microscopy , Marcel Dekker, New York, (2001)

90) K. Eckhard, X. Chen, F. Turcu, W. Schuhmann, Phys. Chem. Chem. Phys. 8 (2006) 5359-5365

91) G.G. Stoney, Proc. R. Soc. Lond. A, 82 (1909) 172-175.

92) S.V. Evdokimov, Russ. J. Electrochem+ 36 (2000) 236-239

93) S.V Evdokimov, Russ. J. Electrochem+ 36 (2000) 489-494

94) H. Vogt, Electrochim. Acta 25 (1980) 527-531

95) S. J. Ardizzone, P. Siviglia, S. Trasatti, J. Electroanal. Chem. 122 (1981) 395-401

96) S. J. Ardizzone, G. Fregonara, S. Trasatti, Electrochim. Acta 35 (1990) 263-267

97) D. Baronetto, N. Krstajic, S. Trassati, Electrochim. Acta 39 (1994) 2359-2362

98) H. Vogt, Electrochim. Acta 39 (1994) 1981-1983

99) R. F. Savinell, R. L. Zeller III, J. A. Adams, J. Electrochem. Soc. 137 (1990) 489-494

100) E.H. Calderon, R. Wühtrich, P. Mandin, G. Foti, C. Comninellis, J. Appl. Electrochem. 39 (2009) 1379-1384

101) E.H. Calderon, A. Katsaounis, R. Wühtrich, P. Mandin, G. Foti, C. Comninellis, J. Appl. Electrochem. 39 (2009) 1827-1833

102) G. Lodi, C. De Asmundis, S. Ardizzone, E. Sivieri, S. Trasatti, Surf. Technol. 14 (1981) 335-343

103) A.G. Pshenichnikov, Y.G. Chirkov, V.I. Rostokin, Russ. J. Electrochem+ 38 (2002) 213-219

104) N.P. Brandon, G.H. Kelsall, J. Appl. Electrochem. 15 (1985) 475-484

105) I.G. Malenkov, J. Eng. Phys. Thermophys, 20 (1971) 704-708

106) J. Zhou, Y. Zu, A.J. Bard, J. Electroanal. Chem. 491 (2000) 22-29

107) J.L. Fernandez, A.J. Bard, Anal. Chem. 75 (2003) 2967-2974

108) A. Minguzzi, M.A. Alpuche-Aviles, J. Rodriguez Lopez, S. Rondini, A.J. Bard, Anal. Chem. 80 (2008) 4055-4064.

109) K. Eckhard, W. Schuhmann, Electrochim. Acta 53 (2007) 1164-1169.

110) C. M. Sanchez-Sanchez, J. Rodriguez-Lopez, A. J. Bard, Anal. Chem. 80 (2008) 3254-

3260

111) C. M. Sanchez-Sanchez, A. J. Bard Anal. Chem. 81 (2009) 8094–8100.

112) Y. Shen, M. Trauble, G. Wittstock, Anal Chem 80 (2008) 750-759.

113) Y. Shen, M. Trauble, G. Wittstock, PCCP 10 (2008) 3635-3644.

114) A. Dobrzeniecka, A.R. Zeradjanin, J. Masa, J. Stroka, M. Goral, W. Schuhmann, P. J. Kulesza, ECS Transactions 35 (2011) 33-44

115) A. Maljusch, T.C. Nagaiah, S. Schwamborn, M. Bron, W. Schuhmann, Anal. Chem. 82 (2010) 1890-1896

116) L.A. De Faria, S. Trasatti, J. Electroanal. Chem. 340 (1992) 145-152

117) R. Vigano, J. Taraszewska, A. Daghetti. S. Trasatti, J. Electroanal. Chem. 182 (1985) 203-209

118) M. Thomassen, B. Borresen, G. Hagen, R. Turnold, Electrochim. Acta 50 (2005) 1157-1167

119) R.G. Compton, in *Electrode Kinetics: Electrodes*, Elsevier Science Publisher, Amsterdam, 1987, 326-338

120) K. Karnicka, K. Eckhard, D.A. Guschin, L. Stoica, P.J. Kulesza, W. Schuhmann, Electrochem. Commun. 9 (2007) 1998-2002

121) L. Guadagnini, A. Maljusch, X. Chen, S. Neugebauer, D. Tonelli, W. Schuhmann, Electrochim. Acta 54 (2009) 3753-3758

122) A. Okunola, T. Chikka-Nagaiah, X. Chen, K. Eckhard, W. Schuhmann, M. Bron, Electrochim. Acta 54 (2009) 4971-4978

123) X. Chen, K. Eckhard, M. Zhou, M. Bron, W. Schuhmann, Anal. Chem. 81 (2009) 7597-7603

124) B.B. Katemann, A. Schulte, W. Schuhmann, Chem. Eur. J. 9 (2003) 2025-2033

125) M. Nebel, K. Eckhard, T. Erichsen, A. Schulte, W. Schuhmann, Anal. Chem. 82 (2010) 7842–7848

126) G.N. Martelli, R. Ornelas, G. Faita, Electrochim. Acta 39 (1994) 1551-1558

127) R.P.H. Gasser, P.R. Vaight Nature 221 (1969) 166-167

128) C. Amatore, J.M. Saveant, D. Tessier, J. Electroanal. Chem. 147 (1983) 39-51

129) J. Murayama, I. Abe, Electrochim. Acta 48 (2003) 1443-1450

130) G. Wu, Z. Chen, K. Artyushkova, F. H. Garzon, P. Zelenay ECS Transactions 16 (2008) 159-170.

131) R.C. Engstrom, M. Weber, D.J. Wunder, R. Burgess, S. Winquist, Anal. Chem. 58 (1986) 844-848

132) A.J. Bard, F.F. Fan, J. Kwak, O. Lev, Anal. Chem. 61 (1989) 132-138

133) A.R. Zeradjanin, T. Schilling, S. Seisel, M. Bron, W. Schuhmann, Anal. Chem. 83 (2011) 7645-7650.

134) L.I. Krishtalik, Electrochim. Acta 26 (1981) 329-337

135) H. Vogt, Electrochim. Acta 23 (1978) 203-205

136) K. Stephan, H. Vogt, Electrochim. Acta 24 (1979) 11-18

137) H.J. Vogt, Appl. Electrochem. 19 (1989) 713-719

138) M. Alkan, M. Oktay, M.M. Kocakerim, M. Copur, M. J. Hazard. Mater. 119 (2005) 13-18

139) L.J.J. Janssen, J.G. Hoogland, Electrochim. Acta 15 (1970) 1667-1676

140) D.R. Hodgson, Electrochim. Acta 41 (1996) 605-609

141) H. Wendt, Electrochim. Acta 39 (1994) 1749-1756

142) J.M. Chin Kwie Joe, L.J.J. Janssen, S.J.D. Van Strelen, J.H.G. Verbunt, W.M. Sluvter, Electrochim. Acta 33 (1988) 769-779.

143) A.R. Zeradjanin, F. La Mantia, J. Masa, W. Schuhmann, Utilization of the catalyst layer at gas evolving electrodes – interplay of morphology and active surface area, *accepted in Electrochimica Acta*

144) B.V. Tilak, V.I. Birss, J. Wang, C.-P. Chen, S.K. Rangarajan, S.K. J. Electrochem. Soc. 148 (2001) D113-D120

145) A.S. Pilla, E.O. Cobo, M.M.E. Duarte, D.R. Salinas, J. Appl. Electrochem. 27 (1997) 1283-1289

146) S.M. Hoseinieh, F. Ashrafizadeh, F, M.H. Maddahi, J. Electrochem. Soc. 157 (2010) E50-E56

147) S.V. Evdokimov, Russ. J. Electrochem+ 36 (2000) 259-264

148) Lj.M. Gajić-Krstajić, T.Lj. Trišović, N.V. Krstajić, Coross. Sci. 46 (2004) 65-74

149) R. Chen, V. Trieu, H. Natter, K. Stöwe, W.F. Maier, R. Hempelmann, A. Bulan, J. Kintrup, R. Weber, Chem. Mater. 22 (2010) 6215-6217

150) J.A. Harrison, J. Appl. Electrochem. 15 (1985) 495-501

151) A.J. Appleby, J.H Zagal, J. Solid State Electrochem. 15 (2011) 1811-1832

152) E. Gileadi, J. Solid State Electrochem. 15 (2011) 1359-1371

153) F.B. Li, A.R. Hillman, S.D. Lubetkin, D.J. Roberts, J. Electroanal. Chem. 335 (1992) 345-362

154) F.B. Li, S.D. Lubetkin, D.J. Roberts, A.R. Hillman, J. Chem. Soc. Chem. Comm. 2 (1994) 159-160

155) G. Ertl, Science 254 (1991) 1750-1755

156) G. Ertl, Angew. Chem. Int. Edit. 47 (2008) 3524-3535

157) M. Eiswirth, K. Krischer, G. Ertl, Surf. Sci. 202 (1988) 565-591

158) J.O'M. Bockris, Nature 159 (1947) 401-402

159) H. Dau, C. Limberg, T. Reier, M. Risch, S. Roggan, P. Strasser, Chem. Cat. Chem. 2 (2010) 724-761.

160) S. Trasatti S. J. Electroanal. Chem. 33 (1971) 351-378

161) C. Angelinetta, S. Trasatti, Lj.D. Atanasoska, Z.S. Minevski, R.T. Atanasoski, Mater. Chem. Phys. 22 (1989) 231-247

162) O. Wolter, J. Heitbaum, Ber. Bunsenges. Phys. Chem. 88 (1984) 2-6

163) M. Wohlfahrt-Mehrens, J. Heitbaum, J. Electroanal. Chem. 237 (1987) 251-260

164) A.C.C. Tseung, S. Jasem, Electrochim. Acta 22 (1977) 31-34.

165) K.E. Johnson, ECS Interface 16 (2007) 38-41.

166) M.M. Huang, Y. Jiang, P. Sasisanker, W.G. Driver, H. Weingärtner, J. Chem. Eng. Data 56 (2011) 1494-1499

167) T. Singh, A. Kumar, J. Phys. Chem. B 112 (2008) 12968-12972

168) C. Wakai, A. Oleinikova, M. Ott, H. Weingärtner, J. Phys. Chem. B 109 (2005) 17028-17030

169) J.F.C. Boodts, S. Trasatti, J. Electrochem. Soc. 37 (1990) 3784-3789

170) J. Gaudet, A.C. Tavares, S. Trasatti, D. Guay, Chem. Mater. 17 (2005) 1570-1579

171) T. Arikawa, Y. Murakami, Y. Takasu, J. Appl. Electrochem. 28 (1998) 511-516

172) V.V. Losev, N. Ya Bune, L.E. Chuvaeva, Electrochim. Acta, 34 (1989) 929-942

173) L. Zhuang, J. Jin, H. D. Abruna, J. Am. Chem. Soc. 129 (2007) 11033-11035

174) I. Wachs, Catal. Today 27 (1996) 437-455

175) R. Li, Z. Jiang, Y. Guam, H. Yang, B. Liu, J. Raman Spectrosc. 40 (2009) 1200-1204

176) P. Castelli, S. Trasatti, F.H. Pollak, W.E. O'Grady, J. Electroanal. Chem. 210 (1986) 189-194

177) S.Y. Mar, C.S. Chen, Y.S. Huang, K.K. Tiong, Appl. Surf. Sci. 90 (1995) 497-504

178) Y.S. Huang, F.H. Pollak, Solid State Commun. 43 (1982) 921-924

179) J. K. Norskov, J. Rossmeisl, A. Logadottir, L. Lindqvist, J. R. Kitchin, T. Bligaard, H. Jonsson, J. Phys. Chem. B 108 (2004) 17886-17892

180) W.P. Griffith, J. Chem. Soc. (A) (1968) 1663-1664.

181) S. Nakagawara, T. Goto, M. Nara, Y. Ozawa, K. Hotta, Y. Arata, Anal. Sci. 14 (1998) 691-698

182) S. Trasatti S. J. Electroanal. Chem. 54 (1974) 437-441

183) Y.S. Huang, S.S. Lin, C.R. Huang, M.C. Lee, T.E. Dann, F.Z. Chien, Solid State Commun. 70 (1989) 517-522

184) W.H. Weber, In *Raman Scattering in Materials Science*; W.H. Weber, R. Merlin, Eds. Springer (2000) Chapter 6, pp. 249.

185) C. Julien, M. Massot, S. Rangan, M. Lemal, D. Guyomard, J. Raman Spectrosc. 33 (2002) 223-228

186) V.G. Hadjiev, M.N. Iliev, I.V. Vergilov, J.Phys. C. Solid State Phys. 21 (1988) L199-L201

187) E. Cazzanelli, A. Kuzmin, G. Mariotto, E. Mironova-Ulmane, J. Phys. Condens. Matter 15 (2003) 2045-2052

188) L. Burgio, R.J.H. Clark, S. Firth, Analyst 126 (2001) 222-227

189) O.N. Shebanova, P.J. Lazor, J. Raman Spectrosc. 34 (2003) 845-852

9. APPENDIX

9.1 …FROM GERMAN CULTURE… *(from Johann Wolfgang Von Goethe)*

The man who masters himself is delivered from the force that binds all creatures.

(Die Geheimnisse)

It is easier to perceive error than to find truth, for the former lies on the surface and is easily seen, while the latter lies in the depth, where few are willing to search for it. (The Maxims and Reflections of Goethe)

In science it is a service of the highest merit to seek out those fragmentary truths attained by the ancients, and to develop them further.

Ingratitude is always a kind of weakness. I have never known men of ability to be ungrateful.

Generosity wins favor for every one, especially when it is accompanied by modesty.

To live in a great idea means to treat the impossible as though it were possible. It is just the same with a strong character; and when an idea and a character meet, things arise which fill the world with wonder for thousands of years.

Rest not! Life is sweeping by;

Go and dare before you die.

Something mighty and sublime

Leave behind to conquer time! ("Haste Not-Rest Not")

9.2…AD IUDICIUM…(*some taughts of Nikola Tesla)*

Our first endeavors are purely instinctive prompting of an imagination vivid and undisciplined. As we grow older reason asserts itself and we become more and more systematic and designing. But those early impulses, though not immediately productive, are of the greatest moment and may shape our very destinies.

I am credited with being one of the hardest workers and perhaps I am, if thought is the equivalent of labor, for I have devoted to it almost all of my waking hours. But if work is interpreted to be a definite performance in a specified time according to a rigid rule, then I may be the worst of idlers. Every effort under compulsion demands a sacrifice of life-energy. I never paid such a price.

The scientists from Franklin to Morse were clear thinkers and did not produce erroneous theories. The scientists of today think deeply instead of clearly. One must be sane to think clearly, but one can think deeply and be quite insane.

Today's scientists have substituted mathematics for experiments, and they wander off through equation after equation, and eventually build a structure which has no relation to reality.

If Edison had a needle to find in a haystack, he would proceed at once with the diligence of the bee to examine straw after straw until he found the object of his search. I was a sorry witness of such doings, knowing that a little theory and calculation would have saved him ninety per cent of his labor.

Marconi is a good fellow. Let him continue. He is using seventeen of my patents.

Einsteins relativity work is a magnificent mathematical garb which fascinates, dazzles and makes people blind to the underlying errors. The theory is like a beggar clothed in purple whom ignorant people take for a king. Its exponents are brilliant men but they are metaphysicists rather than scientists.

Let the future tell the truth and evaluate each one according to his work and accomplishments. The present is theirs; the future, for which I really worked, is mine.

Perhaps it is better in this present world of ours that a revolutionary idea or invention instead of being helped and patted, be hampered and ill-treated in its adolescence — by want of means, by selfish interest, pedantry, stupidity and ignorance; that it be attacked and stifled; that it pass through bitter trials and tribulations, through the heartless strife of commercial existence. So do we get our light. So all that was great in the past was ridiculed, condemned, combated, suppressed — only to emerge all the more powerfully, all the more triumphantly from the struggle.

9.3. CURRICULUM VITAE

Aleksandar R. Zeradjanin

Junior Researcher (and Doctoral candidate)
Center for Electrochemistry
Anal. Chem. - Elektroanalytik & Sensorik
Ruhr-Universität Bochum
Universitätsstr. 150; NC 04/788
D-44780 Bochum, Germany

Tel.: +492343226202; FAX: +492343214683
Internet: www.rub.de/elan
E-mail **:** aleksandar.zera@gmail.com

Birthdate: August 14th, 1979
Birthplace: Novska, Croatia

EDUCATION

Doctoral candidate, Chemistry: from 21. April 2009 at Ruhr University Bochum, by supervision of Prof. Wolfgang Schuhmann

M.S.,Chemical Engineering: Faculty of Chemical Technology and Metallurgy, University of Belgrade, Serbia, july 2008.

Master thesis: Electrochemical characteristics of rechargeable battery system polyaniline/lead dioxide (Mentor Prof. B.N. Grgur, Department for Physical Chemistry and Electrochemistry)

RESEARCH INTERESTS – electrocatalysis and development of new electroanalytical approaches; synthesis and characterization of oxides for Cl_2 and O_2 evolution; non-noble catalysts for the O_2 reduction; oxide supported Pt-based catalysts for the ORR; technical ORR for chlor-alkali technology, ORR and OER in batteries, lead acid batteries, electroconducting polymers, H_2 evolution…

RESEARCH EXPERIENCE

Faculty of Chemistry, Ruhr University Bochum, Germany

- Center for Electrochemistry, 5 months, 05/2012-09/2012

1) Electrocatalysis of oxygen evolution reaction in PEM electrolysers

- Department for Analytical Chemistry - working group for electroanalysis and sensors **–** 3 years and 4 months, 01/2009-04/2012

3) BMBF project - improvement of efficiency of chlorine evolution on dimensionally stable anodes - 3 years, doctoral research

2) BMBF project - electrochemical characterization of gas-diffusion electrodes - 1 month, guest resrearcher

1) Umicore project - testing new support materials for electrocatalysts in fuel cells - 3 months, guest researcher

Faculty of Technology and Metallurgy, University of Belgrade, Serbia (Department for Physical Chemistry and Electrochemistry) **-** associate researcher in exploring electroconducting polymers as electrode materials for batteries – 6 months; January/July (2008)

SCIENTIFIC PRESENTATIONS

Oral Presentations at Conferences

1) Regional ISE meeting for the South-East Europe (RSE-SEE), Belgrade, Serbia, June 2010

2) ISE annual meeting Niigata, Japan, September 2011

3) ISE annual meeting Prague, Czech Republic, August 2012

Poster Presentations

1) CUSO – Nanoelectrochemistry summer school, Villars, Switzerland, September 2010

2) GDCH – German Chemical Society Meeting, Bochum, Germany, September 2010

3) SECM workshop – Frejus, France, October 2010

4) ELCAT – electrocatalysis meeting – Alicante, Spain, November 2011

5) 12th Fischer Symposium – Lübeck, Germany, June 2012,

6) 2nd Ertl Symposium – Stutgart, Germany, June 2012

Additionally Represented at

1) 219th ESC meeting, Monteral, Canada, May 2010

2) XXI International symposium on bioelectrochemistry and bioenergetics, Cracow, Poland, May 2011

3) International Workshop „From imaging techniques towards physical properties“ Bochum, Germany, March 2012

4) ECHEMS8th 2012, Molecular Surface Science and Catalysis, Bertinoro, Italy, June 2012

Oral Presentations as a Part of the BMBF Project "Innovative Technologien für Ressourceneffizienz – Rohstoffintensive Produktionsprozesse: Effizienzsteigerung bei der Chlor- Herstellung“ (FKZ 033R018E) –

1) TU Berlin, October 2009

2) Bayer Materials Science, Leverkusen, March 2010

3) University of Erlangen- Nürnberg, May 2010

4) Bochum University, June 2010

5) Bayer Materials Science, Leverkusen, February 2011

6) Universitär des Saarlandes, Saarbrücken, May 2011

7) University of Erlangen- Nürnberg, June 2011

8) TU Berlin, October 2011

9) Nano X, Saarbrücken, May 2012

REWARDS AND RECOGNITIONS

1) Fellowship of Ruhr University Bochum, January – December 2009

2) Reward for „the best poster for applied electrochemistry“ CUSO – nanoelectrochemistry summer school, Villars, Switzerland, September 2010

3) Invitation for the special issue of the Electrochimica Acta, based on selected

original contributions made at the conference – ISE annual meeting, Niigata, Japan, September 2011

4) Invited lecture in Max Planck Institute – “Functionality of oxide electrodes for electrocatalytic gas evolving reactions”, Düsseldorf, Germany, February 2012

PUBLICATIONS

1) „Visualization of chlorine evolution at dimensionally stable anodes by means of scanning electrochemical microscopy“

Aleksandar R. Zeradjanin, Thorsten Schilling, Sabine Seisel, Michael Bron, Wolfgang Schuhmann – ***Analytical Chemistry*** *83, 7645-7650, 2011*

2) „Scanning electrochemical microscopy for investigation of multicomponent bioelectrocatalytic films”

Anna Dobrzeniecka, **Aleksandar Zeradjanin**, Justus Masa, Jadwiga Stroka, Wolfgang Schuhmann, Pawel J. Kulesza – ***ECS transactions****, 35 (26) 33-44, 2011*

3) „Application of SECM in tracing of hydrogen peroxide at multicomponent non-noble electrocatalyst films for the oxygen reduction reaction“

Anna Dobrzeniecka, **Aleksandar Zeradjanin**, Justus Masa, Andrea Puschhof, Jadwiga Stroka, Pawel J. Kulesza, Wolfgang Schuhmann – ***Catalysis Today****, invited edition, http://dx.doi.org/10.1016/j.cattod.2012.03.060*

4) „Microstructural impact of anodic coatings on the electrochemical chlorine evolution reaction“

Ruiyong Chen, Vinh Trieu, **Aleksandar R. Zeradjanin**, Harald Natter, Detre Teschner, Jürgen Kintrup, Andreas Bulan, Wolfgang Schuhmann, Rolf Hempelmann – ***PCCP*** *14, 7392–7399 ,2012*

5) „Utilization of the catalyst layer of dimensionally stable anodes – Interplay of morphology and active surface area“

Aleksandar R. Zeradjanin, Fabio La Mantia, Justus Masa, Wolfgang Schuhmann - ***Electrochimica Acta****, invited edition, http://dx.doi.org/10.1016/j.electacta.2012.04.101*

6) „Role of water in the chlorine evolution reaction at RuO_2 based electrodes – understanding electrocatalysis as a resonance phenomena“

Aleksandar R. Zeradjanin, Nadine Menzel, Peter Strasser, Wolfgang Schuhmann – ***ChemSusChem,*** *DOI number: 10.1002/cssc.201200193*

7) „Evaluation of catalytic performance of gas evolving electrodes using local electrochemical noise measurements“

Aleksandar R. Zeradjanin, Edgar Ventosa, Aliaksandr Bandarenka, Wolfgang Schuhmann- ***ChemSusChem****, DOI number: 10.1002/cssc.201200262*

8) „Electrochemical characteristics of rechargeable polyaniline | lead dioxide cell“

Branimir N. Grgur, **Aleksandar R. Zeradjanin**, Milica M. Gvozdenović, Miodrag. D. Maksimović, Tomislav Lj. Trišović, Branimir Z. Jugović

Journal of Power Sources*, 217, 193-198, 2012*

9) „Spatial distribution of electrocatalytic activity on gas evolving electrodes – electrohemical microscopic imaging as an insight into macrokinetics“

Aleksandar R. Zeradjanin, Edgar Ventosa, Justus Masa, Leonard Stoica, Wolfgang Schuhmann – completed manuscript

10) „Selective electrocatalytic promotion of chlorine and oxygen evolution at ternary Ti-Ru-Ir based oxide – impact of local equlibriums”

Aleksandar R. Zeradjanin, Nadine Menzel, Wolfgang Schuhmann, Peter Strasser

-completed manuscript

11) „Evaluation of kinetic constants on porous nonnoble catalyst layers for oxygen reduction reaction *via* microelectrode”

Anna Dobrzeniecka, **Aleksandar R. Zeradjanin**, John Henry, Beata Baranowska, Andrea Puschhof, Jadwiga Stroka, Pawel J. Kulesza, Wolfgang Schuhmann

- completed manuscript

12) „Stress induced morphological pattern as efficient electrode for oxygen evolution reaction“ **Aleksandar R. Zeradjanin**, Ruiyong Chen, Bernd Schley, Vinh Trieu, Harald Natter, Rolf Hempelmann, Wolfgang Schuhmann

- in preparation

COOPERATIONS

1) AG Bayer Materials Science - Dr. Jürgen Kintrup and Dipl. Ing. Andreas Bulan

2) TU Berlin - Prof. Peter Strasser's group

3) UdS Saarbrücken - Prof. Rolf Hempelman's group

4) FAU Erlangen - Prof. Patrik Schmuki's group (Robert Hahn...)

5) FAU Erlangen - Prof. Stefan Rosiwal's group

6) NanoX - (Dr. Elin Hamaberg...), Saarbrücken

7) Bayer Technology Service – Dr. Stefanie Eiden

8) Fritz Haber Inst. Berlin - Prof. Robert Schlögl's group (Dr. Detre Teschner...)

9) University of Warszav - Prof. Pavel Kulesza's group

10) University of Belgrade – Prof. Branimir N. Grgur

11) University Halle-Wittenberg – Prof. Michael Bron

CONTRIBUTION TO THE PROBLEMS OF INTEREST

1) local detection and visualization of chlorine and oxygen on oxide electrodes

2) spatial distribution of activity at gas evolving electrodes and its impact on overall performance

3) morphology-activity relations from angle of oscilations and surface physics

4) methodology for extraction of frequency of gas-bubble detachement and establishing of potential dependent frequency spectra

5) methodology for estimation of functionality of the catalyst coating

6) methodology for estimation of number of exchanged electrons (n) during ORR, using SECM microelectrode

7) investigation of the role of the water during electrocatalytic reactions

8) introduction of characteristic vibrations as catalytic descriptor into electrocatalysis

9) role of local equlibriums on selectivity and faradaic efficiency of oxide electrodes for OER and CER

10) splitting of kinetic and diffusional effects in kinetic analysis, using SECM microelectrode

LANGUAGES

- Serbian (native), English (fluent), German (basic)

ADDITIONAL ACTIVITIES

- Member of ISE (International Society of Electrochemistry)
- Supervision of students

HOBBIES

- Football, chess...

9.4. ABBREAVIATIONS AND SYMBOLS

AFM – atomic force microscopy
BDD – boron doped diamond
CAFM – conductive atomic force microscopy
CER – chlorine evolution reaction
CV – cyclic voltammetry
DEMS – differential electrochemical mass spectrometry
DSA – dimensionally stable anode
EDX – energy dispersive X-ray spectroscopy
EIS – electrochemical impedance spectroscopy
GEE – gas evolving electrode
GER – gas evolving reaction
HER – hydrogen evolution reaction
INT - integer
OCP – open circuit potential
OER – oxygen evolution reaction
ORR – oxygen reduction reaction
RDE – rotating disc electrode
SEM – scanning electron microscope
SECM – scanning electrochemical microscopy
SG-TC – sample-generation/tip-collection
TOF – turnover frequency
UHV – ultra high vacuum

A – reactant
a_A *- stoichiometric coefficient for reactant*
a_i *- chemical activity of specie i*
A_{geo} *- geometric surface area of the sample*
A_{real} *- real surface area*
α_a *- transfer coefficient of anode reaction*
B - product
b - known as Tafel's slope
b_B *- stoichiometric coefficient for product*
B_L *– Levich slope*
ß – symmetry factor of activation barrier

c(R) - concentration of reduced specie in the bulk

c_s(R) – surface concentration of reduced specie

C_v - variation coefficent

D - diffusion coefficient

δ – magnitude of diffusion layer

$E°_{rev,a}$ - reversible electrode potentials of anodic reaction

$E°_{rev,c}$ - reversible electrode potentials of cathodic reaction

ΔE - change in electrode potentials between cathode and anode, defined for standard conditions

dE°/dT – temperature coefficient of electrode potential

ε – energy efficiency of electrode reaction

$ε_g$ – gas fraction

F - Faraday's constant (96500 C/mol)

f(Cl_2) – fugacity of the chlorine gas

$ΔG_r$ - Gibbs free energy of the reaction

$⊿_rH$ – enthalpy of the reaction

I - current intensity

j - current density

j_0 – exchange current density

j_d – diffusional current density

j_k – kinetic current density

K - equilibrium constant

k – rate constant

κ - conductivity of electrolyte

l - characteristic length

l_r – length of resistor

n - number of exchanged electrons

η - overpotential of the reaction

dη/dj - is polarization resistance

θ – contact angle

$θ_{int}$ – coverage with intermediates

σ – surface tension of the electrolyte

Δp – pressure difference across the electrolyte interface

q - voltammetric surface charge*

q_v - normalized charge involved into the bubble turnover

R - universal gas constant

r – radius of microelectrode

r_p – radius of the pore

R_s – ohmic resistance

ρ - resistivity of the electrolyte

S – cross section of resistor

$\Delta_r S$ – entropy of the reaction

T - absolute temperature

t – time

U – voltage

v - scan rate

v_k – kinematic viscosity

v_r – rate of reaction

v_s – stoichiometric number

γ - activity coefficient

W_a - Wagner number

W_{an} - energy consumed on anode

ω - rotation rate